Università degli Studi di Genova

Doctoral Thesis in Physics

Cicle XXVII

Application of Bohmian Mechanics to Quantum Transport: the Conditional Wave Function

Author: Damiano Marian

Supervisor: Prof. Nino Zanghì

External Supervisor: Prof. Xavier Oriols

Qui delle divertite passioni
per miracolo tace la guerra,
qui tocca anche a noi poveri la nostra parte di
ricchezza
ed è l'odore dei limoni.

Vedi, in questi silenzi in cui le cose
s'abbandonano e sembrano vicine
a tradire il loro ultimo segreto,
talora ci si aspetta
di scoprire uno sbaglio di Natura,
il punto morto del mondo, l'anello che non tiene,
il filo da disbrogliare che finalmente ci metta
nel mezzo di una verità.

Eugenio Montale

Contents

Introduction

This Thesis is aimed to apply Bohmian Mechanics to the study of quantum transport in mesoscopic systems. Bohmian Mechanics is an alternative version of Quantum Mechanics in which particles have a definite position and their motion is choreographed by the wave function. This theory has been proposed by Louis de Broglie [28] in 1926, rediscovered independently by David Bohm [28] in 1952 and from the 1980's developed and systematized by the research group formed by Detlef Dürr, Sheldon Goldstein and Nino Zanghì [35]. It provides the same statistical results as those of Orthodox Quantum Mechanics for any conceivable experiment in the contest of non-relativistic quantum phenomena, it solves the famous "Schrödinger cat paradox" (i.e. the measurement problem), it clarifies the role of operators as observables and it derives the collapse postulate of the wave function [29, 32].

This theory has always been regarded as useful to solve issues related to the foundational aspects of Quantum Theory, but otherwise useless. In recent years this has started to change in the Physics community and some researchers have started to use this theory to solve practical problems. Around 2000 Robert E. Wyatt and collaborators started to use Bohmian Mechanics, in particular its hydrodynamical formulation, to solve problems of kinetic chemistry [54, 84] opening a new research line that has been quite successful among theoretical chemists. More recently, Xavier Oriols has used Bohmian Mechanics to find an approximate solution to the many-body quantum problem [67] and his research group has developed the BITLLES simulator for quantum transport in nanoelectronic devices [11]. Salvador Miret-Artés has used this theory for studying classical and quantum trajectories and Ángel Sanz addressing atomic, molecular and optical physics [73, 74].
It should also be mentioned that, very recently, this theory has attracted some experimental interest. Noteworthily, is the experiment performed by the group of Steinberg, which has led to a reconstruction of the photon trajectories by means of weak measurements in a double slit set-up; the measured trajectories turn out to be the ones predicted by Bohmian Mechanics [45].

The present Thesis fits in the wake of the contemporary research aiming at showing the utility of Bohmian Mechanics in solving practical problems. The notion of *conditional wave function*, an exclusive concept of Bohmian Mechanics, is central for explaining how this theory offers not only different numerical tools for solving the long-standing many-body problem, but also new unexplored ways to attack and understand complex quantum problems. In particular, the numerical tools offered by this theory will be used throughout the thesis to create new strategies for analyzing physical situation in which it is not completely clear the correct way to proceed. For example, it will be considered the interaction of an electron with an external apparatus that measures the High-Frequency total electrical current. One obtains in this way novel way of simulating and comprehending the effect of an external environment on a quantum system in this particular regime.

The Thesis is organized as follows. In Chapter 1 the basic notions of Bohmian Mechanics needed for the present Thesis will be presented. It will be motivated why there is a need to look for an alternative version of Quantum Mechanics, both from a fundamental and from a practical point of view. In Chapter 2 the use of the conditional wave function in solving many-body problems will be addressed. First, it will be shown how the collapse postulate is simply understood and derived within Bohm theory (Section 2.1), second it will be presented the dynamical evolution of the conditional wave function (Section 2.2) and finally it will be presented a numerical (approximate) algorithm to solve many-particle problems (Section 2.3). Chapter 3 is focused on studying the measurement of the total current in quantum devices. Specifically, it will be presented a model for measuring the successful transmission of an electron impinging on a tunneling barrier (Section 3.1) and a model for measuring the total electrical current at TeraHertz frequencies in quantum devices (Section 3.2). In Chapter 4 it will be proposed a way to measure the Bohmian velocity of an electron in solid-state systems through the notion of weak measurement. A detailed introduction about weak measurement will be given (Section 4.1). It will be proposed a possible geometry for a device (Section 4.2) and a numerical study for understanding the feasibility of the proposed experiment will be presented (Section 4.3). Finally, in Chapter 5 two different problems will be considered: first, a numerical and theoretical study of the scattering probabilities in a two-particle HOM-type (Hong-Ou-Mandel) experiment (Section 5.1) and second, the understanding the origin of quantum noise within Bohmian Mechanics (Section 5.2).

Six Appendixes complement this Thesis. In Appendix A a path for the development of a new algorithm for solving the many-particle problem beyond the known approximations is presented. In Appendix B an analytical derivation of the electric flux through a surface is provided. Appendix C is devoted to derive analytically the Bohmian velocity from a weak measurement procedure. In Appendix D and Appendix E the derivation

of two-particle probabilities for scattering formalism and for generic wave packets are presented. Appendix F addresses the quantum DC current in ergodic systems.

Publications Related to This Thesis

- Marian, D., Colomés, E., Zhan, Z. & Oriols, X.
  Quantum Noise from a Bohmian perspective: fundamental understanding and practical computation in electron devices
  Journal of Computational Electronics, Special Issue on Noise Modeling, in press (2015). See also arxiv:1410.0530

- Norsen, T., Marian, D. & Oriols, X.
  Can the wave function in configuration space be replaced by single-particle wave functions in physical space?
  Synthese, Special Issue: Space-time and the wave function, 1-27 (2014)
  doi: 10.1007/s11229-014-0577-0, see also arxiv:1410.3676

- Colomés, E., Marian, D. & Oriols, X.
  Understandable algorithm for exchange interaction: Quantum noise in nanoelectronic devices
  Computational Electronics (IWCE), 2014 International Workshop on, 3-6 June 2014
  doi: 10.1109/IWCE.2014.6865811

- Marian, D., Zanghì, N. & Oriols, X.
  On the back-action of THz measurement on the total current of quantum devices
  Computational Electronics (IWCE), 2014 International Workshop on, 3-6 June 2014
  doi: 10.1109/IWCE.2014.6865844

- Albareda, G., Marian, D., Benali, A., Alarcòn, A., Yaro, S. & Oriols, X.
  Book Chapter *Electron Devices Simulation with Bohmian Trajectories*
  in *Simulation of transport in nanodevices, Volume 1: Principles, models and methods*, ISTE Ltd (2014).

- Albareda, G., Marian, D., Benali, A., Yaro, S., Zanghì, N. & Oriols, X.
  Time-resolved electron transport with quantum trajectories
  Journal of Computational Electronics, Special Issue on Quantum Transport Beyond DC, **12**(3), 405-419 (2013).

- Marian, D., Colomés, E. & Oriols, X.
  Time-dependent exchange and tunneling: detection at the same place of two electrons emitted simultaneously from different sources
  Submitted, see also arxiv:1408.1990

In preparation

- Marian, D., Oriols, X. & Zanghì, N.: *Proposal for Measuring the Bohmian Velocity in Mesoscopic Systems using the Weak Value of the Total Electrical Current.*

Chapter 1

Bohmian Mechanics

1.1 Why Looking for an Alternative to the Orthodox Interpretation of Quantum Mechanics?

Orthodox Interpretation of Quantum Mechanics is undoubtedly one of the most successful theories in Physics. It has been tested in several situations and its predictions allowed the discovering of new and surprising phenomena; however its foundational aspects have been matter of debate since its appearing. The reason why Orthodox Interpretation exhibits foundational problems resides essentially on what Erwin Schrödinger has addressed in his famous 1935 paper *The Present Situation in Quantum Mechanics* [77], commonly known as the *Schrödinger "cat paradox" paper*

> One can even set up quite ridiculous cases. A cat is penned up in a steel chamber, along with the following diabolic device (which must be secured against direct interference by the cat): in a Geiger counter there is a tiny bit of radioactive substance, *so* small, that *perhaps* in the course of one hour one of the atoms decays, but also, with equal probability, perhaps none; if it happens, the counter tube discharges and through a relay releases a hammer which shatters a small flask of hydrocyniac acid. If one has left this entire system to itself for an hour, one would say that the cat still lives *if* meanwhile no atom has decayed. The first atomic decay would have poisoned it. The ψ-function of the entire system would express this by having in it the living and the dead cat (pardon the expression) mixed or smeared out in equal parts.
>
> It is typical of these cases that an indeterminacy originally restricted to the atomic domain becomes transformed into macroscopic indeterminacy, which

> can then be *resolved* by direct observation. That prevents us from so naively accepting as valid a "blurred model" for representing reality. In itself, it would not embody anything unclear or contradictory. There is a difference between a shaky or out-of-focus photograph and a snapshot of clouds and fog banks.[77]

The cat's example expresses essentially the concept that the "blurring" of the microscopic description, represented by the wave function, emerges, in a quite embarrassing way, into the macroscopic scale. If this "blurring" is confined to the microscopic scale, where one has no direct control, it is acceptable,

> But serious misgivings arise if one notices that the uncertainty affects macroscopically tangible and visible things, for which the term "blurring" seems simply wrong.[77]

The very same problem expressed by Schrödinger was also addressed by Albert Einstein in the volume *Albert Einstein, philosopher-scientist* [75]. While describing a radioactive atom, he reflects about the exact instant in which it decays. Exactly as Schrödinger he considers the situation in which, along with the atom, the instrument that certifies the decay of the atom, for example a Geiger counter, is included. Moreover, he includes a registration strip upon which a mark is made. This system is very complex and its configuration is of very high dimension, but nevertheless can be in principle treated quantum mechanically. If enough time is awaited, i.e. enough to be sure that the mark on the strip has been made, the wave function of the composed system is spread over all the microscopic configurations that correspond to the different marks' positions on the strip. But the wave function does not contain the definite location of the mark actually occurred. About this argumentation Einstein comments:

> In this consideration the location of the mark on the strip plays the role played in the original consideration by the time of disintegration. The reason for the introduction of the system supplemented by the registration-mechanism lies in the following. The location of the mark on the registration-strip is a fact which belongs entirely within the sphere of macroscopic concepts, in contradistinction to the instant of disintegration of a single atom.[75]

Then he reaches the conclusion that

> If we attempt [to work with] the interpretation that the quantum-theoretical description of the individual system we are forced to the interpretation that

> the location of the mark on the strip is nothing which belongs to the system *per se*, but that the existence of that location is essentially dependent upon the carrying out of an observation made on the registration strip.[75]

This is basically the lesson of the so called Orthodox Interpretation (also known as Copenhagen Interpretation of Quantum Mechanics or Ordinary Quantum Mechanics), settled down by Bohr [19] and Heisenberg [42] around 1927: the act of observing is responsible of the mark on the strip being in a place or in another (or in the cat's example of its being dead or alive). Einstein continues:

> Such an interpretation is certainly by no means absurd from a purely logical standpoints; yet there is hardly likely to be anyone who would consider it seriously.[75]

The problem previously exposed, using the words of Schrödinger and Einstein, is commonly known as the "measurement problem" which is somehow regarded as "the problem" of the Orthodox Interpretation of Quantum Mechanics. Also Richard Feynman was disappointed and somehow embarrassed by the fact that the act of observation has such a central role in the Orthodox Interpretation

> This is all very confusing, especially when we consider that even tough we may consistently consider ourselves always to be the outside observer when we look at the rest of the world, the rest of the world is at the same time observing us, and that often we agree on what we see in each other. Does this mean that my observations become real only when I observe an observer observing something as it happens? This is an horrible viewpoint. Do you seriously entertain the thought without the observer there is no reality? Which observer? Any observer? Is a fly an observer? Ia a star an observer? Was there no reality in the universe before 10^9 B.C. when life began? Or are *you* the observer? Then there is no reality to the world after you are dead? I know a number of otherwise respectable physicists who have bought life insurance.[37]

Ultimately the "measurement problem" is a reflection of a fundamental ambiguity present in the formulation of the orthodox theory of quantum mechanics. Using the words of John Stewart Bell, one realizes that

> Nobody knows what quantum mechanics says *exactly* about any situation, for nobody knows where the boundary really is between wavy quantum systems and the world of particular events.[9]

Then it emerges clearly from the previous quotation that what is ambiguous in the Orthodox Interpretation of Quantum Mechanics, and what is actually the point undigestible to Schrödinger, Einstein and Feynamn, is the undefined line that separates the macroscopic and microscopic world: the Schrödinger's cat is nothing else than a manifestation of this fundamental ambiguity in the theory.
During the last fifty years many different theories have been proposed to solve the problem exposed above, only to name a few: Bohmian Mechanics [15, 35, 68], Ghirardi-Rimini-Weber theory [38] and Many Worlds Interpretation [36]. Each theory solves the measurement problem in a different way but all have a common character: observer, observation, measurement etc. do not play any fundamental role in the theory. Bohmian Mechanics says that the wave function is not everything and adds to it definite positions for the particles; Ghirardi-Rimini-Webber theory (or its variants known as Spontaneous Collapse Models) provides a different dynamical evolution for the wave function, introducing a stochastic process responsible for the collapse of the wave function at macroscopic scale while maintaing usual Schrödinger dynamics at microscopic level; Many Worlds Interpretation assumes that at every splitting of the wave function there actually exist two different worlds, in the Schrödinger example, one with the dead cat and the other with the alive cat. Ghirardi-Rimini-Webber theory and Many Words Interpretation will not be treated in the present thesis, while in the following of this Chapter the principal characteristics of Bohmian Mechanics will be presented.

1.2 Particles with Definite Positions

The main idea of Bohmian Mechanics is to insist when saying particles to mean particles: particles follow trajectories, i.e. they have always definite positions in space at a given time. In this theory the wave function evolves according to (the usual) Schrödinger equation

$$i\hbar\frac{\partial\Psi(x_1,x_2,\cdots,x_N,t)}{\partial t}=\mathcal{H}\Psi(x_1,x_2,\cdots,x_N,t), \tag{1.1}$$

where $\mathcal{H}=-\sum_{i=1}^{N}\frac{\hbar^2}{2m_i}\frac{\partial^2}{\partial x_i^2}+V(x_1,x_2,\cdots,x_N,t)$ is the usual Hamiltonian composed by a free part and a general interacting potential V. The wave function *guides* the particles motion through the so-called *guidance law*: for a system of N particles whose configuration at time t is $\mathbf{X}(t)=(X_1(t),X_2(t),...,X_N(t))$, where $X_i(t)$ denotes the actual potions of particle i at time t in the physical space, it reads

$$\frac{dX_i(t)}{dt} = v_i|_{\mathbf{x}=\mathbf{X}(t)} = \frac{\hbar}{m_i}\mathrm{Im}\frac{\Psi^*\nabla_i\Psi}{\Psi^*\Psi}\Big|_{\mathbf{x}=\mathbf{X}(t)}, \tag{1.2}$$

where m_i is the mass of particle i, Im denotes the imaginary part, and ∇_i the gradient relative to the 3 coordinates of particle i.[1] Equation (1.2) is written to be valid both for particles with spin and without spin. For the former the wave function is a spinor $\Psi : \mathbb{R}^{3N} \to \mathbb{C}^k$, i.e. a function of the configuration with k complex components, then $\Psi^*\Psi$ is the scalar product in $\mathbb{C}^k$. For the latter the wave function is complex-valued, i.e. $\Psi : \mathbb{R}^{3N} \to \mathbb{C}$, then in Equation (1.2) the term Ψ^* cancels out.
Since Equation (1.1) does not involve the configuration of the particles $\mathbf{X}(t)$, its solution is unique once the initial wave function Ψ_0 at time $t = t_0$ is specified. Note that Equation (1.2) consists of 3 components of particle i out of $3N$ component of the vector field v^Ψ on configuration space $\mathbb{R}^{3N}$. Then Equation (1.2) can be summarized, for $i = 1, ..., N$ as

$$\frac{d\mathbf{X}(t)}{dt} = \mathbf{v}^\Psi(\mathbf{X}(t)). \tag{1.3}$$

Because Ψ is known from Equation (1.1), once the initial configuration is specified $\mathbf{X}(t_0)$, Equation (1.3) determines the history of the configuration $\mathbf{X}(t)$. Hence Bohmian Mechanics is a *deterministic* theory: once Ψ_0 and $\mathbf{X}(t_0)$ are specified the entire history is determined by Equations (1.1) and (1.2). The state of the system in Bohmian Mechanics is then completely specified by the pair $(\mathbf{X}(t), \Psi)$ at any time.

1.3 Conditional Wave Function

The conditional wave function is a unique tool belonging to Bohmian Mechanics, it is a precise and unambiguous definition of the wave function of a subsystem. Consider N interacting quantum particles (a close system, ultimately the entire universe) described by their wave function $\Psi(x_1, x_2, ..., x_N, t)$ and their configuration $\mathbf{X}(t) = (X_1(t), X_2(t), ..., X_N(t))$, the wave function of particle 1 is simply given by fixing all the actual positions of the remaining particles

[1] In the present thesis a bold variable indicates a point in the configuration space, while a non-bold variable indicates a point in the physical space. Capital letters denote the actual positions of particles, while lowercase letters denote generic positions.

$$\psi_1(x_1,t) = \Psi(x_1,x_2,...,x_N,t)|_{x_2=X_2(t),...,x_N=x_N(t)} = \Psi(x,X_2(t),...,X_N(t),t). \quad (1.4)$$

Note that the conditional wave function of Equation (1.4) depends on time in two different ways; the usual time dependence plus the time dependence on the other particles positions $(X_2(t),...,X_N(t))$. In the same way it is possible to define the wave function of all the other particles, for example particle's 2 conditional wave function is simply: $\psi_2(x_2,t) = \Psi(X_1(t),x_2,X_3(t),...,X_N(t),t)$. An important consequence of the definition of the conditional wave function given by Equation (1.4) is that Equation (1.2) may be re-written, for each particle, in terms of its associated conditional wave function

$$\frac{dX_i(t)}{dt} = \frac{\hbar}{m_i}\mathrm{Im}\frac{\nabla_i\Psi}{\Psi}\Big|_{\mathbf{x}=\mathbf{X}(t)} = \frac{\hbar}{m_i}\mathrm{Im}\frac{\nabla\psi_i}{\psi_i}\Big|_{x_i=X_i(t)}. \quad (1.5)$$

Thus, in order to obtain the trajectories of the N particles it is only needed, in principle, to know which is the conditional wave function of each particle. The conditional wave function is a central object in the developing of the present Thesis; its characteristics will be described in details in Chapter 2 and will be used throughout the Thesis.

1.4 Quantum Equilibrium Hypotesis, Equivariance and Empirical Equivalence

Bohmian Mechanics makes the same empirical prediction of Ordinary Quantum Mechanics, whenever the latter is non-ambiguous. In fact, the right hand side of the *guidance equation* (1.2) can be understood as $v_i = j_i/\rho$, evaluated at the configuration point $\mathbf{X}(t)$, where j_i is the standard *probability current* associated with particle i and ρ is the standard *probability density*. As consequence of Equation (1.1), the probability current and density obey the continuity equation

$$\frac{\partial\rho}{\partial t} + \sum_i \nabla_i j_i = 0. \quad (1.6)$$

If one considers an ensemble of systems with the same wave function Ψ but random configurations $\mathbf{X}$ moving with configuration-space velocity $\mathbf{v}$, it is easy to see that the probability distribution $P(\mathbf{X},t)$ over the ensemble should evolve according to

$$\frac{\partial P}{\partial t} + \sum_i \nabla_i (P v_i) = 0. \tag{1.7}$$

Comparison with Equation (1.6) shows that, since $v_i = j_i/\rho$, $P = \rho$ is a solution. Thus, if the initial configurations $\mathbf{X}(t_0)$ in the ensemble are chosen with distribution $P[\mathbf{X}(t_0) = \mathbf{x}] = \rho(\mathbf{x}, t_0) = \Psi^*(\mathbf{x}, t_0)\Psi(\mathbf{x}, t_0)$ - the so-called *quantum equilibrium hypothesis* - it is then a consequence of Equations (1.1) and (1.2) jointly that

$$P[\mathbf{X}(t) = \mathbf{x}] = \rho(\mathbf{x}, t) = \Psi^*(\mathbf{x}, t)\Psi(\mathbf{x}, t) \tag{1.8}$$

for all t. It is thus clear that Bohmian mechanics reproduces the statistical predictions of Ordinary Quantum Mechanics for position measurements, and hence also for any other type of measurement whose outcome is ultimately registered in the position of some *pointer*. This means that Bohmian mechanics is *empirically equivalent* to Ordinary Quantum Mechanics, thus the two theories can not be tested against each other.

1.5 Can a Clear Theory be Useful for Computing and Understanding Quantum Phenomena?

After having exposed the principal features of Bohmian Mechanics it is important to come back to the question posed in the title of Section 1.1: *Why looking for an alternative to the Orthodox Interpretation of Quantum Mechanics?* As briefly exposed, this theory is an alternative version of Quantum Mechanics that does not need any concept of observer or observation in its foundations, it provides a clear and unambiguous way to define the wave function of a subsystem and clearly explains the results of any conceivable experiment giving the same empirical predictions of the Ordinary Quantum Mechanics (whenever the latter is non-ambiguous).

There exists another reason, at least for the author of the present thesis, for considering an alternative version of Quantum Mechanics: It could provide new "practical applications" going beyond of those of standard framework. This is exactly the main subject of the present thesis. With "practical application" is intended any support of the theory in order to solve specific problems (such as: the interaction of a small quantum system with an external environment; the solution of a numerical inaccessible problem, as

for example the many-particle Schrödinger equation, by means of new tools and new approximations, etc.), to deeply investigate the physical origin of quantum phenomena inside of the theory (for example noise in quantum transport) and to attack some very complex problems in a direct and unambiguous way without the introduction of additional postulates (such as: the famous "collapse postulate" of the wave function; the introduction of ad-hoc "operators" for some particular experiments, etc.).
Stepping back to the last quotation used at the end of Section 1.1, when summarizing what Bell calls the *first class problem* of quantum theory (such as the measurement problem, the awkward notions of operator, measurement, observer etc.), he continues

> This is the first class problem and, as we all know, it does not matter at all in practice. [...] It doesn't matter in practice and it is very much a question of debate among physicists whether or not you should worry about a question of principle before it becomes a question of practice.[9]

The present work somehow contradicts this last statement: It could be the case that a (ontologically) clear theory becomes relevant for questions of practice, especially in all the situations where "nobody knows what quantum mechanics says *exactly*"[9]. In fact, if the problem on the foundation of quantum theory was the fundamental ambiguity on the division between the classical and quantum world, nowadays many experiments, applications etc. are exactly performed in the boundary of this two worlds: A complete and non-ambiguous theory allows to describe these situations in a clear and perhaps intuitive way. In the specific case of Bohmian mechanics, the notion of conditional wave function becomes fundamental to study these physical regimes and this is why it is the main object of the present thesis.

Chapter 2

The Many-Body Problem: Use of the Conditional Wave Function

Ordinary Quantum Mechanics usually does not attribute a wave function for a single part of a larger quantum mechanical system. The standard way to proceed is to *trace out* certain degrees of freedom ending up with the so-called *reduced density matrix*. Instead Bohmian Mechanics uses the notion of *conditional wave function* already introduced in Section 1.3. The present Chapter is devoted to analyze the main characteristics of this quantum mechanical object with a particular attention to its usefulness in understanding many-body problems. It will be explained its role in the *derivation* of the so called collapse postulate, its *dynamical evolution* and its practical use for solving many-particle quantum problems. In this Chapter to simplify the discussion, spinless particles will be considered. All the discussion can be reformulated for particles with spin using the notion of *conditional density matrix* [33].

2.1 Understanding Collapse

The first many-body problem considered is the interaction of a quantum system with an apparatus. As already explained in Chapter 1, in Bohmian Mechanics there is no separation between "measuring apparatus" and a "quantum system", both are treated at the same footing, taking care that a suitable interaction between them is modeled. While analyzing this interaction some interesting feature of the conditional wave function will be addressed. In particular, as it will be seen in more detail later in the present Chapter, the conditional wave function obeys the usual one-particle Schrödinger equation in the expected type of situation in which the particle in question is suitably isolated from its environment. Nevertheless in general (when there is non-trivial interaction among

particles) the conditional wave function will evolve in an unusual (non-unitary) way. To give a sense of the possible behavior and also to provide a sense of how the measurement axioms of ordinary Quantum Mechanics can instead be derived, from a careful analysis of appropriate kinds of interactions in Bohmian Mechanics, it will be explained how the one-particle wave function associated with a quantum system *collapses* when there is a proper interaction with another system such as a *measuring device*. First it will be exposed how ordinary quantum theory deals with a measurement process with the introduction of the collapse of the wave function postulate, then the derivation of the collapse within Bohmian Mechanics with a simple analytically-solvable toy model will be illustrated in details. The discussion of the collapse will be done in a practical situation: the transmission of an electron impinging upon a tunneling barrier.

2.1.1 Collapse in the Orthodox Interpretation of Quantum Mechanics

As already said in Chapter 1 the Orthodox Interpretation associates only a wave function to a physical system. Within the first non-relativistic quantization language, the evolution of this wave function is defined by a law and a postulate. The law is the usual Schrödinger equation, which states that (when the system is not measured) the wave function evolves unitarily and deterministically. The postulate provides the collapse of the wave function when a measurement on the physical system is performed. Its enunciate can be found in many textbooks, as for example in the Cohen-Tannoudji [22]:

> If the measurement of physical quantity $\mathcal{A}$ on the system in the state $|\Psi\rangle$ gives result a_n, the state of the system immediately after the measurement is the normalized projection $\frac{P_n|\Psi\rangle}{\sqrt{\langle\Psi|P_n|\Psi\rangle}}$, of $|\Psi\rangle$ onto the eigensubspace associated with a_n

where a_n is the eigenvalue of the corresponding operator $\hat{A}$ which describes the physical quantity $\mathcal{A}$ and P_n is the projection operator onto the subspace $\mathcal{H}_n$ of the total Hilbert space $\mathcal{H}$. This means that once it is measured (and not before), the system gets fully projected to one of the eigenstates in a non-unitary evolution. After the collapse, the *new* wave packet evolves again according to the time-dependent Schrödinger equation until a new measurement is done.

This postulate requires a new non-unitary operator $\hat{A}$ (different from the Hamiltonian which is present in the Schrödinger equation) able to encapsulate all the interactions of the quantum systems with the rest of the particles. This operator is the only tool through which the possible results of a measurement can be determined. In principle

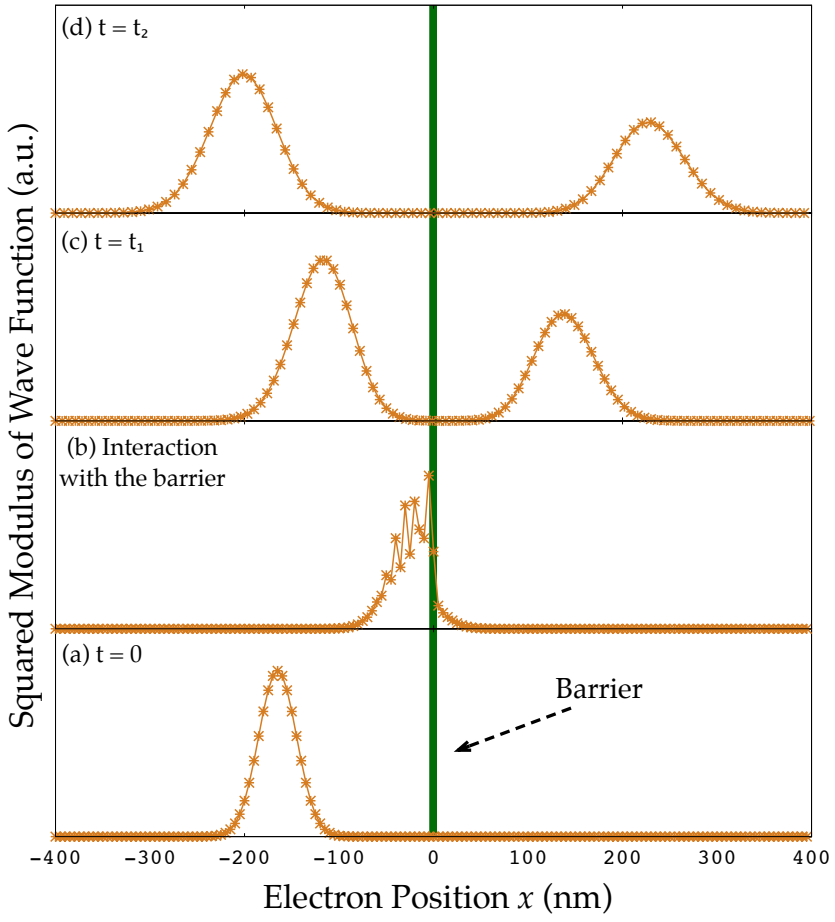

FIGURE 2.1: Evolution of the squared modulus of the wave function of an electron impinging on a tunneling barrier (green solid line). Four different times are plotted corresponding to (a) initial time, (b) the moment when the wave function interacts with the barrier, (c) the time t_1 when it occurs the first measurement and (d) time t_2 corresponding to the second measurement. At time t_1 and t_2, because of the unitary evolution, the electron can be detected at both sides of the barrier.

nothing is known about this operator except that it is a (hermitian $\hat{A} = \hat{A}^\dagger$) function whose (real) eigenvalues a_n of its spectral decomposition are the possible results of the measurement.

Why the collapse postulate is necessary within the orthodox quantum theory is briefly explained in the following example: Imagine to have a typical scenario in which an electron is impinging upon a partially transparent barrier. Electron transport through the barrier takes place by tunneling. Electron is either transmitted or reflected, but not both! [16, 24, 61] An electron is transmitted with a probability T, while is reflected with probability $R = 1 - T$. Each electron, after measurement, will appear randomly at the left or the right of the barrier. In the idealized situation just considered the electron wave function can be modeled as one dimensional, $\Psi(x, t)$, where x is the transport direction. In Figure 2.1 the (unitary) evolution of such wave function solution of Equation (1.1)

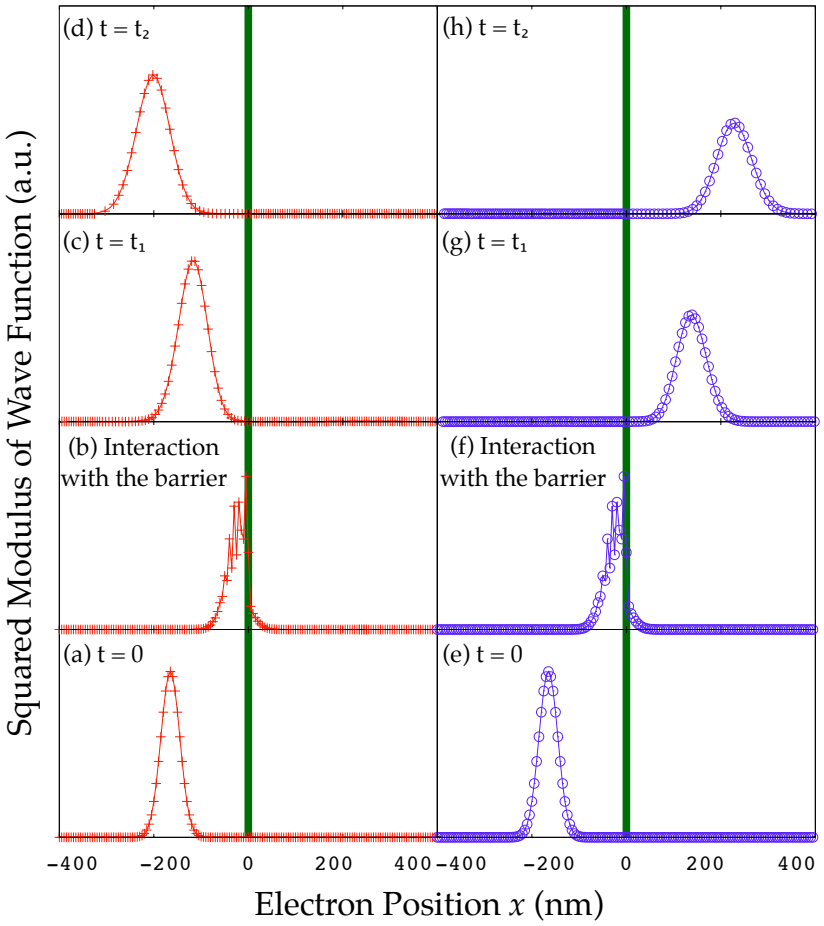

FIGURE 2.2: (a), (b), (c) and (d) Non unitary evolution of the wave function for a reflected electron detected at time t_1 on the left side. (e), (f), (g) and (h) Non unitary evolution of the wave function for a transmitted electron detected at time t_1 on the right side. Symbols are the same of Figure 2.1

is reported. In the one particle Schrödinger equation, it is assumed that the potential barrier $V(x)$ is centered at $x = 0$ and different from zero only for $-b/2 < x < b/2$, where b is the width of the barrier. In Figure 2.2 the evolution of the same electron, but undergoing a measurement at time $t = t_1$ after the interaction with the barrier, is plotted. For simplicity, in the present conceptual discussion a reasonable (but ad-hoc) operator is assumed. Such operator provides the following perturbation of the wave function. If the electron is *randomly* measured as a reflected electron at t_1, the transmitted part of the wave function is eliminated. This measuring process corresponds to Figures 2.2 (c) and (d) where only the reflected wave function survives after t_1. Equivalently, the measurement process associated to a transmitted electron corresponds to eliminating the reflected part, as seen in Figures 2.2 (g) and (h).[1]

[1]The measurement described in most textbooks is called "projective" (*strong*) measurement. There exists, for example, another type of measurement known as *weak* measurement, which is useful to describe situations where the effects of the apparatus on the measured system is just a small perturbation. The latter will be analyzed in details in Chapter 4.

Now, by comparing the evolutions of the wave functions in Figure 2.1 and Figure 2.2, it is obvious that the former is not enough to describe the evolution of the electron wave function undergoing to a measurement process. By looking at Figure 2.1, it could be the case that an electron found at time t_1 on the right (transmitted) can be found in a later time t_2 on the left as a reflected electron (see the evolution of the probability density in Figure 2.1). This sequence of probabilities is wrong. Experimental results confirm that once, say time t_1, the electron is detected at one side, in a later time t_2 it is always found at the same side. Then, one gets a very valuable lesson from the Copenhagen explanation: the (unitary) Schrödinger equation alone is not enough, it is necessary to introduce the collapse (postulate) of the wave function.

The collapse postulate ultimately implies the introduction of an operator $\hat{A}$, which varies from experiment to experiment, able to get the correct experimental results. It is important to say that over the years, physicists have identified the operators, by developing instincts on which are the effects of measurements on the wave function. There are scenarios (as the one depicted in Figure 2.2) where is quite obvious which operator is the *right* one. On the contrary, for example, when measuring the total (conduction plus displacement) current it is not at all obvious which are the relevant operators. Is this measurement process *continuous* or *instantaneous*? Does it provide a *strong* or a *weak* perturbation of the wave function? The answers to these questions are certainly not simple. Bohmian Mechanics provides a clear answer to these *technical* questions on how to find the *right* operator. In Chapter 3 this problem will be addressed in details; for the moment it is enough to focus only on the collapse of the wave function when system is undergoing a measurement. The following subsection is dedicated to expose the theoretical treatment of the collapse within Bohmian Mechanics.

2.1.2 Theoretical Treatment of Collapse with Bohmian Mechanics

In the following to facilitate the discussion, the simplest possible multi-particle system is taken: two spinless particles moving in one spatial dimension. Suppose that particle 1 is "the quantum system to be measured" and particle 2 represents the center of mass coordinate of the macroscopic pointer of a measuring device associated with quantum mechanical operator $\hat{A}$. Suppose the full system is initially in a product state

$$\Psi(x_1, x_2, 0^-) = \chi(x_1)\phi(x_2) \tag{2.1}$$

where $\chi(x_1)$ is an arbitrary linear combination of $\hat{A}$ eigenstates

$$\chi(x_1) = \sum_n c_n \chi_n(x_1) \quad \text{with} \quad \hat{A}\chi_n(x_1) = a_n \chi_n(x_1) \tag{2.2}$$

and $\phi(x_2)$ is a narrow gaussian packet centered at $x_2 = 0$ representing the measuring device in its *ready* state.

In a realistic description of a measurement, the "quantum system" and the "measuring device" would need to interact in a way that drives the wave function Ψ into a set of macroscopically-disjoint channels in the configuration space, with each channel corresponding to a distinct perceivable possible outcome of the measurement. In the context of the present simplified two-particle toy-model, the overall idea can be adequately captured by positing, for example, an impulsive interaction Hamiltonian like

$$\hat{H} = \lambda\, \delta(t) \hat{A} \hat{P}_{x_2} \tag{2.3}$$

where $\hat{p}_{x_2}$ is the momentum operator for the pointer.[2]

In the special case that the "quantum system" happens already to be in an eigenstate χ_m of $\hat{A}$, this interaction leaves the two-particle system in the state $\Psi(x_1, x_2, 0^+) = \chi_m(x_1)\phi(x_2 - \lambda a_m)$. In light of the quantum equilibrium hypothesis (Section 1.4), it thus follows that the the actual position X_2 of the pointer will, with unit probability, lie near the value λa_m indicating the pre-measurement (eigen)value a_m of $\hat{A}$. The pointer, in short, points to the value normally associated with $\hat{A}$ in this situation. In the general case, however, the interaction Hamiltonian takes the state in Equation (2.1) to

$$\Psi(x_1, x_2, 0^+) = \sum_n c_n \chi_n(x_1) \phi(x_2 - \lambda a_n) \tag{2.4}$$

in which the pointer is in an entangled superposition with the system. This final state reflects the notorious measurement problem of Ordinary Quantum Mechanics. But for the Bohmian theory, there is no problem: the empirically observed outcome is not to be found in the wave function, but instead in the actual final pointer position $X_2(0^+)$. Again in light of the *quantum equilibrium hypothesis*, this will, with probability $|c_n|^2$, be near the value λa_n indicating that the outcome of the measurement was a_n.[3]

[2] The interaction Hamiltonian in Equation (2.3) was firstly introduced by von Neumann [82] to describe exactly the measurement situation in orthodox quantum theory.

[3] It is assumed here that the spacing, $|\lambda(a_n - a_{n+1})|$, between adjacent possible pointer positions is small compared to the width, w, of ϕ.

Now consider how the conditional wave function for the "quantum system" evolves during the measurement. Prior to the interaction, when the joint two-particle wave function is still given by Equation (2.1), the conditional wave function for particle 1 is

$$\psi_1(x_1, 0^-) = \chi(x_1)\phi(x_2)\big|_{x_2=X_2(t)} \sim \sum_n c_n\chi_n(x_1). \tag{2.5}$$

This corresponds to the initial superposed wave function that would be attributed to the "quantum system" in Ordinary Quantum Mechanics. But the post-interaction Ψ, given by Equation (2.4), involves disjoint channels of support in the configuration space. The final pointer position, $X_2(0^+)$, will randomly (depending on the initial conditions) end up in the support of *just one* of these channels. That is, $\phi(x_2 - \lambda a_n)|_{x_2=X_2(0^+)}$ will (approximately) *vanish* for all n except the particular value, n', satisfying $X_2(0^+) \approx \lambda a_{n'}$, which corresponds to the actual result of the measurement. And so the post-interaction conditional wave function for particle 1 will be

$$\psi_1(x_1, 0^+) \;=\; \sum_n c_n\chi_n(x_1)\phi(x_2 - \lambda a_n)\big|_{x_2=X_2(0^+)} \sim \chi_{n'}(x_1). \tag{2.6}$$

That is, the interaction causes the initially superposed wave function for particle 1 to *collapse* to the appropriate eigenfunction (corresponding to the realized outcome of the measurement) even though the wave function of the joint system evolves exclusively unitarily according to the two-particle Schrödinger equation. Bohmian Mechanics thus *explains*, from the point of view of a theory in which all particles are treated in a fully uniform and fully quantum way, how the wave functions of sub-systems may evolve exactly as described (at the price of non-uniform treatment and additional *ad hoc* postulates) in Ordinary Quantum Mechanics.

It is interesting to analyze the same physical situation considered in Section 2.1.1 from the Bohmian perspective. An electron impinges on a tunneling barrier and its wave function is partially reflected, with probability R, and partially transmitted, with probability $T = 1 - R$. Again one of the most simple multi-particle system one can consider is composed of two degrees of freedom. The interaction can be provided by Equation (2.3) with the specification of the quantum mechanical operator $\hat{A}$ as follows:

$$\hat{A} \equiv A(x_1) = \Theta(x_1) - \Theta(-x_1), \tag{2.7}$$

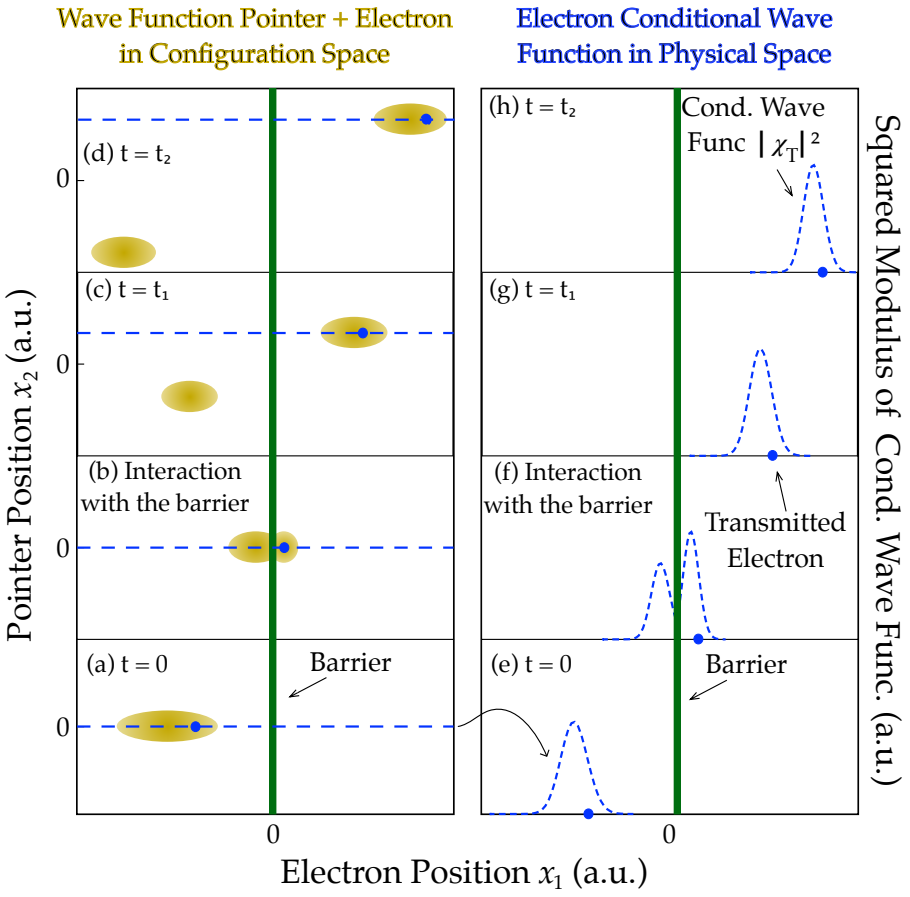

FIGURE 2.3: a), b), c) and d) Schematic evolution of the modulus square of the wave function $\Psi(x_1, x_2, t)$ of the many particle system in the configuration space. a) Time $t = 0$ the electron is located at the left of the barrier and the pointer is the "ready" state $x_2 = 0$. b) The electron suffer interaction with the barrier. c) and d) Interaction with the pointer shows up. The horizontal line corresponds to the cut in the configuration space which defines the conditional wave function of the electron.
e), f), g) and h) Evolution of the conditional wave function for a transmitted electron. It is clearly shown that at times $t = t_1$ and $t = t_2$ survives only the transmitted part of the electron wave function.

where $\Theta(x)$ is the Heaviside step function, thus providing an operator that attributes eigenvalue -1 if the particle is reflected and eigenvalue $+1$ if the particle is transmitted.

In Figure 2.3 it is considered an initial wave function of the complete system pointer *plus* electron at time $t = 0$ as a product of two single particle wave function as in Equation (2.1). The interaction Hamiltonian Equation (2.3) is activated from time $t = t_1$ till time $t = t_2$, namely the system is electron is measured in this interval of time. In this schematic example the measurement can be modeled as a projective measurement if the following relation is satisfied:

$$\lambda \Delta t \Delta a \gg 1, \tag{2.8}$$

where $\Delta t = t_2 - t_1$ is the interval of the interaction and $\Delta a = a_T - a_R$ is the difference between the two eigenvalues of the operator $A(x_1)$ in Equation (2.7). The wave function of the electron after the interaction with the barrier in Figure 2.3 can be written as:

$$\chi(x_1) = \chi_T(x_1) + \chi_R(x_1), \tag{2.9}$$

thus the action of the operator in Equation (2.3) on the eigenvectors of the wave function in Equation (2.9) is

$$\begin{aligned} A(x_1)\chi_T(x_1) &= a_T\chi_T(x_1) \quad \text{with} \quad a_T = +1, \\ A(x_1)\chi_R(x_1) &= a_R\chi_R(x_1) \quad \text{with} \quad a_R = -1. \end{aligned} \tag{2.10}$$

The complete wave function Ψ at time $t < t_1$ is

$$\Psi(x_1, x_2, t < t_1) = [\chi_T(x_1) + \chi_R(x_1)]\,\phi(x_2). \tag{2.11}$$

When the measurement is performed the wave function is shifted in the pointer direction x_2 forming an entangled superposition of the form

$$\Psi(x_1, x_2, t > t_1) = \chi_T(x_1)\phi_T(x_2) + \chi_R(x_1)\phi_R(x_2). \tag{2.12}$$

Because Bohmian Mechanics in addition to the wave function posited definite positions for the particle, one has that the electron position will be in one of the two channels in the configuration space depicted in Figure 2.3 c) and d). In that specific case the electron is transmitted thus the pointer moves up. It is important to underline how trivially the measurement is explained within Bohmian Mechanics, only a *channelized* (unitary) time-evolution of 2D wave function plus two Bohmian trajectories, one for the electron and another for the measuring apparatus are needed. Already at this level the "measurement problem" exposed in Chapter 1 has completely disappeared: because in each run of the experiment the electron is either transmitted or reflected (never both!), the pointer has always a definite position (moving up or moving down). Thus stepping back to the famous "cat paradox" problem, the paradox does not simply exist: the cat is always dead or alive!

It is now quite trivial to *derive* the collapse for the conditional wave function of the electron, in the case of Figure 2.3 one has:

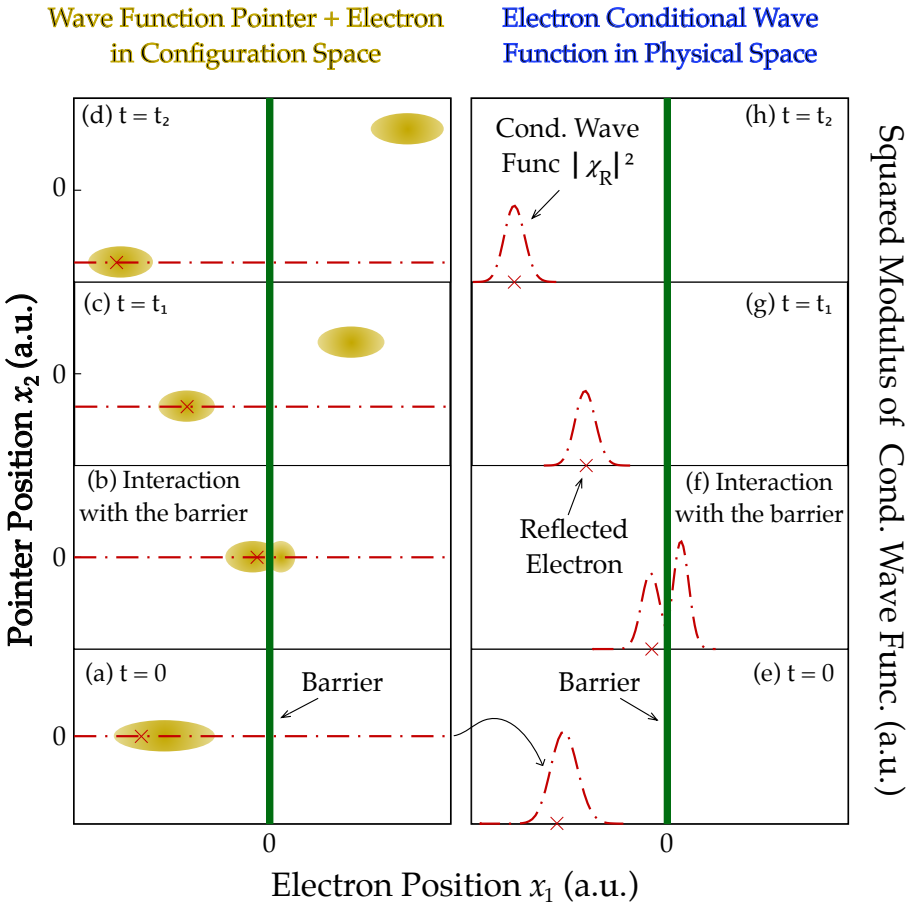

FIGURE 2.4: Same symbols of Figure 2.3. Because the electron is transmitted, in g) and h) only the reflected part of the conditional wave function of the electron survives.

$$\psi_1(x_1, t > t_1) = \chi_T(x_1,t)\phi_T(x_2,t) + \chi_R(x_1,t)\phi_R(x_2,t)\Big|_{x_2=X_2(t)} \sim \chi_T(x_1,t), \qquad (2.13)$$

obtaining only the transmitted part of the electron conditional wave function. The same analysis can be done for a different experiment where the electron is reflected, in Figure 2.4 is reported this case. One can observe that at time $t > t_1$ the interaction with the pointer provides that only the reflected part of the electron conditional wave function survives:

$$\psi_1(x_1, t > t_1) = \chi_T(x_1,t)\phi_T(x_2,t) + \chi_R(x_1,t)\phi_R(x_2,t)\Big|_{x_2=X_2(t)} \sim \chi_R(x_1,t). \qquad (2.14)$$

While the wave function provides only statistical information about the experimental results, with the help of the Bohmian trajectories, it has been possible to recover the

individual result of each experiment. In fact for each experiment the pointer of the detector is either moving up (corresponding to a transmitted electron) or moving down (reflected electron), while an ensemble of repeated experiments (where the initial positions of the particles, both the electron $X_1(0)$ and the detector $X_2(0)$, are selected according to the squared modulus of the wave function at the initial time $|\Psi(x_1, x_2, 0)|^2$) reproduce the same statistical results.

It is important to emphasize that, the collapse in Bohmian theory is naturally derived. Such a natural derivation of the collapse behavior demystifies the measurement process. The non-unitary evolution of the wave function of a measured system is achieved simply slicing the enlarged wave function (which includes the apparatus) in the configuration space. In fact, it is important to note that the evolution of $\psi_1(x_1, t)$ (the electron *conditional wave function*) is not unitary, even though the evolution of Ψ is. This characteristic will be further investigated in next Section analyzing the evolution of the conditional wave function in general situations. Finally, the reader will find a quite realistic numerical simulation for a "transmitted charge detector" in Section 3.1.

2.2 Dynamical Evolution of the Conditional Wave Function

Once explained how naturally the measurement problem and the postulate of the collapse of the wave function are derived in Bohmian Mechanics, it is possible to elaborate more on the other features of the conditional wave function. It is very interesting, for several reasons that will be clarified later, to have an independent dynamical evolution for the conditional wave function. In fact, looking at the definition given in Equation (1.4) the conditional wave function is given in term of the many-particle wave function of the entire system. Thus, although useful to derive the collapse postulate in a trivial way, it seems to have no other utility. This is not the case, it is possible to track out the dynamical evolution of each conditional wave function in terms of a Schrödinger-type equation. Investigating on this equation two important facts are realized: the conditional wave function has a general non-unitary and non-linear evolution (thus no surprise if it is able to reproduce the *collapse* behavior) and in such a situation in which the subsystem under investigation is decoupled from its environment it obeys the usual Schrödinger equation.

2.2.1 General Schrödinger-Type Equation for the Conditional Wave Function

A crucial point, underlying the behavior discussed in last Section, is that the conditional wave function (for, say, particle 1) depends on time in two ways, through the Schrödinger time-evolution of Ψ, and also through the time-evolution of X_2. For a simple two particle system, in a potential $V(x_1, x_2)$, it is possible to derive a Schrödinger-type equation for the conditional wave function of particle 1 as follows:

$$\begin{aligned} i\hbar\frac{\partial}{\partial t}\psi_1(x_1,t) &= i\hbar\frac{\partial\Psi(x_1,x_2,t)}{\partial t}\Big|_{x_2=X_2(t)} + i\hbar\frac{dX_2}{dt}\frac{\partial\Psi(x_1,x_2,t)}{\partial x_2}\Big|_{x_2=X_2(t)} \\ &= -\frac{\hbar^2}{2m_1}\frac{\partial^2\psi_1(x_1,t)}{\partial x^2} + V\left[x_1, X_2(t), t\right]\psi_1(x_1,t) \\ &\quad + i\hbar\frac{dX_2}{dt}\psi_1'(x_1,t) - \frac{\hbar^2}{2m_2}\psi_1''(x_1,t), \end{aligned} \tag{2.15}$$

where it has been defined

$$\psi_1'(x_1,t) = \frac{\partial\Psi(x_1,x_2,t)}{\partial x_2}\Big|_{x_2=X_2(t)} \tag{2.16}$$

and

$$\psi_1''(x_1,t) = \frac{\partial^2\Psi(x_1,x_2,t)}{\partial x_2^2}\Big|_{x_2=X_2(t)}. \tag{2.17}$$

The Schrödinger-type equation for ψ_1 can thus be re-written as

$$i\hbar\frac{\partial\psi_1}{\partial t} = -\frac{\hbar^2}{2m_1}\frac{\partial^2\psi_1}{\partial x_1^2} + V_1^{\text{eff}}(x_1,t)\psi_1, \tag{2.18}$$

where

$$V_1^{\text{eff}}(x_1,t) = V[x_1, X_2(t), t] + A_1(x_1,t) + B_1(x_1,t) \tag{2.19}$$

is the *conditional potential* $V[x_1, X_2(t), t]$ felt by particle 1 plus two additional terms:

$$A_1(x_1,t) = i\hbar\frac{dX_2}{dt}\frac{\psi_1'(x_1,t)}{\psi_1(x_1,t)} \tag{2.20}$$

and

$$B_1(x_1,t) = -\frac{\hbar^2}{2m_2}\frac{\psi_1''(x_1,t)}{\psi_1(x_1,t)}. \tag{2.21}$$

It is important to stress that the terms A_1 and B_1 in Equations (2.20)-(2.21) depend on $\psi_1(x_1,t)$ itself, making the whole equation non-linear. A different path for the same deduction of the $A_1(x_1,t)$ and $B_1(x_1,t)$ terms can be found in [67]. These terms, which can be complex (with real part and imaginary part), have units of energy. Then, since V_1^{eff} is also complex (the pseudo-Hamiltonian is not hermitian), the norm of the conditional wave function solution of (2.18) is not conserved. This explains why such conditional wave functions have no problem in describing the measurement *collapse* mentioned in Section 2.1.2.

At this point, it is worthwhile to underline the interplay between conditional wave functions and Bohmian trajectories. Certainly, the trajectory $X_1(t)$ is influenced by the conditional wave functions $\psi_1(x,t)$. Nothing relevant here. However, the trajectory $X_1(t)$ does also have an influence on $\psi_2(x_1,t)$. The trajectory $X_1(t)$ modifies $\psi_2(x_2,t)$ through V_2^{eff}. Then, $X_2(t)$ is affected and it modifies V_1^{eff}, affecting $\psi_1(x_1,t)$.

2.2.2 Conditional Wave Function for Separable Quantum Systems

In the special case of a factorizable (i.e., non-entangled) two-particle wave function, $\Psi(x_1,x_2,t) = \alpha(x_1,t)\beta(x_2,t)$, one has

$$\psi_1'(x_1,t) = \alpha(x_1,t)\frac{\partial\beta}{\partial x_2}\Big|_{x_2=X_2(t)}, \tag{2.22}$$

so that

$$A_1(t) = i\hbar\frac{dX_2}{dt}\frac{\partial\beta/\partial x_2}{\beta}\Big|_{x_2=X_2(t)} \tag{2.23}$$

is independent of x_1. Similarly,

$$\psi_1''(x,t) = \alpha(x,t)\frac{\partial^2\beta}{\partial x_2^2}\Big|_{x_2=X_2(t)}, \tag{2.24}$$

so that

$$B_1(t) = -\frac{\hbar^2}{2m_2}\frac{\partial^2\beta/\partial x_2^2}{\beta}\Big|_{x_2=X_2(t)} \tag{2.25}$$

is also independent of x_1.

Thus, whenever two particles are un-entangled, the only x_1-dependence in the effective potential V_1^{eff} arises from the conditional potential, $V[x_1, X_2(t), t]$ (and, of course, similarly for the other particle). The Schrödinger-like equations describing the time-evolution of the conditional wave functions thus become *linear*. They remain in general non-unitary, in so far as A_1 and B_1 will still be (complex!) functions of time. But in this case, these terms simply give rise to an overall multiplicative time-dependent constant factor which cancels out anyway in the guidance formula, Equation (1.5). Thus the terms might as well simply be dropped, in which case the individual single-particle wave functions will obey precisely the usual single-particle Schrödinger equations.

So far, it has been shown only the admittedly unremarkable fact that in a non-entangled two-particle system, the Bohmian conditional wave functions, which are exactly equivalent to the wave functions that would be attributed to the two particles in this situation by Ordinary Quantum Mechanics, evolve just as Ordinary Quantum Mechanics says. Namely: each one obeys its own autonomous one-particle Schrödinger equation. The appearance of the conditional potential is interesting, in the sense that for genuinely interacting particles this gives a particular, uniquely-Bohmian candidate for the potential energy field *experienced by* each particle separately. However, any genuine interactions between the particles will take an initially un-entangled state into an entangled one, thus removing the context that implied that each conditional wave function should evolve according to its own autonomous Schrödinger equation! So there is no free lunch here. If the particles interact at all (or happen to begin in an entangled state) then it is not possible to reproduce the *exact* Bohmian dynamics by looking exclusively at the conditional wave functions for separable systems. But there are physical situations in which only the conditional potential $V[x_1, X_2(t), t]$ is enough to well reproduce the particle trajectories. Even more, in such situations, the conditional wave function becomes an indispensable tool to deal with many-particle problems, providing an algorithm to solve the many-particle Schrödinger equation, this is the main subject of the following Section.

2.3 Numerical Algorithm for Solving Many-Body Problems with the Conditional Wave Function

So far the conditional wave function has been used in a simple two-particle toy model: Its use has been fruitful to solve conceptual problems such as the “cat paradox” and the

"collapse postulate". Nevertheless, it is interesting to go beyond a simple two-particle model and see whether with the help of the conditional wave function it is possible to solve many-particle quantum problems. In fact, it is well known that the many-particle Schrödinger equation (1.1) is unsolvable for more than $N > 10$ particles, with nowadays computer capabilities, because it requires to compute the wave function $\Psi(\mathbf{x}, t)$ in the N-dimensional configuration space.[4] Already in 1929, Dirac writes

> The general theory of quantum mechanics is now almost complete. The underlying physical laws necessary for the mathematical theory of a large part of physics and the entire chemistry are thus completely known, and the difficulty is only that the exact application of these laws leads to equations much too complicated to be soluble.[27]

and later Born rephrases:

> It would indeed be remarkable if Nature fortified herself against further advances in knowledge behind the analytical difficulties of the many-body problem.[20]

underling the impossibility of solving the many-particle Schrödinger equation.
In the following, a practical algorithm to solve the many-particle Schrödinger equation with the use of the conditional wave function will be presented. Before discussing in details the numerical procedure for a general system of N interacting particles in Section 2.3.2, the fundamental approximations required to implement the algorithm are explained in Section 2.3.1 with an example for a two particle system interacting through a non separable potential.

2.3.1 The Small Entanglement Approximation

It is very interesting to use the conditional wave function in general scenarios. Nevertheless, the discussion in Section 2.2.2 suggests that if, in some sense, the amount of entanglement remains sufficiently small, it might be possible to arrive at a reasonably accurate approximation to the exact Bohmian dynamics by dropping A and B terms and treating each particle as a (Bohmian) quantum system moving under the influence of the conditional potential defined through the other particle (Bohmian) position.

[4] Assume, for example, a system with $N = 10$ particles confined in a 1D region of $10nm$, discretized with a spatial step of $\Delta x = 0.1$ nm, a grid of 100 points for each dimension is obtained. Then, the total number of points in the configuration space for the 10 particles is $100^{10} = 10^{20}$. Using 4 bytes (32 bits) to store the complex value of the wave function at each grid point, the information contained in a 10-particle wave function would require more than $3 \cdot 10^8$ Terabytes (TB).

This suggests a kind of first-order approximation for the potential developed at the end Section 2.2.1: for each particle it is retained the conditional potential term in V_i^{eff} and set the other terms to zero in Equation (2.19)

$$V_i^{\text{eff}} \approx V(x_1, x_2, t)\Big|_{x_i=x \text{ and } x_n=X_n(t)\forall n\neq i}. \tag{2.26}$$

On the grounds that this should work perfectly when there is no entanglement, this approach can be called the "small entanglement approximation" or SEA. But note that there is no clear *a priori* reason to expect the SEA to work well when there is even just a little entanglement. It could be, for example, that as soon as any entanglement develops, the small entanglement approximation breaks down completely, giving particle trajectories that are wildly unphysical and/or blatantly different from those of ordinary Bohmian mechanics. Computationally speaking, it is significantly easier to track two functions of a spatial coordinate, than to track a single function of two spatial coordinates. Moreover, the computational superiority only increases with the number of particles: for N particles and a spatial grid of M points, numerically solving the full N-particle Schrödinger equation requires tracking the value of Ψ at M^N points; whereas numerically solving N coupled single-particle Schrödinger equations requires tracking values at only $M \times N$ points. Thus, the approach suggested here holds real promise for those interested in efficient many-body calculations.

2.3.1.1 Numerical Example in the Small Entanglement Approximation: Limitation and Validity

As a first example, it is interesting to study the dynamical evolution of the conditional wave functions, using the *small entanglement approximation*, in the following situation, consider two particles in 1D interaction through the "Coulomb-like" potential:

$$V_C(x_1, x_2) = C \cdot \frac{q^2}{4\pi\epsilon_r\epsilon_0} \frac{1}{\sqrt{(x_1 - x_2)^2 + a_C^2}} f(x_1, x_2), \tag{2.27}$$

with $\epsilon_r = 11.6$ and ϵ_0 being the free space dielectric constant. To avoid numerical irrelevant complications, the parameter $a_C = 1.2\ nm$ avoids the divergence character of the Coulomb potential when $x_1 = x_2$. The function $f(x_1, x_2) = exp(-(x_1 - x_2)^2/\sigma_C)$, with $\sigma_C = 15\ nm$, allows to define the Coulomb interaction only when the particles are at a relative distance less then approximatively 60 nm. These conditions mimic the solution of the 3D Poisson equation in a mesoscopic device with screening and with an active region of 60 nm [67]. The parameter C in Equation (2.27) is a-dimensional and

it will be tuned in order to increase (or decrease) the amount of interaction. As initial two-paticle wave function a product state $\Psi(x_1, x_2, 0) = \phi_a(x_1)\phi_b(x_2)$ of two gaussian wave packets is chosen. The wave packets ϕ_a and ϕ_b have opposite central momentums $k_a = -k_b$ and central positions $x_a = -x_b$. The Schrödinger equation for the two-particle system implies the following Schrödinger-type equation for the one-particle wave function of particle 1:

$$\begin{aligned} i\hbar\frac{\partial\psi_1(x_1,t)}{\partial t} &= \left[-\frac{\hbar^2}{2m_1}\frac{\partial^2}{\partial x_1^2} + V_C(x_1, X_2(t))\right]\psi_1(x_1,t) \\ &- \frac{\hbar^2}{2m_2}\frac{\partial^2\Psi(x_1,x_2,t)}{\partial x_2^2}\Big|_{x_2=X_2(t)} + i\hbar\frac{dX_2(t)}{dt}\frac{\partial\Psi(x_1,x_2,t)}{\partial x_2}\Big|_{x_2=X_2(t)} \end{aligned} \tag{2.28}$$

and for particle 2:

$$\begin{aligned} i\hbar\frac{\partial\psi_2(x_2,t)}{\partial t} &= \left[-\frac{\hbar^2}{2m_2}\frac{\partial^2}{\partial x_2^2} + V_C(X_1(t), x_2)\right]\psi_2(x_2,t) \\ &- \frac{\hbar^2}{2m_1}\frac{\partial^2\Psi(x_1,x_2,t)}{\partial x_1^2}\Big|_{x_1=X_1(t)} + i\hbar\frac{dX_1(t)}{dt}\frac{\partial\Psi(x_1,x_2,t)}{\partial x_1}\Big|_{x_1=X_1(t)} \end{aligned} \tag{2.29}$$

The mass are $m_1 = m_2 \equiv 0.067 * m_0$, where m_0 is the free electron mass. Under the *small entanglement approximation*, these exact equations reduce to the pair:

$$i\hbar\frac{\partial\psi_1(x_1,t)}{\partial t} = \left[-\frac{\hbar^2}{2m_1}\frac{\partial^2}{\partial x_1^2} + V_C(x_1, X_2(t))\right]\psi_1(x_1,t), \tag{2.30}$$

$$i\hbar\frac{\partial\psi_2(x_2,t)}{\partial t} = \left[-\frac{\hbar^2}{2m_2}\frac{\partial^2}{\partial x_2^2} + V_C(X_1(t), x_2)\right]\psi_2(x_2,t). \tag{2.31}$$

Note that the Schrödinger type equation for the conditional wave function of particle 1 in the *small entanglement approximation* has the conditional potential $V_C(x_1, X_2(t)$ which depends explicitly on the actual position of particle 2 (the same happens for the conditional wave function of particle 2). This implies that this approximation already embodies a possible interchange of energy, for example, between the two particles. As already said, there is no reason to expect that this approximation will give good results even when the entanglement is very small. In order to quantify the discrepancy of the small entanglement approximation from the exact 2D solution of the problem it is convenient to define the following quantity:

$$\text{Deviation}(t) = \lim_{M\to\infty} \frac{1}{M} \sum_{\alpha=1}^{M} \sqrt{(X_1^{1D}(t)^\alpha - X_1^{2D}(t)^\alpha)^2 + (X_2^{1D}(t)^\alpha - X_2^{2D}(t)^\alpha)^2} \quad (2.32)$$

where X^{1D}s are the trajectories calculated with the 1D solution in the small entanglement approximation, X^{2D}s are the exact solution of the two particle Schrödinger equation and the index α indicates the different run of the experiment. The initial position of the Bohmian trajectories are chosen according to the *quantum equilibrium hypothesis*, i.e. $|\Psi(x_1, x_2, 0)|^2$.

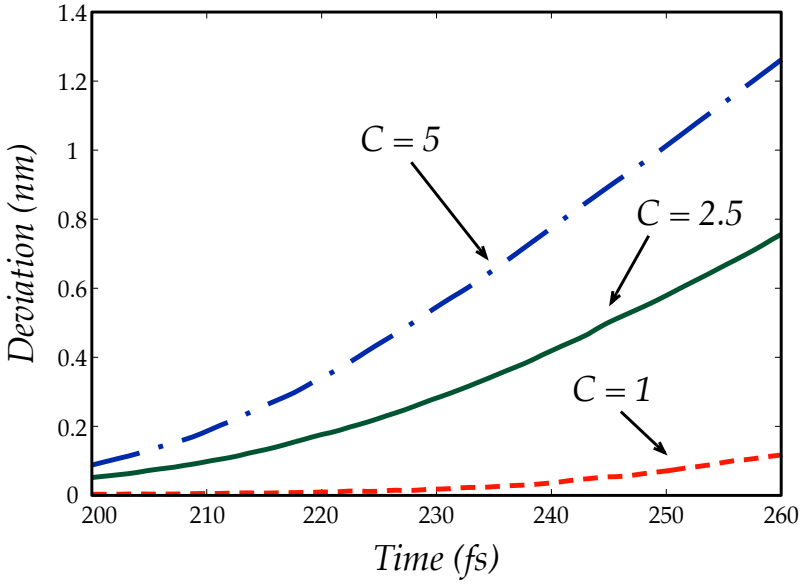

FIGURE 2.5: Deviation from the exact 2D trajectories of the 1D approximate solution calculated from Equation (2.32) for $C = 1$ (red dashed line), $C = 2.5$ (green solid line) and $C = 5$ (blue dashed dotted line) in Equation (2.27).

In Figure 2.5 the deviation defined in Equation (2.32) is plotted in function of time for three different values of the parameter C in Equation (2.27). Firstly, one can note that for $C = 1$ the SEA gives good results: thus as expected the *small entanglement approximation* is accurate whenever the entanglement is not relevant. It is also clear that the deviation increase as time grows. In addition, for larger values of C the deviation increase. In order to investigate better this point, in Figure 2.6 the deviation at time $t = 260\ fs$ of the simulation is reported for different values of C in Equation (2.27). It is shown that for small values of C the deviation is negligible (as expected from the discussion in Section 2.2.2), while is bigger for larger values of C. From Figure 2.6 it is possible to identify three different regions: for $C = 0$ till $C \approx 7.5$ the deviation increases, for $C > 7.5$ till $C \approx 20$ decreases and for $C > 20$ increases again.

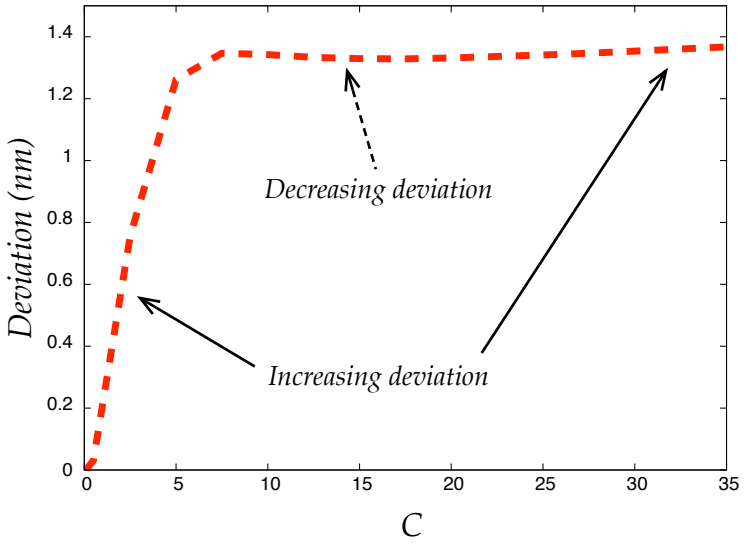

FIGURE 2.6: Deviation from the exact 2D trajectories of the 1D approximate solution calculated from Equation (2.32) at time $t = 260\ fs$ in function of the parameter C in Equation (2.27).

2.3.2 A Practical Algorithm for Solving the Many-Particle Schrödinger Equation

The previous numerical example suggests that the use of the conditional wave function, in the *small entanglement approximation*, can be an original tool in order to deal with the many-body quantum systems. The ideas exposed in the following were proposed by X. Oriols and they can be found for example in Refs. [67, 68]. Consider a general quantum system composed of N particles interacting through a potential V. The generalization of the dynamics, reported in Section 2.2.1, for the single-particle conditional wave function of particle 1, $\psi_1(x_1,t)$, for a system of N interacting particles reads:

$$i\hbar\frac{\partial\psi_1(x_1,t)}{\partial t} = \Big\{ -\frac{\hbar^2}{2m}\nabla_1^2 + V_1(x_1,\mathbf{X}_{N-1}(t),t) + A_1(x_1,\mathbf{X}_{N-1}(t),t) + iB_1(x_1,\mathbf{X}_{N-1}(t),t)\Big\}\psi_1(x_1,t). \tag{2.33}$$

As already said the numerical values of the potentials A_1 and B_1 are in principle unknown and in order to use the previous equation they need some educated guesses.[5] On the other hand, the total potential energy among the N electrons that appears in Equation (1.1), has been divided into two parts:

[5]In the present Section a variable in the configuration space is denoted with a bold letter as always and subscript to indicate the numbers of degrees of freedom considered.

$$\begin{aligned} V(x_1, \mathbf{X}_{N-1}(t), t) &= V_1(x_1, \mathbf{X}_{N-1}(t), t) + \\ &+ V_{N-1}(\mathbf{X}_{N-1}(t), t). \end{aligned} \tag{2.34}$$

The term $V_1(x_1, \mathbf{X}_{N-1}(t), t)$ can be any type of many-particle potential defined in the position-representation, in particular it can include short-range and long-range Coulomb interactions. The other term $V_{N-1}(\mathbf{X}_{N-1}(t), t)$ in Equation (2.34) without any dependence on x_1 is contained in the coupling potential A_1 in Equation (2.33). The same procedure can be done for the rest of the $N-1$ particles, for example for particle 2 the positions of particles $1, 3, ..., N$ is fixed obtaining the analogous of Equation (2.33) for $\psi_2(x_2, t)$. From a practical point of view, all quantum trajectories $\mathbf{X}_N(t)$ have to be computed simultaneously. In order to gather all the above concepts, hereafter a practical computation is discussed with conditional wave functions by detailing a sequential procedure:

1. At the initial time $t = 0$, fix the initial position of all i-particles, $X_i(0)$, according to the initial probability distribution ($|\Psi(\mathbf{x}_N, 0)|^2$), and their associated single-particle wave function $\psi_i(x_i, 0)$.

2. From all particle positions, compute the exact value of the potential $V_i(x_i, \mathbf{X}_{N-1}(0), 0)$ for each particle. An approximation for the terms A_i and B_i is required at this point. (In the *small entanglement approximation* they are simply set equal to zero, but there can be other possibilities.)

3. Solve each single-particle Schrödinger equation, Equation (2.33), from $t = 0$ till $t = dt$.

4. From the knowledge of the single-particle wave function $\psi_i(x_i, dt)$, it is possible to compute the new velocities $v_i(dt)$ for each i-particle (see Equation (1.5)).

5. With the previous velocity, compute the new position of each i-particle as $X_i(dt) = X_i(0) + v_i(dt)dt$.

6. Finally, with the set of new positions and wave functions, repeat the whole procedure (steps 1 till 5) for another infinitesimal time dt till the total simulation time is finished.

The advantage of the above algorithm using Equation (2.33) instead of the many-particle Schrödinger equation (Equation (1.1)) is that, in order to find approximate trajectories, $X_i(t)$, it is not needed to evaluate the wave function and potential energies in

the whole configuration space, but only over a smaller number of configuration points, $\{x_i, \mathbf{X}_{N-1}(t)\}$, associated with those trajectories defining the highest probabilities according to $|\Psi(\mathbf{x}_N, t)|^2$.

For spinless electrons, the exchange interaction is naturally included in Equation (2.33) through the terms A_i and B_i. Due to the Pauli exclusion principle, the modulus of the wave function tends to zero, $|\psi(x_i, \mathbf{X}_{N-1}(t), t)| \to 0$, in any neighborhood of x_i such that $|x_i - \mathbf{X}_{N-1}(t)| \to 0$. Thus, both terms, $A_i(x_i, \mathbf{X}_{N-1}(t), t)$ and $B_i(x_i, \mathbf{X}_{N-1}(t), t)$, have asymptotes at $x_i \to \mathbf{X}_{N-1}(t)$ that *repel* the $i-$ particle from other electrons. However, in order to exactly compute the terms A_i and B_i one has to know the total wave function, which is in principle unknown. There are however a few ways to introduce the symmetry of the wave function without dealing directly with these two coupling terms [3, 4, 67]. The presented schematic algorithm is the base of a quantum transport simulator named BITLLES.[6]

In Appendix A the reader can found preliminary results for going beyond the numerical scheme in the *small entanglement approximation* just presented here.

[6]BITLLES is the acronym of *Bohmian Interacting Transport for non-equiLibrium eLEctronic Structures*. See the website *http://europe.uab.es/bitlles*

Chapter 3

On the Measurement of the Total Current in Quantum Devices

The present Chapter is devoted to investigate the characteristics and functionality of Quantum Devices. In particular the conditional wave function, introduced in the previous Chapter, will be used extensively. One of the problems of describing Quantum Devices resides on characterizing its interactions with an external (Big!) system such as an apparatus. With Quantum Device is generally denoted an electronic system working in the quantum regime: it seems obvious, but the crucial point is exactly that every physical quantity (such as for example the mean current, noise etc.) is defined in the same way that for classical electronic devices but the quantity involved obeys quantum rules. The necessity of decreasing the dimensions of the devices in the future years has been established by the International Technology Roadmap for Semiconductors, thus reaching in the near future to work with devices in deep quantum regimes and in particular working at high frequency. While for classical and semiclassical devices there exist good simulation tools for studying the behavior of such systems there no exist the same for Quantum Devices in high frequency regime. In the following of the present Chapter, two models of apparatus will be presented.

The structure of the present Chapter is the following: in Section 3.1 and in Section 3.2 two different apparatus' models will be presented. The first model, called *transmitted charge detector* will be analyzed in Section 3.1.1 with the derivation of a Schrödinger equation for one electron in the active region of a device and for the center of mass of a macroscopic apparatus. Then, in Section 3.1.2 the exact Bohmian velocity, for the pointer and the apparatus will be computed, while Section 3.1.3 is devoted to the computation of the total current for an electron in the active region of a device. Section 3.1.4

and Section 3.1.5 conclude the first model presenting the numerical simulation. Within this model, a first study of the influence of the apparatus on the measured system will be provided. The second model of apparatus, able to measure the total electrical current at high frequency, will be studied in Section 3.2. In particular, as it will be seen, this second model uses the notion of the conditional wave function to study the interaction between the measured electron and the registering apparatus.

3.1 Transmitted Charge Detector

As already mentioned, Bohmian Mechanics does not differentiate between measuring and non-measuring evolutions, everything is treated quantum mechanically even the "classical" measuring apparatus [29, 35, 68]. Consider an apparatus composed by K degrees of freedom, i.e. particles that form the pointer of a measuring apparatus (for example, the ammeter), identified by $\mathbf{y} = \{y_1, ..., y_K\}$. Then, the Bohmian positions of these degrees of freedom $\mathbf{Y}(t) = \{Y_1(t), ..., Y_K(t)\}$ (when a particular initial position is selected according to the *quantum equilibrium hypothesis*), specifies the output of the measurement at a particular time t without ambiguity. Because of the pointer, it is mandatory to deal with a wave function $\Upsilon(\mathbf{x}, \mathbf{y}, t)$ whose equation is the Schrödinger equation (in the enlarged configuration space) completely analogous to Equation (1.1). The pointer positions $\mathbf{Y}(t)$ and the system positions $\mathbf{X}(t)$ move according to their equations of motions equivalent to Equation (1.2). The (Bohmian) positions of a *good* pointer $\mathbf{Y}(t)$ are supposed to be correlated with the system position $\mathbf{X}(t)$. As already said, the stochasticity nature of the quantum measurement is recovered here because in the experimental setup the initial Bohmian positions $\mathbf{Y}(t = 0)$ and $\mathbf{X}(t = 0)$ have to be selected according to the quantum equilibrium condition. The Bohmian explanation of the measurement process has, however, two technical difficulties:

1. The first difficulty appears because one has to specify which is the Hamiltonian that determines the evolution of the system plus apparatus. This difficulty is similar to specifying which is the operator that provides good information about the measuring process in the *Orthodox* Quantum Mechanics.

2. The second difficulty is related to the computational limitations that one has when solving the many-particle Schrödinger equation. The Schrödinger equation with the addition of the pointer degrees of freedom is most of the times unsolvable. This technical difficulty is not present when using operators because they act only on the system wave function.

3.1.1 Specifying the System plus Apparatus Schrödinger Equation

The idea of including the pointer as an additional degree of freedom in the Schrödinger equation was already proposed by von Neumann in 1932 within Orthodox Quantum Mechanics, when trying to provide a macroscopic explanation of the *collapse* of the wave function. The interaction Hamiltonian considered here is the same introduced in Ref. [82]:

$$H_{int} = -i\hbar\lambda A(\mathbf{x}) \sum_{j=1}^{K} \frac{\partial}{\partial y_j}, \tag{3.1}$$

where, as in Section 2.1, A represents the property of the measured system. The sum over $j = 1, ..., K$ represents the interaction with each single degree of freedom of the pointer. Then the general Schrödinger equation one is interested to solve is

$$\begin{aligned} i\hbar\frac{\partial \Upsilon(\mathbf{x},\mathbf{y},t)}{\partial t} &= \Big(\sum_{k=1}^{N} -\frac{\hbar^2}{2m^*}\frac{\partial^2}{\partial x_k^2} + \sum_{j=1}^{K} -\frac{\hbar^2}{2m}\frac{\partial^2}{\partial y_j^2} + V(\mathbf{x},t) + \\ &- i\hbar\lambda A(\mathbf{x}) \sum_{j=1}^{K} \frac{\partial}{\partial y_j}\Big)\Upsilon(\mathbf{x},\mathbf{y},t) \end{aligned} \tag{3.2}$$

where m^* is the effective mass the electron and m is the mass of a particle composing the pointer.

At the end of this subsection the aim will be of reducing the enormous complexity of the problem of $N + K$ degrees of freedom in $N + 1$ degrees of freedom: N for the electrons in the active region of the device and only one for the pointer. Then only one electron in the device will be considered to carry out the simulations.

First of all, consider the center of mass ξ of the pointer degrees of freedom:

$$\xi = \sum_{j=1}^{K} y_j \frac{m}{M} = \sum_{j=1}^{K} y_j \frac{1}{K} \tag{3.3}$$

with M the sum of the mass of all particles, and the relative positions ξ_j for $j = 2, .., K$ as:

$$\begin{aligned} \xi_2 &= y_1 - y_2 \\ \xi_3 &= y_1 - y_3 \\ &\cdots \\ \xi_K &= y_1 - y_K. \end{aligned} \tag{3.4}$$

Therefore, it is possible to make a change of variables from $\Upsilon(\mathbf{x}, \mathbf{y}, t)$ to $\Upsilon(\mathbf{x}, \boldsymbol{\xi}, t)$. Then the spatial derivatives are computed from the chain rule:

$$\frac{\partial \Upsilon(\mathbf{x}, \mathbf{y}, t)}{\partial y_i} = \frac{\partial \Upsilon(\mathbf{x}, \boldsymbol{\xi}, t)}{\partial \xi} \frac{\partial \xi}{\partial y_i} + \sum_{j=2}^{K} \frac{\partial \Upsilon(\mathbf{x}, \boldsymbol{\xi}, t)}{\partial \xi_j} \frac{\partial \xi_j}{\partial y_i}. \tag{3.5}$$

In particular, using Equation (3.3) and Equation (3.4), it is obtained for y_1:

$$\frac{\partial \Upsilon(\mathbf{x}, \mathbf{y}, t)}{\partial y_1} = \frac{\partial \Upsilon(\mathbf{x}, \boldsymbol{\xi}, t)}{\partial \xi} \frac{1}{K} + \sum_{j=2}^{K} \frac{\partial \Upsilon(\mathbf{x}, \boldsymbol{\xi}, t)}{\partial \xi_j} \tag{3.6}$$

and for $y_i \neq y_1$:

$$\frac{\partial \Upsilon(\mathbf{x}, \mathbf{y}, t)}{\partial y_i} = \frac{\partial \Upsilon(\mathbf{x}, \boldsymbol{\xi}, t)}{\partial \xi} \frac{1}{K} - \frac{\partial \Upsilon(\mathbf{x}, \boldsymbol{\xi}, t)}{\partial \xi_i}. \tag{3.7}$$

In conclusion the final result is:

$$\sum_{j=1}^{K} \frac{\partial \Upsilon(\mathbf{x}, \boldsymbol{\xi}, t)}{\partial y_j} = \frac{\partial \Upsilon(\mathbf{x}, \boldsymbol{\xi}, t)}{\partial \xi}, \tag{3.8}$$

meaning that the total momentum of the $j = 1, ..., K$ particles is equal to the momentum of the center of masses. Repeating the previous procedure for the kinetic energy, it is easy to realize that for the spatial derivative of y_1 one gets:

$$\frac{\partial^2 \Upsilon(\mathbf{x}, \mathbf{y}, t)}{\partial y_1^2} = \frac{\partial^2 \Upsilon(\mathbf{x}, \boldsymbol{\xi}, t)}{\partial \xi^2} \frac{1}{K^2} + 2 \sum_{j=2}^{K} \frac{\partial^2 \Upsilon(\mathbf{x}, \boldsymbol{\xi}, t)}{\partial \xi_j \partial \xi} \frac{1}{K} + \sum_{j=2}^{K} \sum_{h=2}^{K} \frac{\partial^2 \Upsilon(\mathbf{x}, \boldsymbol{\xi}, t)}{\partial \xi_j \partial \xi_h} \tag{3.9}$$

and for $y_i \neq y_1$ one gets:

$$\frac{\partial^2 \Upsilon(\mathbf{x},\mathbf{y},t)}{\partial y_i^2} = \frac{1}{K^2}\frac{\partial^2 \Upsilon(\mathbf{x},\boldsymbol{\xi},t)}{\partial \xi^2} - 2\frac{\partial^2 \Upsilon(\mathbf{x},\boldsymbol{\xi},t)}{\partial \xi_i \partial \xi}\frac{1}{K} + \frac{\partial^2 \Upsilon(\mathbf{x},\boldsymbol{\xi},t)}{\partial \xi_i^2}. \tag{3.10}$$

Then, concluding that:

$$\sum_{i=1}^{K}\frac{\partial^2 \Upsilon(\mathbf{x},\mathbf{y},t)}{\partial y_i^2} = \frac{1}{K}\frac{\partial^2 \Upsilon(\mathbf{x},\boldsymbol{\xi},t)}{\partial \xi^2} + \sum_{j=2}^{K}\sum_{h=2}^{K}\frac{\partial^2 \Upsilon(\mathbf{x},\boldsymbol{\xi},t)}{\partial \xi_j \partial \xi_h} + \sum_{l=2}^{K}\frac{\partial^2 \Upsilon(\mathbf{x},\boldsymbol{\xi},t)}{\partial \xi_l^2}. \tag{3.11}$$

Equation (3.2) after the change of variables becomes:

$$\begin{aligned} i\hbar\frac{\partial \Upsilon(\mathbf{x},\boldsymbol{\xi},t)}{\partial t} &= \Big(\sum_{k=1}^{N} -\frac{\hbar^2}{2m^*}\frac{\partial^2}{\partial x_k^2} + \sum_{j=2}^{K} -\frac{\hbar^2}{2m}\frac{\partial^2}{\partial \xi_j^2} + V(\mathbf{x},t) + \\ &+ \sum_{l=2}^{K}\sum_{j=2}^{K} -\frac{\hbar^2}{2m}\frac{\partial^2}{\partial \xi_l \partial \xi_j} - \frac{\hbar^2}{2M}\frac{\partial^2}{\partial \xi^2} - i\hbar\lambda A(\mathbf{x})\frac{\partial}{\partial \xi}\Big)\Upsilon(\mathbf{x},\boldsymbol{\xi},t). \end{aligned} \tag{3.12}$$

In the Hamiltonian of Equation (3.12) the degrees of freedom $\{\mathbf{x},\xi\}$ and $\{\xi_2,...,\xi_K\}$ are separable because there is not any interacting potential merging them. Therefore, one can assume that the wave function can be written as:

$$\Upsilon(\mathbf{x},\xi,\xi_2,\xi_3,..,\xi_K,t) = \Upsilon_a(\mathbf{x},\xi,t)\Upsilon_b(\xi_2,\xi_3,..,\xi_K,t). \tag{3.13}$$

Then, decomposing the previous Schrödinger equation as:

$$\begin{aligned} &\frac{1}{\Upsilon_a}i\hbar\frac{\partial \Upsilon_a}{\partial t} - \frac{1}{\Upsilon_a}\left(\sum_{k=1}^{N} -\frac{\hbar^2}{2m^*}\frac{\partial^2}{\partial x_k^2} + V(\mathbf{x},t) - \frac{\hbar^2}{2M}\frac{\partial^2}{\partial \xi^2} - i\hbar\lambda A(\mathbf{x})\frac{\partial}{\partial \xi}\right)\Upsilon_a \\ &\qquad = -\frac{1}{\Upsilon_b}i\hbar\frac{\partial \Upsilon_b}{\partial t} + \frac{1}{\Upsilon_b}\left(\sum_{j=2}^{K} -\frac{\hbar^2}{2m}\frac{\partial^2}{\partial \xi_j^2} + \sum_{l=2}^{K}\sum_{j=2}^{K} -\frac{\hbar^2}{2m}\frac{\partial^2}{\partial \xi_l \partial \xi_j}\right)\Upsilon_b. \end{aligned} \tag{3.14}$$

Therefore, it is possible to neglect the other $\{\xi_2,...,\xi_K\}$ degrees of freedom and concentrate only on the center of mass ξ and $\{\mathbf{x}\}$ electrons:

$$i\hbar\frac{\partial\Psi(\mathbf{x},\xi,t)}{\partial t}=\left(\sum_{k=1}^{N}-\frac{\hbar^2}{2m^*}\frac{\partial^2}{\partial x_k^2}+V(\mathbf{x},t)-\frac{\hbar^2}{2M}\frac{\partial^2}{\partial\xi^2}-i\hbar\lambda A(\mathbf{x})\frac{\partial}{\partial\xi}\right)\Psi(\mathbf{x},\xi,t), \quad (3.15)$$

where it has been defined $\Upsilon_a \equiv \Psi(\mathbf{x},\xi,t)$. A pure time-dependent terms in the potential is neglected because it has no effect on the Bohmian trajectories. In the following, only one electron in the active region of the device will be considered, for example $x_1 \equiv x$, in order to perform numerical simulation. Before detailing the numerical simulations of Equation (3.15), two things are missing: the explicit expression of $A(\mathbf{x})$ and to study theoretically the influence of the interaction term in the Hamiltonian on the trajectories of the apparatus. In order to study the latter the derivation of the *guidance equation* will be derived from the polar form of the wave function.

3.1.2 Derivation of Quantum Hamilton-Jacobi and Continuity Equations

It is possible to derive the Quantum Hamilton-Jacobi and the Continuity equation from Equation (3.15) writing the wave function in the polar form. Hereafter it is considered for simplicity only a 2D version of Equation (3.15):

$$\Psi(x,\xi,t)=R(x,\xi,t)e^{\frac{i}{\hbar}S(x,\xi,t)}, \quad (3.16)$$

with $R(x,\xi,t)>0$ and $S(x,\xi,t)$ real-valued functions. Inserting Equation (3.16) in the Equation (3.15) one obtains:

$$\begin{aligned}
i\hbar\frac{\partial R(x,\xi,t)}{\partial t} &- \frac{\partial S(x,\xi,t)}{\partial t}R(x,\xi,t)=-\frac{\hbar}{2m^*}\frac{\partial^2 R(x,\xi,t)}{\partial x^2}+\\
&- \frac{i\hbar}{m^*}\frac{\partial R(x,\xi,t)}{\partial x}\frac{\partial S(x,\xi,t)}{\partial x}-\frac{i\hbar}{2m^*}\frac{\partial^2 S(x,\xi,t)}{\partial x^2}R(x,\xi,t)+\\
&+ \frac{1}{2m^*}\left(\frac{\partial S(x,\xi,t)}{\partial x}\right)^2 R(x,\xi,t)-\frac{\hbar^2}{2M}\frac{\partial^2 R(x,\xi,t)}{\partial\xi^2}+\\
&- \frac{i\hbar}{M}\frac{\partial R(x,\xi,t)}{\partial\xi}\frac{\partial S(x,\xi,t)}{\partial\xi}+\frac{1}{2M}\left(\frac{\partial S(x,\xi,t)}{\partial\xi}\right)^2 R(x,\xi,t)+\\
&- \frac{i\hbar}{2M}\frac{\partial^2 S(x,\xi,t)}{\partial\xi^2}R(x,\xi,t)+\\
&- i\hbar\lambda A(x)\frac{\partial R(x,\xi,t)}{\partial\xi}+\lambda A(x)\frac{\partial S(x,\xi,t)}{\partial\xi}R(x,\xi,t). \quad (3.17)
\end{aligned}$$

Taking the real part of Equation (3.17) one gets the Quantum Hamilton-Jacobi equation

$$\begin{aligned}\frac{\partial S(x,\xi,t)}{\partial t} &= -\frac{1}{2m^*}\left(\frac{\partial S(x,\xi,t)}{\partial x}\right)^2 + \frac{\hbar^2}{2m^* R(x,\xi,t)}\frac{\partial^2 R(x,\xi,t)}{\partial x^2} + \\ &- \frac{1}{2M}\left(\frac{\partial S(x,\xi,t)}{\partial \xi}\right)^2 + \frac{\hbar^2}{2MR(x,\xi,t)}\frac{\partial^2 R(x,\xi,t)}{\partial \xi^2} + \\ &- \lambda A(x)\frac{\partial S(x,\xi,t)}{\partial \xi}, \end{aligned} \tag{3.18}$$

while the imaginary part of Equation (3.17) gives:

$$\begin{aligned}\frac{\partial R(x,\xi,t)}{\partial t} &= -\frac{1}{m^*}\frac{\partial R(x,\xi,t)}{\partial x}\frac{\partial S(x,\xi,t)}{\partial x} - \frac{1}{2m^*}\frac{\partial^2 S(x,\xi,t)}{\partial x^2}R(x,\xi,t) + \\ &- \frac{1}{M}\frac{\partial R(x,\xi,t)}{\partial \xi}\frac{\partial S(x,\xi,t)}{\partial \xi} - \frac{1}{2M}\frac{\partial^2 S(x,\xi,t)}{\partial \xi^2}R(x,\xi,t) + \\ &- \lambda A(x)\frac{\partial R(x,\xi,t)}{\partial \xi}. \end{aligned} \tag{3.19}$$

If one multiplies Equation (3.19) for $2R(x,\xi,t)$ and defines $\rho(x,\xi,t) = R^2(x,\xi,t)$, obtains the Continuity equation:

$$\begin{aligned}\frac{\partial \rho(x,\xi,t)}{\partial t} &+ \frac{\partial}{\partial x}\left[\rho(x,\xi,t)\frac{1}{m^*}\frac{\partial S(x,\xi,t)}{\partial x}\right] + \\ &+ \frac{\partial}{\partial \xi}\left[\rho(x,\xi,t)\left(\frac{1}{M}\frac{\partial S(x,\xi,t)}{\partial \xi} + \lambda A(x)\right)\right] = 0. \end{aligned} \tag{3.20}$$

From Equation (3.20) it can be extrapolated the bohmian velocity, for both the electron in the active region of the device and the center of mass of the pointer

$$v_x = \frac{1}{m^*}\frac{\partial S(x,\xi,t)}{\partial x}, \tag{3.21}$$

$$v_\xi = \frac{1}{M}\frac{\partial S(x,\xi,t)}{\partial \xi} + \lambda A(x), \tag{3.22}$$

where it can be observed that the velocity of the electron in the device is exactly what one expects from the usual derivation for Bohmian Mechanics, while the velocity of the pointer is proportional to the gradient of the phase S, as usual, and has an additional term proportional to the measured quantity A. Notwithstanding, the velocity of the

electron v_x is not unchanged by the influence of the apparatus: as a matter of fact the phase $S(x,\xi,t)$ is not separable in the variable x and ξ, i.e. $S(x,\xi,t) \neq S(x,t) + S(\xi,t)$. In the following the explicit computation of $A(x)$ will be detailed.

3.1.3 The Relationship Between the Total Current on the Ammeter and the Bohmian Trajectories of the System

It is common to compute the electrical current on the (simulated) surface S_D of Figure 3.1, while a real measurement is done on the (non-simulated) surface S_A. It is then crucial to understand in which extension is the current on S_A equal to that on S_D. In fact, these currents will be only equal if one considers the *total current* $I_T(t) = I_c(t) + I_d(t)$, where $I_c(t)$ and $I_d(t)$ are respectively the conduction (or particle) and displacement components. Since the Maxwell equations ensure that the total current density $J(\vec{x},t)$ is a vector with a null divergence, then it is possible to write $\int_S \vec{J}(\vec{x},t)\cdot d\vec{s} = 0$ for a closed surface $S = \{S_D, S_A, S_L\}$.[1] In particular, see the parallelepiped in the left side of Figure 3.1 for a two terminal device. Then, one can assume $\int_{S_L} \vec{J}(\vec{x},t)\cdot d\vec{s} = 0$ in Figure 3.1, so finally one gets $\int_{S_D} \vec{J}(\vec{x},t)\cdot d\vec{s} = -\int_{S_A} \vec{J}(\vec{x},t)\cdot d\vec{s}$.

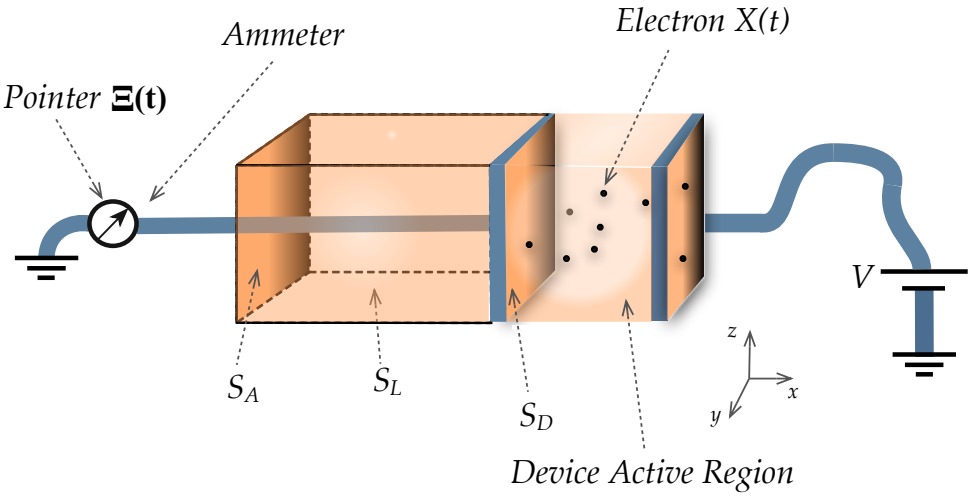

FIGURE 3.1: Schematic representation of a two terminal device.

The function $A(\vec{x})$ in Equation (3.15) has then to be related to the total current $I_T(t)$ of the system, meaning that $I_T(t)$ has to be somehow linked to the positions $\vec{X}(t)$ of the particle of the system. The total current measured by an ammeter, $I_T^\alpha(t)$,[2] for a particular trajectory $\vec{X}^\alpha(t) \equiv \{X^\alpha(t), Y^\alpha(t), Z^\alpha(t)\}$, can be defined as the time-derivative of the following *conduction* plus *displacement* charges:

[1] From this Section until the end of this Chapter it is used a vector to indicate a 3D variable while no vector indicates a 1D variable.

[2] In the following the upper index α indicates the particular run of an experiment. In each experiment the position of the particles will be selected, as always, according to the *quantum equilibrium hypothesis*.

$$I_T^{\alpha}(t) = \frac{d\left(Q_c(\vec{X}^{\alpha}(t)) + Q_d(\vec{X}^{\alpha}(t))\right)}{dt} \equiv \frac{dQ\left(\vec{X}^{\alpha}(t)\right)}{dt}, \tag{3.23}$$

where the *conduction* charge has been defined as:

$$Q_c(\vec{x}) = -q \int_{S_D} dy'\, dz' \int_{x'=x_D}^{\infty} dx' \delta(\vec{x}' - \vec{x}), \tag{3.24}$$

being q the (unsigned) electron charge and x_D the x-position of the lateral surface S_D formed by the points $0 \leq y' \leq L_y$ and $0 \leq z' \leq L_z$, with L_y and L_z are the lengths of the side of the surface S_D. The conduction charge is $Q_c(\vec{x}) = -q$ only if the electron is located at the right of x_D. Identically, it can be interpreted the *displacement* charge in Equation (3.23), as:

$$Q_d(\vec{x}) = \int_{S_D} \epsilon(x') \vec{E}(x, y, z, x_D, y', z') \cdot d\vec{s}, \tag{3.25}$$

being $\vec{E}(x, y, z, x_D, y', z')$ the electric field generated at the point $\vec{x}' = \{x_D, y', z'\}$ of the surface S_D by one electron at $\vec{x} = \{x, y, z\}$. It is important to emphasize that $Q_d(\vec{x})$ is different from zero independently of the distance between the electron and the surface. The generalization of $Q_c(\vec{x})$ and $Q_d(\vec{x})$ to an arbitrary number of electrons in the active region of the device $Q_c(\vec{x}_1, .., \vec{x}_N)$ and $Q_d(\vec{x}_1, .., \vec{x}_N)$ follows straightforwardly. Finally, in the ammeter model considered, the von Neumann term A in Equation (3.15) is the *conduction* plus *displacement* charges defined in Equations (3.24) and (3.25), i.e.

$$A(\vec{x}) = -\frac{Q(\vec{x})}{q}, \tag{3.26}$$

where the (irrelevant) minus sign is just to provide a positive pointer movement when an electron moves from left to right in Figure 3.1, which correspond to a negative net current. Certainly, other models for the ammeter are possible, however, it will be seen next that the one proposed here implies that the total current $I_T^{\alpha}(t)$ is directly related, with great accuracy, to the acceleration of the pointer. Hereafter, a detailed computations of the *conduction* and *displacement* charges defined in Equations (3.24) and (3.25). Specifically, an expression that tells which is the charge in a given surface when an electron is in a generic position $\vec{x}$ is required. In order to achieve this it can be defined the following function:

$$Q(\vec{x}) := \epsilon\Phi(\vec{E}(\vec{x})) + N(\vec{x}). \tag{3.27}$$

As already said, the two terms in Equation (3.27) represent the two contribution to the total current $I_T = I_c + I_d$, i.e. the particle current and the displacement current. By definition, $\Phi(\vec{E}(\vec{x}))$ is the (scalar) flux of the electric field generated by the electron $\vec{x}$ on the surface S_D:

$$\Phi(\vec{E}(\vec{x})) = \int_{S_D} \vec{E}(\vec{x}) \cdot d\vec{s} \tag{3.28}$$

The position of the electron is $\vec{x} = (x, y, z)$ and the surface S_D is a plane of area $L_y \cdot L_z$ perpendicular to the $\hat{x}$ direction placed in $x = x_D$, i.e. defined by the points $\{x_D, 0 \leq y' \leq L_y, 0 \leq z' \leq L_z\}$, exactly as in Figure 3.1. In the computation of the flux of the electric field, only the x component contribute, thus

$$E_x(x, y, z; x_D) = \frac{q}{4\pi\epsilon} \frac{(x_D - x)}{[(x_D - x)^2 + (y' - y)^2 + (z' - z)^2]^{3/2}}. \tag{3.29}$$

The flux is then:

$$\Phi(E_x(x, y, z; x_D)) = \int_0^{L_z} \int_0^{L_y} \frac{q}{4\pi\epsilon} \frac{(x_D - x)}{[(x_D - x)^2 + (y' - y)^2 + (z' - z)^2]^{3/2}} dy' dz'. \tag{3.30}$$

In Appendix B it is reported the analytical development of Equation (3.30) which gives:

$$\begin{aligned}\Phi(E_x(x,y,z;x_D)) &= \frac{q}{4\pi\epsilon}\tan^{-1}\left(\frac{(L_y-y)(L_z-z)}{(x_D-x)\sqrt{(x_D-x)^2+(L_y-y)^2+(L_z-z)^2}}\right)+\\ &+ \frac{q}{4\pi\epsilon}\tan^{-1}\left(\frac{z(L_y-y)}{(x_D-x)\sqrt{(x_D-x)^2+(L_y-y')^2+(z)^2}}\right)+\\ &+ \frac{q}{4\pi\epsilon}\tan^{-1}\left(\frac{y(L_z-z)}{(x_D-x)\sqrt{(x_D-x)^2+(y)^2+(L_z-z)^2}}\right)+\\ &+ \frac{q}{4\pi\epsilon}\tan^{-1}\left(\frac{zy}{(x_D-x)\sqrt{(x_D-x)^2+(y)^2+(z)^2}}\right). \qquad (3.31)\end{aligned}$$

In the simple case in which the particle is located in $x = (x, L_y/2, L_z/2)$, it moves only in the $\hat{x}$ direction and when $L_y = L_z \equiv L$ and $S = L^2$, expression (3.31) becomes

$$\Phi(E_x(x;x_D)) = \frac{q}{\pi\epsilon}\tan^{-1}\left(\frac{S}{4(x_D-x)\sqrt{(x_D-x)^2+\frac{S}{2}}}\right). \qquad (3.32)$$

The term $N(x)$ is due to the particle current and is simply

$$N(x) = q\Theta(x_D - x). \qquad (3.33)$$

It is worthwhile to note that in Equation (3.32) appears a discontinuity in $x = x_D$ and that the function changes sign when an electron cross the discontinuity point. The physical meaning of this term is, as already said, the flux of the electric field generated by a particle in a generic position x, the change of sign is simply explained by the scalar product that appears in Equation (3.28). The meaning of the discontinuity is explained observing Equation (3.33), this expression is 0 if the particle position is less than x_D instead is exactly q, the charge, when the particle position in greater than x_D, so the gap in Equation (3.33) exactly compensate the discontinuity in Equation (3.32), meaning that the displacement current contribution is globally zero.
One can also observe that the sum of the two terms guarantee the continuity of the function $Q(x)$.

3.1.4 The Many-particle Schrödinger Equation of the System plus Apparatus

It is possible to perform the numerical simulation of a 2D version of Equation (3.15) with the results for the *conduction* and *displacement* charges just computed. It is considered that the system and the pointer are described by just one particle x and ξ. Hereafter the explicit equation simulated is rewritten:

$$i\hbar\frac{\partial\Psi(x,\xi,t)}{\partial t} = \Big(-\frac{\hbar^2}{2m^*}\frac{\partial^2}{\partial x^2} + V(x,t) - \frac{\hbar^2}{2M}\frac{\partial^2}{\partial\xi^2} + i\hbar\lambda\frac{Q(x)}{q}\frac{\partial}{\partial\xi}\Big)\Psi(x,\xi,t). \tag{3.34}$$

At this point, it is relevant to compute the Bohmian velocity of such center of masses. By inserting the polar form of the wave function $\Psi(x,\xi,t) = R(x,\xi,t)e^{\frac{i}{\hbar}S(\mathbf{r},\xi,t)}$ into Equation (3.34), one obtains the corresponding Hamilton-Jacobi and the continuity equations (exactly as in Section 3.1.2) from which it can be defined the pointer velocity as

$$v_\xi(x,\xi,t) = \frac{1}{M}\frac{\partial S(x,\xi,t)}{\partial\xi} - \lambda\frac{Q(x)}{q}. \tag{3.35}$$

Since the mass M is very large (it is important to recall that the degree of freedom ξ represents the center of mass of all the particles forming the pointer), the first term in the right hand side of Equation (3.35) can be neglected. Therefore, for a particular trajectory $\{X^\alpha(t), \Xi^\alpha(t)\}$, it turns out that the acceleration of the pointer, i.e. the time derivative of Equation (3.35), is proportional to the total current of the system defined in Equation (3.23) (and which explicit expression has been derived in Section 3.1.3):

$$\frac{dv_\xi(X^\alpha(t),\Xi^\alpha(t),t)}{dt} \approx -\lambda\frac{dQ(X^\alpha(t))/q}{dt} = -\frac{\lambda}{q}I^\alpha(t). \tag{3.36}$$

Hereafter Equation (3.34) is numerically solved. Consider that the initial wave function is a product of two Gaussian wave packets $\Psi(x,\xi,0) = \psi(x,0)\phi(\xi,0)$. The central kinetic energies, central positions and spatial dispersion being respectively $E_x = 0.1\ eV$, $x_c = -100\ nm$ and $\sigma_x = 8\ nm$ for the particle, and $E_\xi = 0\ eV$, $\xi_c = 0\ nm$ and $\sigma_\xi = 0.5\ nm$ for the pointer. The system consists of an electron (with m^* equal to 0.068 the electron free mass) impinging upon an Eckart barrier $V(x,t) = V_0/\cosh^2[(x - x_{bar})/w]$ with $V_0 = 0.3\ eV$, $x_{bar} = -50\ nm$ and $w = 1\ nm$ (see the line at $x = -50\ nm$ in Figure 3.2). The pointer of the apparatus ξ (with $M \approx 75000\ m^*$) interacts with the system through

the term $i\hbar\lambda Q(\mathbf{x})\partial/\partial\xi$ with $\lambda = 50\ nm/ps$. It has been considered a lateral surface with $S_D = 900\ nm^2$ located at $x_D = 75\ nm$ so that of $Q(x)$, defined in Equations (3.23), (3.24) and (3.25), is only different from zero on the right hand side of the plots in Figure 3.2. It is indicated this region by a (apparatus) rectangle in the configuration space.

The numerical solution of the modulus of $\Psi(x, \xi, t)$ is plotted at four different times. At the initial time $t = 0$, Figure 3.2 (a), the entire wave function is at the left of the barrier. At a later time t_0 the wave function has split up into reflected and transmitted parts due to the barrier, see Figure 3.2 (b). At this time, because the electron has not yet arrived at the transmitted charge detector, the wave function has the following form:

$$\Psi(x, \xi, t_0) = [\psi_T(x, t_0) + \psi_R(x, t_0)]\, \phi(\xi, t_0). \tag{3.37}$$

Then, Figure 3.2 (c) and (d), the interaction of the detector with the transmitted part of the wave function appears. For time $t > t_0$ the transmitted part of the wave function is shifted up in the ξ direction while the reflected part does not move. In fact, the *local* velocity of the wave packet in the ξ direction becomes different from zero for the transmitted part and, according to Equation (3.35), the pointer moves when it is located in the transmitted part. The interaction with the apparatus thus produces two channels in the configuration space, one corresponding to the electron being transmitted and the other corresponding to the electron being reflected, getting an entangled superposition among the electron and the apparatus.

In Figure 3.2 is also plotted the actual positions of the system and detector $\{X(t), \Xi(t)\}$ for four different possible initial positions $\{X(0), \Xi(0)\}$, corresponding (say) to four distinct runs of the experiment (labelled by $\alpha = 1, ..., 4$). Of the four possible evolutions shown, three have the electron transmitting ($\alpha = 2, 3, 4$) and one has it reflecting ($\alpha = 1$). While the pointer position $\Xi(t)$ does not move for the reflected particle, its evolution for the transmitted ones clearly shows a movement. In conclusion, looking at the *detector* position it can be perfectly certified if the particle has been reflected ($X(t) < -50\ nm$ and $\Xi(t) = 0\ nm$) or transmitted ($X(t) > -50\ nm$ and $\Xi(t) \approx 15\ nm$). It is important to underline how trivially the measurement is explained within Bohmian Mechanics, only a *channelized* (unitary) time-evolution of 2D wave function plus two Bohmian trajectories, one for the system and another for the measuring apparatus are needed.

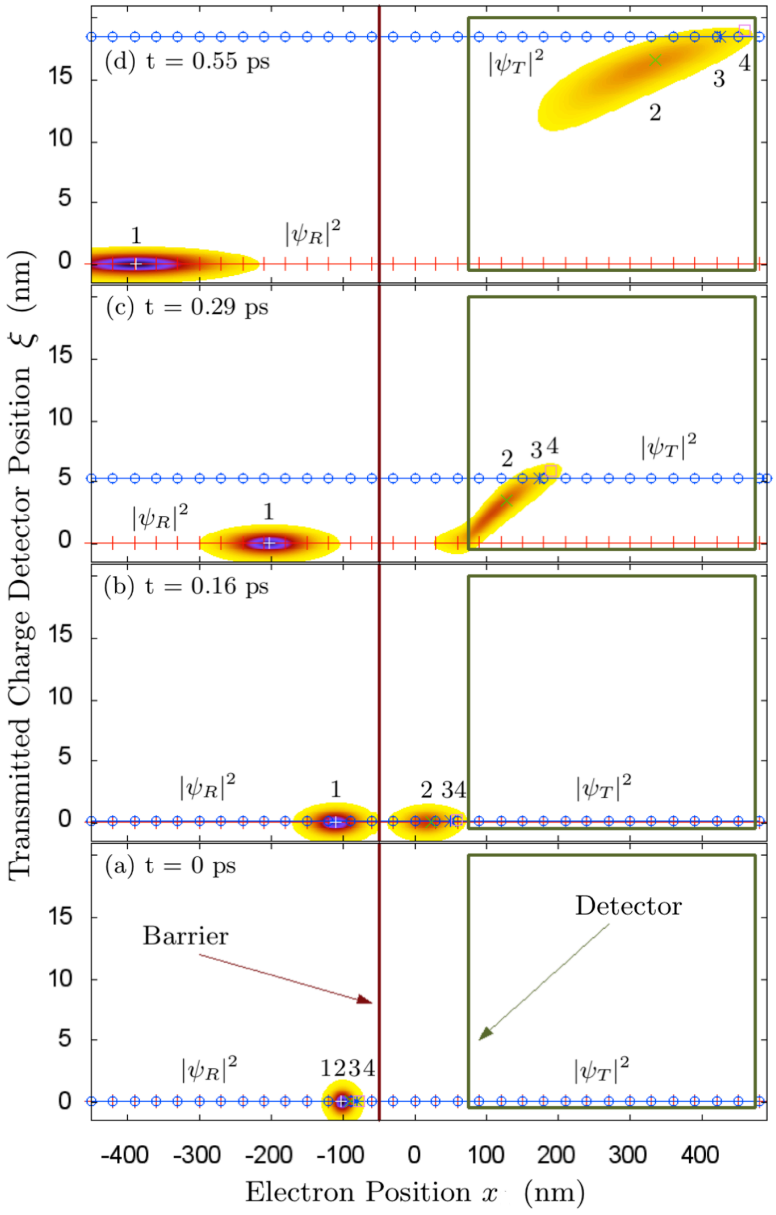

FIGURE 3.2: Time evolution of the squared modulus of $\Psi(x, \xi, t)$ at four different times computed from Equation (3.34). The system barrier is indicated by a solid line and the region on the configuration space where the system-apparatus interaction is nonzero by a rectangle. The time evolution of four trajectories $\{X^\alpha(t), \Xi^\alpha(t)\}$ with different initial positions are presented with $+$ ($\alpha = 1$), $\times$ ($\alpha = 2$), $*$ ($\alpha = 3$) and $\square$ ($\alpha = 4$). The transmitted trajectories ($\square$, $*$, and $\times$) at (c) and (d) have different pointer positions associated to $\Xi^\alpha(t)$ for $\alpha = 2, 3, 4$ because their evolution does only depend on the transmitted wave packet. The pointer position associated with the reflected trajectory ($+$) with $\alpha = 1$ does not move because there is no interaction between this trajectory and the apparatus. The $+$ line indicates the modulus of the conditional wave function $|\psi_R|^2 = |\Phi(x, \Xi^{\alpha=1}(t), t)|^2$, while the $\odot$ line corresponds to $|\psi_T|^2 = |\Psi(x, \Xi^{\alpha=3}(t), t)|^2$.

3.1.4.1 Numerical Derivation of the Collapse

Once the complete measurement process is solved in the enlarged configuration space (system *plus* detector), it is possible to describe the same measurement in the electron subspace with the help of the conditional wave function. The key point illustrated here is that the collapse of the conditional wave function for the electron, which collapse is of course postulated (see Section 2.1.1) in Ordinary Quantum Mechanics, instead arises naturally and automatically in Bohmian Mechanics. It is simply a consequence of slicing the unitary-evolving (2D) wave function Ψ along the (moving) line $\xi = \Xi(t)$, resulting $\psi(x,t) = \Psi(x, \Xi(t), t)$. In Figure 3.2 two solid horizontal lines are plotted corresponding to a slice of the wave function at two different values of $\Xi(t)$ (i.e. for two different experiments). In Figure 3.3 the evolution of these (time-dependent) slices of the many-particle wave function is reported, the *conditional wave function* for the electron, for the trajectories $\alpha = 1$ and $\alpha = 3$ from Figure 3.2. It can be clearly seen that if the particle is reflected, as is the case for $\alpha = 1$, the position of the pointer does not change with time and, after the interaction with the detector has been performed, the electron's *conditional wave function* includes only a reflected part. See Figures 3.3 (c) and (d). On the other hand, when the particle is transmitted (e.g., $\alpha = 3$), it is the reflected part of the *conditional wave function* which collapses away, leaving only the transmitted packet. See Figures 3.3 (g) and (h). Note in particular that the evolution of $\psi(x,t)$ (the electron's *conditional wave function*) is not unitary, even though the evolution of Ψ is.

While the wave function provides only statistical information about the experimental results, with the help of the Bohmian trajectories, it has been possible to recover the individual result of each experiment. In fact for each experiment the pointer of the detector is either moving (corresponding to a transmitted electron) or not (reflected electron), while an ensemble of repeated experiments (where the initial positions of the particles, both the electron $X(0)$ and the detector $\Xi(0)$, are selected according to the squared modulus of the wave function at the initial time $|\Psi(x, \xi, 0)|^2$) reproduce the same statistical results.

Thus with the previous numerical example the collapse-behaviour of the wave function of a transmitted (or reflected) electron has been reproduced. Apart from irrelevant technicalities (related on how the measuring apparatus is defined) the results in Figure 2.2 and Figure 3.3 are conceptually identical. It is important to emphasize that, the collapse in Bohmian theory is naturally derived. Such a natural derivation of the collapse behavior demystifies the measurement process. The non-unitary evolution of the wave function of a measured system is achieved simply slicing the enlarged wave function (which includes the apparatus) in the configuration space. Even more, the fact that the apparatus, in the example called *transmitted charge detector*, is directly treated into the Hamiltonian

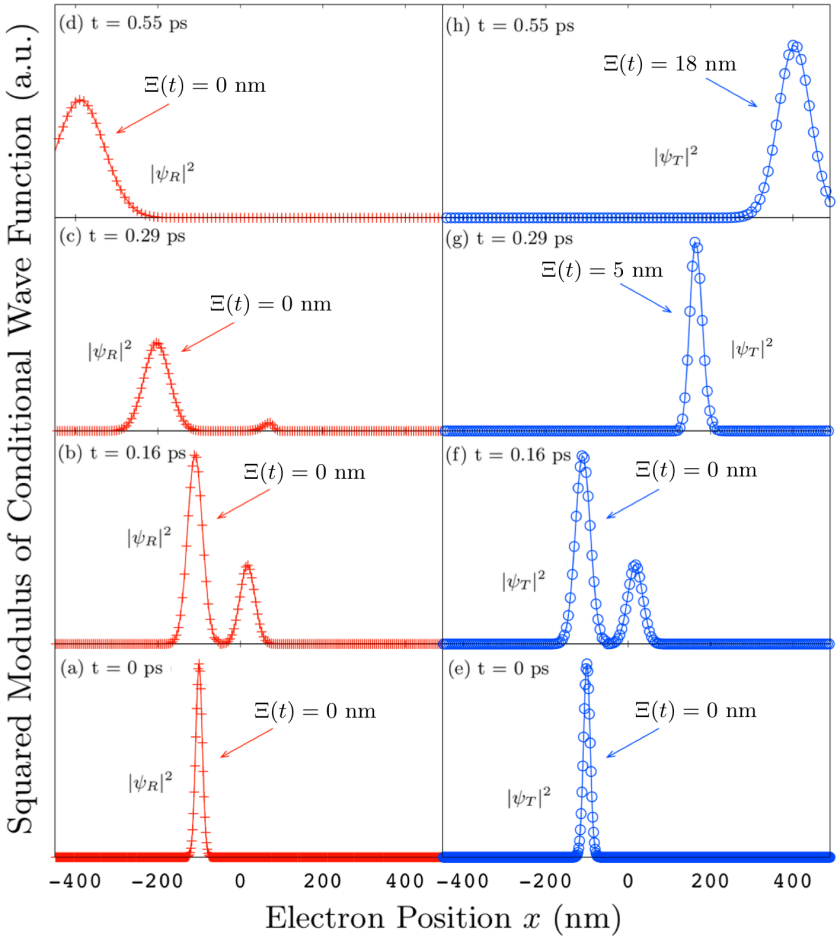

FIGURE 3.3: The + line in (a), (b), (c) and (d) is the time evolution of the squared modulus of the conditional wave function associated to the trajectory $\alpha = 1$ in Figure 3.2, i.e. $\psi_R = |\Psi(x, \Xi^{\alpha=1}(t), t)|$. The $\odot$ line in (e), (f), (g) and (h) is the squared modulus of the conditional wave function associated to the trajectory $\alpha = 3$ in Figure 3.2. i.e. $\psi_T = |\Psi(x, \Xi^{\alpha=3}(t), t)|$. The actual detector position $\Xi(t)$ is plotted at each time in order to compare these results with those in Figure 3.2.

of the Schrödinger equation allows to study such a situation where it is not completely clear which is its actual effect on the measured system and where it is difficult to find the *right* operator able to reproduce the experimental results (see Chapter 4 to enlarge this point).

3.1.5 Solving the System plus Apparatus Schrödinger Equation

Once the first technical difficulty (i.e. specifying how the ammeter is included in the Hamiltonian) is solved, one must discuss about the difficulties of solving the Schrödinger equation including the system and apparatus degrees of freedom. *Can the inclusion of the pointer degrees of freedom in the Schrödinger equation be avoided without loosing*

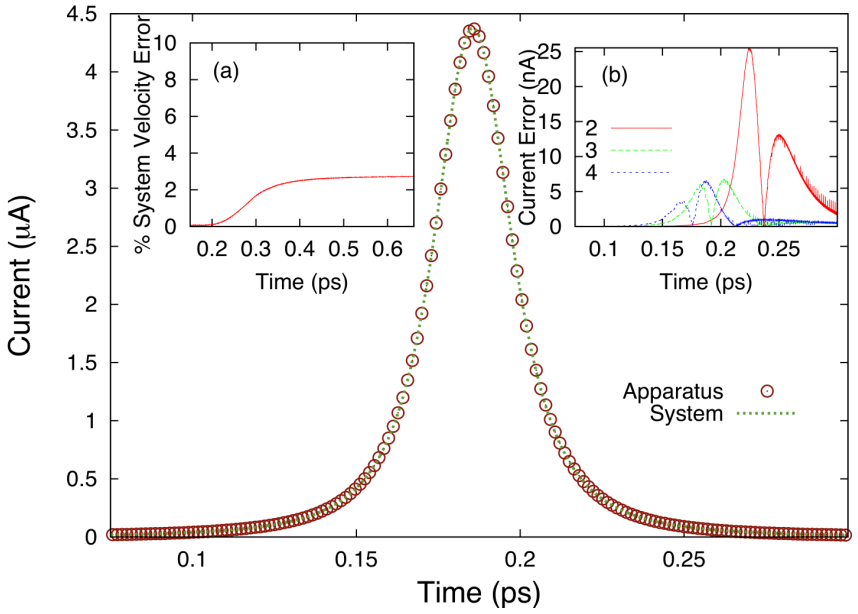

FIGURE 3.4: Total current associated to the $*$ trajectory $\{X^3(t), \Xi^3(t)\}$ of Figure 3.2 as a function of time defined from the acceleration of the pointer trajectory computed from Equation (3.34) (with ammeter) in (red) circles and from the system trajectory computed from a single particle Schrödinger equation (without ammeter) in (green) dotted lines. For commodity, the sign of the current has been reversed. (a) Relative (ensemble) error for the system Bohmian velocity when comparing the solution from Equation (3.34) (with ammeter) and from a single particle Schrödinger equation (without ammeter). (b) Absolute error of the system current of the $\times$ ($\alpha = 2$), $*$ ($\alpha = 3$) and $\square$ ($\alpha = 4$) trajectories when comparing the solution from Equation (3.34) (with ammeter) and from a single particle Schrödinger equation (without ammeter).

much accuracy? The answer to this question is affirmative whenever the apparatus induces a small distortion on the system. The distortion on the system's trajectories can be quantified by defining the relative (ensemble) error of the system velocity:

$$\langle \delta v(t) \rangle = \lim_{M_\alpha \to \infty} \frac{\sum_{\alpha=1}^{M_\alpha} |v_\lambda^\alpha(t) - v_0^\alpha(t)|}{\sum_{\alpha=1}^{M_\alpha} |v_\lambda^\alpha(t)|}. \tag{3.38}$$

It has been defined $v_\lambda^\alpha(t)$ as a system Bohmian velocity when one use Equation (3.34) with $\lambda = 50\ nm/ps$, while $v_0^\alpha(t)$ when one does not consider the apparatus ($\lambda = 0$) in Equation (3.34). The latter is equivalent to solving directly a single particle Schrödinger equation for the electron in the device. One can see in the inset (a) of Figure 3.4 that the relative error on the velocity defined in Equation (3.38) is less than 3 %. Then, if the inclusion of the pointer is avoided, the total current can be computed directly from the system trajectory $X_0^\alpha(t)$ without apparatus, with a small error. This result is

confirmed by the (green) dotted line in Figure 3.4 that corresponds to the total current using Equation (3.23) from the system trajectories using a single particle Schrödinger equation (or Equation (3.34) when $\lambda = 0$). The absolute error in the prediction of the current $I_T(t)$ in one particular experiment is defined as the difference (in absolute value) between the exact value in (red) circles and the approximate value in a dotted (green) line. See the absolute error for the three transmitted trajectories in the inset (b) of Figure 3.4.

Summarizing, if the back action of the apparatus on the system trajectories is not much relevant, one can avoid the explicit computation of the pointer trajectory and simulate just the system, i.e. the single particle Schroödinger equation is enough to compute the system trajectories and thus the electrical current $I_T(t)$ from them. The reason why the agreement between the current computed from the pointer trajectory and the system trajectory is so good is because the main distortion of the system trajectory comes from the barrier, not from the apparatus. The former splits the initial wave packet into two separated parts (transmitted and reflected components), while the latter provides a small *adiabatic* perturbation on the system trajectories as seen in Figure 3.2. It is very important to emphasize, however, that the change from Equation (3.34) to a single particle Schrödinger equation is only technical, without any fundamental implication. The real pointer of the ammeter is $\Xi(t)$, not $X(t)$. However, when the measurement apparatus has a small (3 % of error in the numerical example) effect on the system and the pointer position does perfectly specify the value of the total current of the system (see Figure 3.4), and it can be avoided the explicit simulation of the pointer in order to surpass computational burdens.

It has to be discussed that the movement of the pointer (see Figure 3.4) is not macroscopic (it moves only a few nanometers), however, it can be demonstrated that for other parameters (of the pointer wave packet with different λ and S_D), $\Xi(t)$ would have a macroscopic movement.

Finally, it can be demonstrated that the conclusions explained here about the correlation and errors of the system and the pointer positions are not affected by increasing the number of electrons.

The apparatus just proposed can only certify if the electron has been transmitted or reflected. A step further can be done: *can an Ammeter be modeled more realistically?* In particular: *can this Ammeter certify instantaneously the value of the total current?* The next Section is devoted to investigate this point in detail.

3.2 Ammeter for High-Frequency Current

One can simply observe that the experimental characterization of an electronic device is based on fixing an external (DC or AC) voltage at the borders of the simulation box and then measuring the electrical current flowing through it. In the previous Section a model of Ammeter able to capture the back-action on the system has been derived. At the same time, as discussed at the end of Section 3.1.5 this Ammeter is not able to capture the instantaneous value of the total current but it has only able to certify if an electron has been transmitted or reflected. Thus, the following idea can be pursued: Enlarge as much as possible the interaction of the electrons in the active region of the device with the surrounding particles, i.e. taking into account not only the center of mass but possibly many degrees of freedom. A crucial point in this investigation will be the conditional wave function and its use in the small entanglement approximation explained in Section 2.3.1. This procedure can significantly help when dealing with devices working at Tera Hertz (THz) frequencies as it will be seen below, when the total quantum current (with particle and displacement components) is repeatedly measured at very small time intervals.

As already said, the traditional procedure to describe the interaction between the electrons of the system and those of the ammeter (the cables, the environment, etc.) is by *encapsulating* them into a non-unitary operator. However, again the same questions arise: *Which is the operator that determines the (non-unitary) evolution of the wave function when measuring the total current? Is it "continuous" or "instantaneous"? with a "weak" or "strong" perturbation of the wave function?* [80] As already said, the answers are certainly not simple. It has to be said again that over the years physicists have identify the operators, by developing instincts on which are the effects of measurements on the wave function. To the best of knowledge of the author of this thesis, no such (THz) current operator has been presented. In any case, if one want to extract reliable information about the current measured at very high frequencies, taking into account the back-action seems mandatory.

Before entering in the details of the model proposed here, it is important to clarify a feature of Bohmian Mechanics: any mean value of an observable can be calculated from the ensemble trajectories. Hereafter it is reported a simple demonstration of that, while more details can be found in Ref. [68].

3.2.1 Any Mean Value of an Observable can be Calculated from Ensemble Trajectories

If needed, Bohmian mechanics can make use of operators, but only as a mathematical tool. Without any physics or fundamental role in the operator. Hereafter it will be briefly explained how it is possible to calculate the mean value of a general hermitian operator with Bohmian trajectories. The *quantum equilibrium hypothesis* at the initial time $t = 0$ can be expressed in terms of the trajectories as follows

$$|\Psi(\mathbf{x},0)|^2 = \lim_{M_\alpha \to \infty} \frac{1}{M_\alpha} \sum_{\alpha=1}^{M_\alpha} \prod_{i=1}^{N} \delta(x_i - X_i^\alpha(0)), \tag{3.39}$$

where the superindex α takes into account the uncertainty in the initial position of the particles. It can be easily demonstrated that the evolution of the above infinite set of quantum trajectories $\alpha = 1, 2, ..., M_\alpha$ reproduce at any time t the probability distribution, $|\Psi(\mathbf{x}, t)|^2$.
One can always write an Hermitian operator $\hat{A}$ and the mean value in the position representation. Then the mean value of this operator over the wave function[3] $\psi(x,t)$ is:

$$\langle \hat{A} \rangle = \int_{-\infty}^{+\infty} \psi^*(x,t) \hat{A} \left(x, -i\hbar \frac{\partial}{\partial x} \right) \psi(x,t) dx. \tag{3.40}$$

Another possibility is to calculate the mean value by defining a spatial average of a "local" magnitude $A_B(x)$ weighted by $|\psi(x,t)|^2$:

$$\langle \hat{A} \rangle = \int_{-\infty}^{+\infty} |\psi(x,t)|^2 A_B(x) dx. \tag{3.41}$$

Because the mean value in Equation (3.40) and Equation (3.41) one can easily identify $A_B(x)$ as:

$$A_B(x) = \mathrm{Re} \left(\frac{\psi^*(x,t) \hat{A} \left(x, -i\hbar \frac{\partial}{\partial x} \right) \psi(x,t)}{\psi^*(x,t)\psi(x,t)} \right) \tag{3.42}$$

[3]Here it is considered for simplicity a single particle in one dimension.

where the real part Re(...) in Equation (3.42) is taken to ensure that the mean value in Equation (3.41) takes always real values. Thus, one can use Equation (3.39) to write $|\Psi(\mathbf{x},t)|^2$ in Equation (3.41), obtaining:

$$\langle A\rangle_\Psi = \lim_{M_\alpha\to\infty}\frac{1}{M_\alpha}\sum_{\alpha=1}^{M_\alpha} A_B(\mathbf{X}^\alpha(t)). \tag{3.43}$$

Equation (3.43) allows to calculate the mean value of an operator $\hat{A}$ from an ensemble of Bohmian trajectories. In fact, for $M_\alpha \to \infty$, by construction, the mean value calculated from Equation (3.43) is equal to the mean value calculated from Equation (3.41).

3.2.2 Simulation with Conditional Wave Function

Consider the two-terminal device depicted in Figure 3.5 a) where THz currents are measured, for example, in the $L-$ammeter. The quantum system is defined by an electron traveling through the active region, while all the rest is considered as part of the measuring apparatus.

In principle, it is needed to consider all the particles of Figure 3.5 a). However, because of the large distance between the system and the ammeter, one can consider only the interaction between the particle x_1, and the nearest electrons, $x_2, ..., x_N$, in the metal surface S_m (see Figure 3.5 b)). Therefore, one can compute the total current on the surface S_L, while the rest of not simulated particles, which do not have a direct effect on the back-action suffered by the particle x_1, are the responsible of translating this value of the total current along the cable until the ammeter. The conditional (Bohmian) wave function [29] of the system (i.e. the wave function of the quantum subsystem in the active region of the device) provides again an excellent tool to numerically computing the interaction between the particles plotted in Figure 3.5 b). Under the small entanglement approximation reported in Section 2.3.1, the conditional (Bohmian) wave function evolves as

$$i\hbar\frac{\partial\psi(x_1,t)}{\partial t} = [H_0 + V]\,\psi(x_1,t) \tag{3.44}$$

where $V = V(x_1, \vec{X}_2(t), ..., \vec{X}_N(t))$ is the conditional Coulomb potential felt by the system and H_0 is its free Hamiltonian.

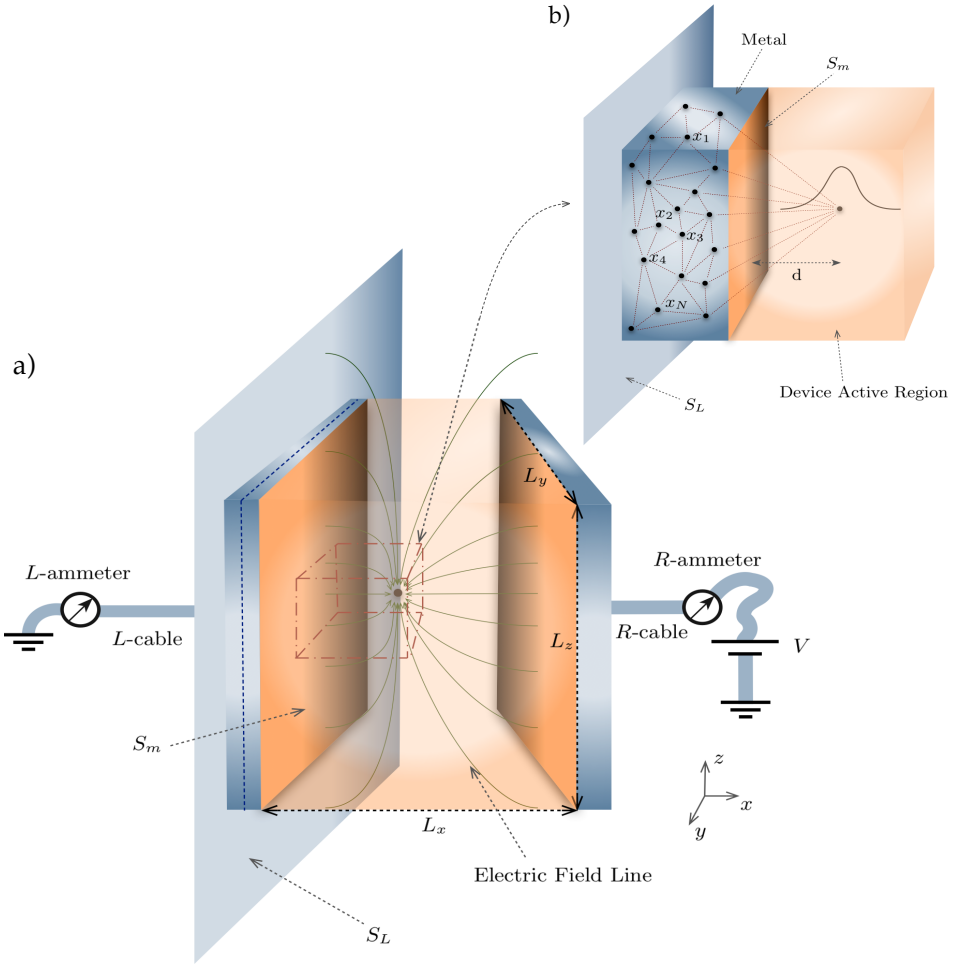

FIGURE 3.5: a) Schematic representation of a two terminal device. The ideal surface S_L collects all the electric field lines (green solid lines). b) Zoom of the red region in a). It is schematically depicted the Coulomb interaction (red dashed lines) and the conditional wave function (black solid line) defined in Equation (3.44).

The total quantum current can be computed as the time derivative of the flux Φ of the electric field $\vec{E}(\vec{x},t)$ produced by all N electrons (system *plus* metal) on the large ideal surface S_L using the relation:

$$I_T(t) = \int_{S_L} \epsilon(\vec{x}) \frac{d\vec{E}}{dt} \cdot d\vec{s} = \sum_{i=1}^{N} \vec{\nabla}\Phi(\vec{X}_i(t))\vec{v}_i(t) \tag{3.45}$$

where the flux Φ depends on each electron position and $\vec{v}_i$ is the Bohmian velocity. Equation (3.45) is nothing else that the generalization of the expression found in Section 3.1.3.[4]

[4]Here it is considered only the displacement component of the total current as it is assumed that the electron does not cross the surface.

3.2.2.1 Simulation of the Electrons in the Metal Surface

Here it is addressed the problem of how the electrons in the metals are exactly simulated. Each electron $\vec{x}_i$ interact with the others electrons in the metal $\vec{x}_2, ..., \vec{x}_{i-1}, \vec{x}_{i+1}, ..., \vec{x}_N$ and with the electron in the active region of the device x_1. The simulations reported hereafter are performed considering the electrons in the metal as classical particles thus obeying to Newton second law:

$$\ddot{\vec{x}}_i = \frac{\vec{F}_i}{m_i}, \tag{3.46}$$

where m_i is the free electron mass. The force $\vec{F}_i$ consists of two contributions, the Coulomb force and a viscosity term (in order to simulate the interaction with phonons):

$$\vec{F}_i = \vec{F}_{Coulomb} - \gamma \vec{v}_i \tag{3.47}$$

where $\gamma = 3.374 \cdot 10^{-17}\ \ Kg/s$. The number of electron in the metal (3D) surface is chosen in accordance with the density of the Copper ($n_{Cu} = 8.43 \cdot 10^{28}\ \ m^{-3}$). In the simulations reported hereafter the surface where the electron in the metal are simulated is of $S_m = 2,5 \cdot 10^{-17}\ m$ for a width of $5 \cdot 10^{-9}\ m$.

3.2.3 Back-Action on the Quantum System

After a numerical simulation along the ideas mentioned before, in Figure 3.6 can be seen that the quantum system is only slightly affected by the interaction with the electrons in the metal. From the comparison in Figure 3.6 of the (conditional) wave function evolving according Equation (3.44) (with ammeter) at the final time of the simulation with the wave function obtained from a Schrödinger evolution in a time independent potential $V(x_1)$ computed as a mean field (without ammeter), one can deduce that the potential $V = V(x_1, \vec{X}_2(t), ..., \vec{X}_N(t))$ in Equation (3.44) is almost separable in x_1 and $\vec{x}_2, ..., \vec{x}_N$ justifying numerically the small entanglement approximation used for performing the simulations.

Varying the parameter d in Figure 3.5 b), i.e the distance between the initial central position of the wave packet and the metal surface S_m, it can be calculated how differently the quantum system is affected because of the interaction with the electrons in the

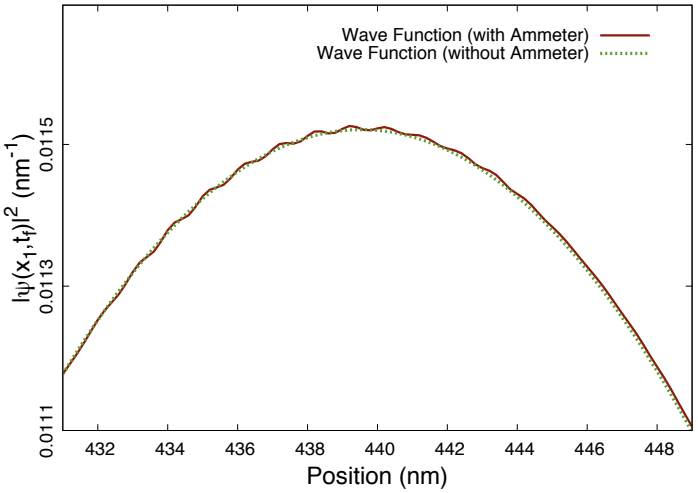

FIGURE 3.6: Comparison at the final time of the simulation (t_f) of the modulus square of the conditional wave function (solid line) evolving according to Equation (3.44) and the wave function without ammeter (dashed line), i.e. considering a Schrödinger evolution in a time independent potential $V(x_1)$ computed as a mean field.

metal. In Figure 3.7 the value of the error (defined in the caption) for different values of d is reported. Not surprisingly the error decreases while increasing the distance. Increasing the distance means diminishing of the strength of the interaction, for this reason this result justifies the use of the *small entanglement approximation* explained in Section 2.3.1.

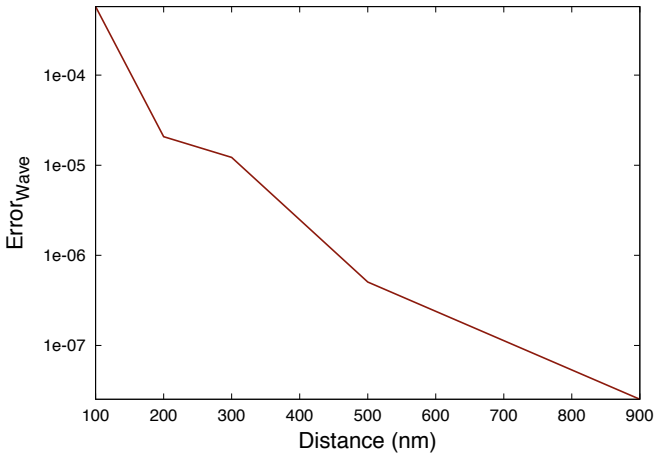

FIGURE 3.7: Error on the wave function computed as $\text{Error}_{wave} = \int |\psi(x_1,t_f) - \psi^{mean}(x_1,t_f)|^2 dx_1$ at the final time of the simulation t_f for different initial values of the distance (parameter d in Figure 3.5 b)) of the electron x_1 from the metal surface S_m. The wave function $\psi(x_1,t_f)$ is computed from Equation (3.44) while $\psi^{mean}(x_1,t_f)$ is computed from a mean field simulation, i.e. imposing an external potential $V(x_1)$.

3.2.4 Computations of the Total Current

The instantaneous current measured in the surface S_L when considering the contribution of all the electrons in the metal or when considering only the electron in the device active region, i.e. without including the apparatus, differs considerably as shown in Figure 3.8.

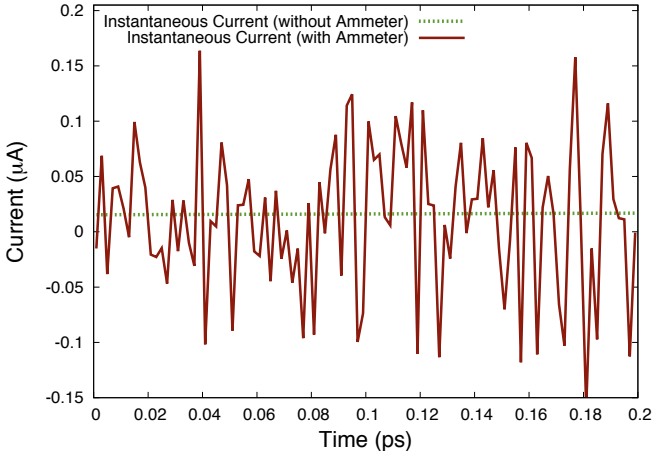

FIGURE 3.8: Value of the total current. With solid line is reported the instantaneous value of the total current calculated from Equation (3.45) (with ammeter) and with dashed lines obtained from a mean field simulation for particle x_1 alone (without ammeter).

The large fluctuations in the current reported in Figure 3.8 means an additional source of noise due to the interaction of the electrons in the metal with the particle x_1 in the active region of the device. Considering this additional source of noise, whose origin is the quantum back-action, is mandatory to get accurate THz predictions.

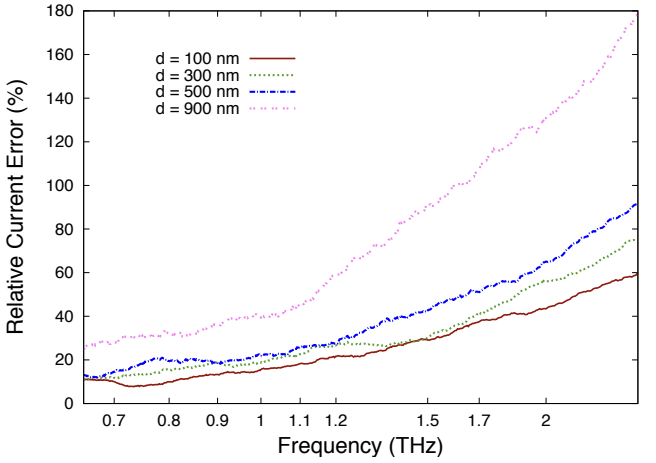

FIGURE 3.9: Relative error for the total current as a function of frequency ($f = 1/T$) calculated as $|\overline{I}_T(t) - \overline{I}_T^{x_1}(t)|/|\overline{I}_T^{x_1}(t)|$. The $\overline{I}_T(t)$ is the mean temporal current at the considered frequency taken from Equation (3.45) (with ammeter) and $\overline{I}_T^{x_1}(t)$ is mean temporal total current obtained from a mean field simulation (without ammeter). The different curves represent different values of the parameter d.

In Figure 3.9 the relative error (defined in the caption) as a function of the frequency ($f = 1/T$) is reported. It can be seen that the error decrease for small frequencies (i.e. for large intervals T for time-averaging). Additionally, it can be seen in Figure 3.9 that when the distance d is increased (different curves in the plot), the relative error in the measured total current grows.

3.2.5 Weak Measurement

From the previous results, it can be clearly seen that when the information of the measured total current is very noisy, the quantum system is only slightly perturbed, and vice versa. This fact is completely in agreement with the fundamental rules of quantum measurement: if one looks for precise information, one has to pay the price of perturbing the system significantly (the so-called collapse of the wave function or strong measurement [82]). On the other hand if one does not require such a precise information (for the instantaneous value of the total current seen in Figure 3.8) one can leave the wave function of the system almost unaltered (known in literature as weak measurement). At this point one can wonder if repeating many times the same (numerical) experiment the mean value of the (weak) measured total current computed from Equation (3.45) is equal to the value obtained without considering the ammeter.

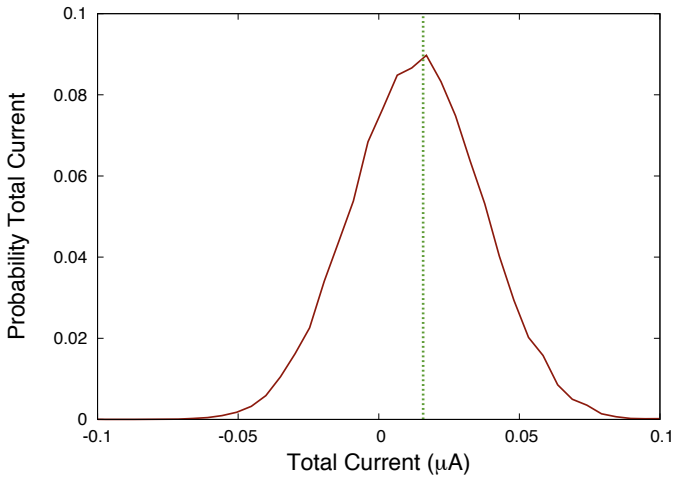

FIGURE 3.10: Red solid line probability distribution of the measured total current from Equation (3.45) in a time interval $T = 0.2\ ps$ of the simulation from 39000 experiments. Green dashed line mean value obtained form a mean field simulation.

In Figure 3.10, the mean value of the probability distribution of the total current (with ammeter) corresponds exactly to the mean value of the total current of the system without ammeter. Let us mention that this mean value is exactly what one would have found by performing several ideal strong measurement on the quantum system and averaging them.

Next Chapter will be devoted to a further inspection of the weak measurement just found: it will be detailed a procedure to compute the weak value of the Bohmian velocity in mesoscopic systems through two measurements of the total current, one weak and one strong. Numerical experiments will support the proposed experiments.

Chapter 4

Weak Measurement of Bohmian Velocity in Mesoscopic Systems

The present Chapter is devoted to a proposal for weak measuring the Bohmian velocity in a mesoscopic system. In the last years an increasing attention has been posed on the utility of weak measurements [1] for exploiting new and fascinating quantum phenomena. A weak measurement implies that the measuring apparatus provides a small perturbation on the measured system and that the output result has a large uncertainty. Although quantum mechanics forbids to measure simultaneously the position and the momentum of a quantum particle in a single experiment, weak measurements realized on a large set of identically prepared systems provide well-defined values of momentum and position of the quantum system. These type of measurements open new paths for wave function [13] or trajectories [45] (which reveal to be exactly the ones predicted by Bohmian mechanics [29, 34]) reconstructions. Up to now, all such experiments are done with (relativistic) photons and, unfortunately, a procedure to perform weak measurements for (non-relativistic) electrons in solid-state devices does not exist. For this reason, this Chapter is devoted to investigate numerically the feasibility of an experiment for weak measuring the Bohmian velocity from the (high-frequency) displacement current measured by an ammeter in a solid-state electronic device. The methodology described in Section 3.2 and the results obtained there will be used in the present Chapter.

4.1 Weak Measurement of Bohmian Velocity from the Total Electrical Current

Hereafter an introduction to the theory of weak measurement will be provided in Section 4.1.1. Then in Section 4.1.2 several important results for the present thesis will be derived. In Section 4.1.2.1 a formula connecting the measurement of the displacement current in a large surface to the momentum of a particle in the active region of the device will be obtained and in Section 4.1.2.2 it will be justified that this measurement is weak. In Section 4.1.2.3 a formula connecting the measurement of the total current in a small surface to the position of the particle will be achieved. These results will be used in Section 4.2 and Section 4.3 to detail a proposed experiment to reconstruct the Bohmian trajectories in a solid state system.

4.1.1 Theory of Weak Measurement

In Section 3.2.5 it has been argued that the measurement scheme proposed in Section 3.2 is *weak*. Hereafter it will be detailed the precise mathematical meaning resuming the main feature of what is known as weak measurement.
In 1988 Aharonov, Albert and Vaidman [1] proposed the idea of generalizing the usual projective measurement. Imagine one wants to measure the position of a particle, the associated operator being $\hat{x}$, the eigenstates of this operator are a continuum with the carnality of $\Re$. One can introduces a general notion of operator, the *so called* POVM (Positive Operator Value Measure), able to embodies the intrinsic uncertainty in a measurement apparatus. For example, it can be chosen the following Gaussian measurement Kraus operator [46]:

$$\hat{A} = \left(\frac{1}{\sqrt{\pi}\sigma_a}\right)^{\frac{1}{2}} \int dx e^{-\frac{(x-x_a)^2}{2\sigma_a^2}} P_x, \tag{4.1}$$

where σ_a is the width of the gaussian, $P_x = |x\rangle\langle x|$ is the projection operator and x_a is the value registered by the measuring apparatus. The operator in Equation (4.1) changes the system initial wave function $\psi_0(x)$ as follows:

$$\psi_f(x) = \mathcal{N}\hat{A}\psi_0(x) = \mathcal{N}\left(\frac{1}{\sqrt{\pi}\sigma_a}\right)^{\frac{1}{2}} e^{-\frac{(x-x_a)^2}{2\sigma_a^2}} \psi_0(x), \tag{4.2}$$

where $\mathcal{N}$ is the normalization constant.
Thus the wave function after the measurement $\psi_f(x)$ will be a Gaussian-weighted sum of projection of the initial wave function $\psi_0(x)$ onto the eigenstates of $\hat{x}$. The operator in Equation (4.1) is quite general, it is interesting to study two limiting cases depending on the width σ_a of the Gaussian. Calling σ_f the width of the wave function (in the position representation), if $\sigma_a \ll \sigma_f$ the operator in Equation (4.1) is a quasi-projection operator and it is referred to a *strong* operator, otherwise if $\sigma_a \gg \sigma_f$ the operator in Equation (4.1) is referred to a *weak* operator.

Defining $\sigma_s \equiv \sigma_a$ and $x_s \equiv x_a$, a strong measurement of the position can be envisioned as reported in Figure 4.1:

- In Figure 4.1 a) it is shown the wave function of the system at time $t = 0$ isolated, evolving unitarily according to the Schrödinger equation.
- In Figure 4.1 b) it is shown the strong operator acting on the system wave function. The strong operator is depicted with a green dashed zone, the width of the gaussian is σ_s and is centered around position x_s.
- In Figure 4.1 c) it is shown the wave function of the system after the application of the Gaussian measurement Kraus operator. It can be seen that what survives is only the part of the wave function that was, at time $t = 0$, around the measured position x_s.

The operator defined in Equation (4.1), with $\sigma_a \ll \sigma_f$, provides a notion of strong measurement near to what it is a real measurement apparatus. Looking at Equation (4.2) one deduces that the wave function $\psi_f(x)$ is almost collapsed around position x_s (see Figure 4.2 c)).

The width of the gaussian, σ_a, defines the precision of the instrument or in other words the reliability of the information extracted from the system by the measurement process. The idea of weak measurement is then to relax and decrease the disturbance of the system undergoing a measurement process. The price to be paid is that the amount of information provided by the measuring apparatus in a single measurement is not reliable. As stated before, the relevant condition is that $\sigma_a \gg \sigma_f$. Defining $\sigma_w \equiv \sigma_a$ and $x_w \equiv x_a$, a weak measurement of the position can be envisioned as reported in Figure 4.2:

- In Figure 4.2 a) it is shown the wave function of the system at time $t = 0$ isolated, evolving unitarily according to the Schrödinger equation.

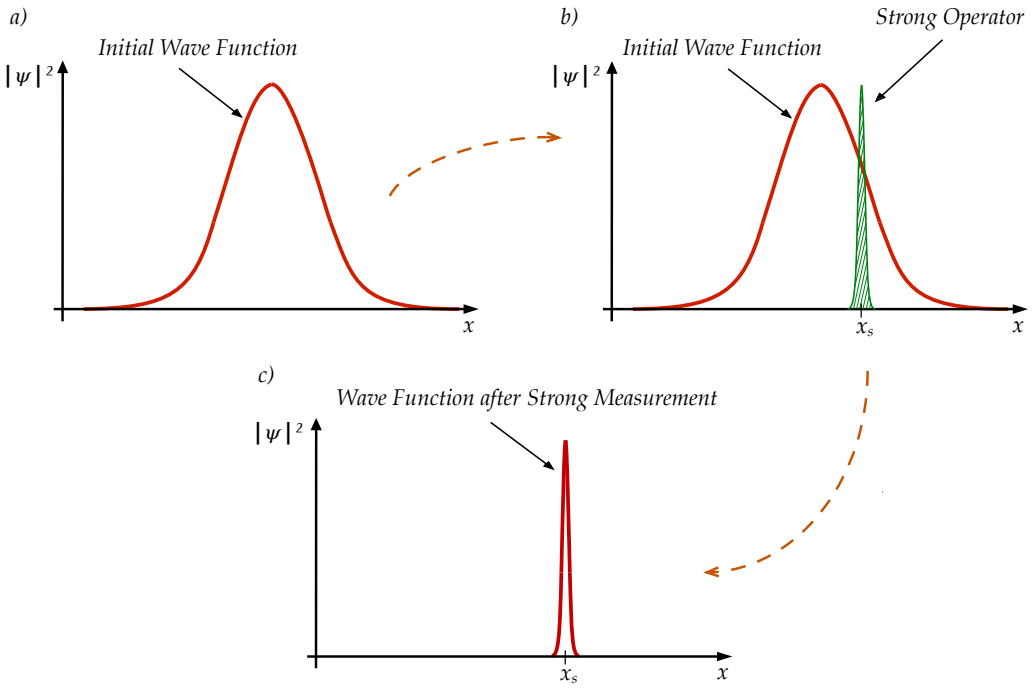

FIGURE 4.1: Schematic representation of a strong measurement process. a) At the initial time $t = 0$ the wave function (red solid line) of the system is not interacting with a measuring apparatus. b) The strong operator (green line) acts on the wave function of the system. c) After the interaction, the wave function of the system collapses around the measured value x_s.

- In Figure 4.2 b) it is shown the weak operator acting on the system wave function. The weak operator is depicted with a yellow dashed zone, the width of the gaussian (that does not enter entirely in the figure) is σ_w and is centered around position x_w
- In Figure 4.2 c) it is shown the wave function of the system after the application of the weak Gaussian measurement Kraus operator. It can be seen that the function is almost equal to the initial one in Figure 4.2 a). It is worthwhile to notice that the wave function of the system does not keep track of the value x_w measured by the apparatus.

An important property of weak measurement is that the mean value of a weak measurement (over an ensemble of identically prepared experiments) is exactly equal to the mean value of the quantity measured. Calling $|\psi\rangle$ the initial wave function one has:

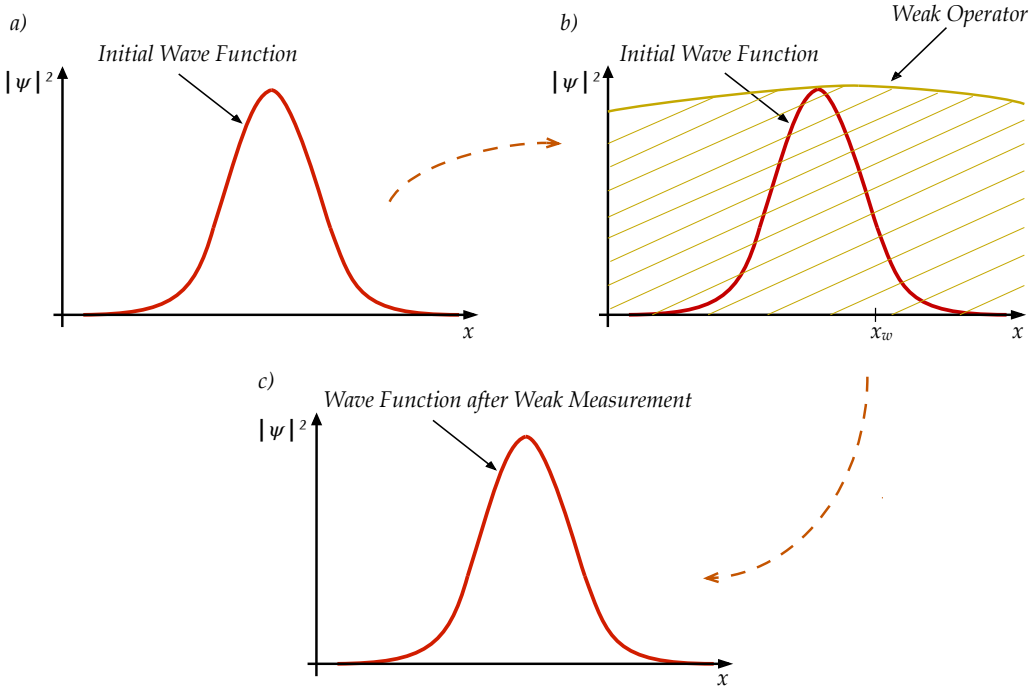

FIGURE 4.2: Schematic representation of a weak measurement process. a) At the initial time $t = 0$ the wave function (red solid line) of the system is not interacting with a measuring apparatus. b) The weak operator (yellow line) acts on the wave function of the system. c) After the interaction, the wave function of the system remains almost unaltered.

$$\begin{aligned}
\langle x_w \rangle &= \frac{1}{\sqrt{\pi}\sigma_a} \int x_w \mathcal{P}(x_w) dx_w = \\
&= \frac{1}{\sqrt{\pi}\sigma_a} \int x_w \langle \psi | \hat{A}^\dagger \hat{A} | \psi \rangle dx_w = \\
&= \frac{1}{\sqrt{\pi}\sigma_a} \int \int x_w e^{-\frac{(x-x_w)^2}{\sigma_w^2}} \langle \psi | x \rangle \langle x | \psi \rangle dx dx_w = \\
&= \int x |\psi(x,0)|^2 dx = \langle x \rangle. \qquad (4.3)
\end{aligned}$$

It is possible to summarize the main feature of a weak measurement: it provides a small perturbation of the wave function (see Equation (4.2)), a single experiment does not provide any reliable information about the measured system (see Figure 4.2) but the mean value (over an ensemble of identically prepared experiments) is the same of the usual strong measurement (see Equation (4.3)).

4.1.2 On the Total Current Measured on Different Metallic Surfaces

In this Section it is analyzed the result found in Equation (3.32) in two different regimes: Firstly, it will be analyzed for a large metallic surface and after for a small metallic surface. The precise definition of "large" and "small" will be explained in details.

4.1.2.1 Total Current on an Large Surface S

It is interesting first of all to evaluate Equation (3.32) in the situation in which $S \gg (x_D - x)^2$: this means that the maximum distance (squared) that an electron in a device can reach form the surface is much smaller than the surface itself. In order to work out an approximate form for Equation (3.32) in this regime it can be considered the following change of variable $\chi = (x_D - x)$, and it can be assumed for simplicity that the electron is located on the left of the surface (i.e. $x < x_D \rightarrow \chi > 0$) then:

$$\Phi(E_x(\chi)) = \frac{q}{\pi\epsilon}\tan^{-1}\left(\frac{S}{4\chi\sqrt{\chi^2+\frac{S}{2}}}\right) = \frac{q}{\pi\epsilon}\tan^{-1}\left(\frac{S}{4\chi^2\sqrt{1+\frac{S}{2\chi^2}}}\right). \tag{4.4}$$

Then, calling $\xi^2 = \frac{2\chi^2}{S}$, Equation (4.4) becomes

$$\Phi(\xi) = \frac{q}{\pi\epsilon}\tan^{-1}\left(\frac{1}{2\sqrt{\xi^2(1+\xi^2)}}\right), \tag{4.5}$$

such that the condition $S \gg \chi^2$ becomes equivalent to $\xi \ll 1$. So Equation (4.5) becomes simply:

$$\Phi(\xi)_{\xi^2 \ll 1} = \frac{q}{\pi\epsilon}\tan^{-1}\left(\frac{1}{2\sqrt{\xi^2}}\right). \tag{4.6}$$

Remembering that $\tan^{-1}(\alpha\xi) + \tan^{-1}(\frac{1}{\alpha\xi}) = \frac{\pi}{2}$ for $\xi > 0$ (this implies that the electron is on the left of the surface) then one has:

$$\Phi(\xi) = \frac{q}{\pi\epsilon}\left[\frac{\pi}{2} - \tan^{-1}(2\xi)\right]. \tag{4.7}$$

In Equation (4.7) the term $\tan^{-1}(2\xi)$ can be expanded obtaining:

$$\Phi(\xi) = \frac{q}{\pi\epsilon}\left[\frac{\pi}{2} - 2\xi + \frac{(2\xi)^3}{3} - ...\right]. \tag{4.8}$$

This last expression, Equation (4.8), can be truncated at first order of ξ. Thus recalling the original variables one arrives at:

$$\Phi(E_x(x; x_D)) = \frac{q}{\pi\epsilon}\left[\frac{\pi}{2} - 2\sqrt{\frac{2}{S}}(x_D - x)\right] \propto x. \tag{4.9}$$

Equation (4.9) is an important results, it demonstrates that the flux of the electric field generated by a particle in a very large surface is proportional to the position of the electron.

Now it can be discussed the general problem considered here, i.e. derive a microscopic analysis of the measurement of the total electrical current in a large metallic surface. In order to do that one has to "enlarge" the system considering also all the electrons composing the metallic surface, as done in Section 3.2.

Without assuming nothing about the dynamics of the the electrons in the metal one can say that they contribute as the electron in the device to the flux of the total electric field as described by Equation (4.9) by superposition principle. One obtains, suppressing the dependence on x_D and making reference to the position of the electron in the device as X_1, the following expression:

$$\Phi(E_x(X_1, X_2, X_3, ..., X_N)) = \alpha X_1 + \alpha \sum_{j=2}^{N} X_j, \tag{4.10}$$

where the actual Bohmian positions of the particles X_i have been used and α is a suitable constant. In expression Equation (4.10) one can clearly see that the total electric flux is due to a contribution from the electron in the system $\propto X_1$ and another due to all the other electrons in the metal. The latter is the additional source of noise found in Section 3.2.

So far, it has been considered that the electron in the active region of the device is not crossing the surface and therefore one gets that the total electric current is due only to the displacement current contribution. So the total current becomes:

$$I_{T_{S_{\text{large}}}} \propto \frac{d\Phi(E)}{dt} = \frac{d}{dt}\left(\alpha X_1(t) + \alpha \sum_{j=2}^{N} X_j(t)\right) \propto v_{x_1} + \sum_{j=2}^{N} v_{x_j}, \tag{4.11}$$

where $v_{x_i} \forall i$ is the x-component of the Bohmian velocity of the i-particle. It will be demonstrated in Section 4.3 numerically that the term $\sum_{j=2}^{N} \langle v_{x_j} \rangle \approx const.$ over an ensemble of repeated experiment. This result is not surprising because it has been already achieved in Section 3.2 that the electrons in the metals act as an additional source of noise not changing the mean value. So, it is possible to write:

$$\langle I_T \rangle_{S_{\text{large}}} \propto \langle p_{x_1} \rangle. \tag{4.12}$$

Equation (4.12) shows that the mean value of the total electrical current in a large metallic surface is proportional to the mean value of the momentum (x-component, i.e. the component perpendicular to the surface) of the quantum particle in the device.

4.1.2.2 Is the Measurement on a Large Surface a Weak Measurement?

In the previous Section it has been demonstrated that the measurement of the total current in a large surface is proportional to the (Bohmian) momentum of the particle in the active region of the device. Here it is addressed the question: is this measurement weak? As seen in Section 4.1.2.1 a weak measurement requires that: the measurement does not perturb (too much) the wave function, that the information extracted from a single experiment is not reliable and that the mean value corresponds exactly to the mean value of a strong measurement of the same quantity. Now, the simulations performed in Chapter 3 turns out to be very useful. There, it was simulated an electron in the active region of a device interacting with others electron in a surface and the total current was measured on a large surface S, exactly the condition considered here.

In Section 3.2.3 and Section 3.2.4 it has been shown that if one wants precise information about the measured system, the perturbation of the wave function is increased, and vice versa (see Figure 3.7 and Figure 3.9 respectively). It has been also proven in Section 3.2.5 that the mean value obtain from the simulations with ammeter is equal to the mean value without ammeter (of the system alone), as clearly shown in Figure 3.10. So, all the conditions exposed at the beginning of this Section are satisfied, thus configuring the measurement of the total current in a large surface as a *weak measurement*. Thus adding the result obtained in Equation (4.12), the weak measurement of the total current can be written in the language of Gaussian measurement Kraus operator as:

$$\hat{I}_w = C_w \int dp e^{-\frac{(p-p_w)^2}{2\sigma_w}} |p\rangle\langle p|, \tag{4.13}$$

where p is the momentum (x-component) of the particle in the device and C_w is suitable constant (for more details see Appendix C).
Now, it will be discussed how the width σ_w of the Gaussian measurement Kraus operator changes with the frequency. It has been seen that depending on the frequency the information about the measured total current changes (see Figure 3.9). In Figure 4.3 it is reported how σ_w varies with the frequency of the measurement. It can be seen that lowering the frequency yelds more precise information about the system (the width of the gaussian decreases). In this sense the proposed experiment works in a regime where the total current is measured at High-Frequency.

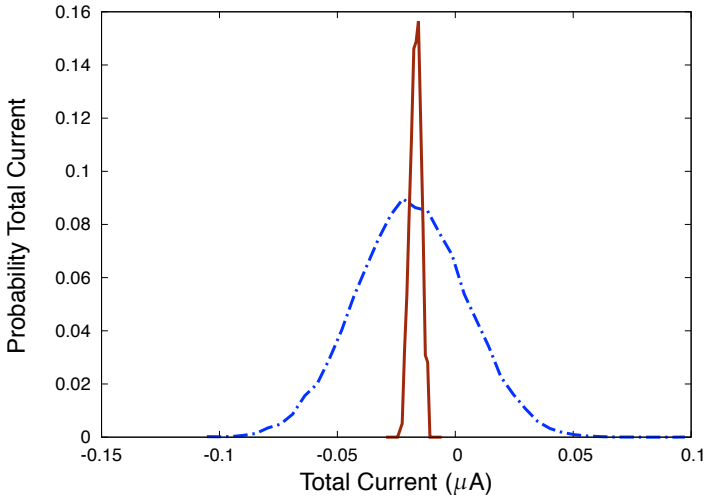

FIGURE 4.3: Blue dashed line probability distribution of the measured total current at a frequency of $f = 5\ THz$. Red solid line probability distribution of the measured total current at $f = 50\ GHz$.

4.1.2.3 Total Current on a Small Surface S

Now, it is interesting to consider the opposite limit in which the surface S where the measurement is performed is very small compared to the distance of the electron from the surface $\chi = x_D - x$. Specifically one has to consider Equation (4.4) in the limit in which $S \ll \chi$ assuming as before that the electron is on the left of the surface, i.e. $\chi > 0$. Making the following change of variable $\xi = \frac{S}{2\chi^2}$ the previous condition becomes equivalent to study the condition $\xi \ll 1$ for the function

$$\Phi(E_x(\xi)) = \frac{q}{\pi\epsilon} \tan^{-1}\left(\frac{\xi}{2\sqrt{1+\xi}}\right), \tag{4.14}$$

it can be easily seen that the first order expansion of the last expression is:

$$\Phi(E_x(x;x_D)) = \frac{q}{4\pi\epsilon}\frac{S}{(x_D-x)^2} \quad \text{for} \quad x < x_D. \tag{4.15}$$

The physical interpretation of this term is quite natural: the contribution of a particle to the total flux measured in a small surface is only relevant when the particle is "near" the surface. This means that the the contribution is relevant when the electron cross the surface. For this reason it has been pointed out that the function (3.32) has a discontinuity in the point $x = x_D$ of the first kind. In order to ensure continuity one has to add to the total flux of the electric field the particle contribution of the current. This is simply proportional to $q\Theta(x - x_D)$ where $\Theta(x)$ is the Heaviside function. Then with the add of this contribution one has that, in the limit of small surface, the particle contribution is the main contribution, when an electron crosses the surface. Extending this result to quantum mechanics is trivial and gives for the total current measured on the small surface:

$$\langle I_T\rangle_{S_{\text{small}}} \propto \langle\delta(x_1 - x_D)\rangle = \int dx_1\psi^*(x_1,t)\delta(x_1-x_D)\psi(x_1,t) \tag{4.16}$$

where $\psi(x_1,t)$ is the wave function of the electron in the device. Equation (4.16) explains the obvious relation that measuring the total current in a small surface provides information whether or not the particle is passed through the surface or not. It is important to mention that in this case one does not need to include all the others electrons in the metal because one can see that the first interaction that the electron in the device suffers is already strong. In principle a treatment including the rest of the electrons of the system can be provided but in this case the result obtained does not change; in fact the electron in the device contributes to the total current only when pass through the small surface and then when the interaction with all the others electrons in the metal is strong (the distance is very small).

Thus it is possible to write the measurement of the total current in a small surface S in the language of the Gaussian measurement Kraus operator as:

$$\hat{I}_s = C_s\int dx e^{-\frac{(x-x_s)^2}{2\sigma_s}}|x\rangle\langle x|, \tag{4.17}$$

with σ_s satisfying the condition exposed in Section 4.1.1 and C_s a suitable constant (see Appendix C).

4.2 Geometry of the Proposed Experiment

Once the theory of weak measurement has been developed and the results in Sections 4.1.2.1, 4.1.2.2 and 4.1.2.3 have been achieved, it is possible to propose a specific device geometry for measuring the Bohmian velocity in mesoscopic systems.

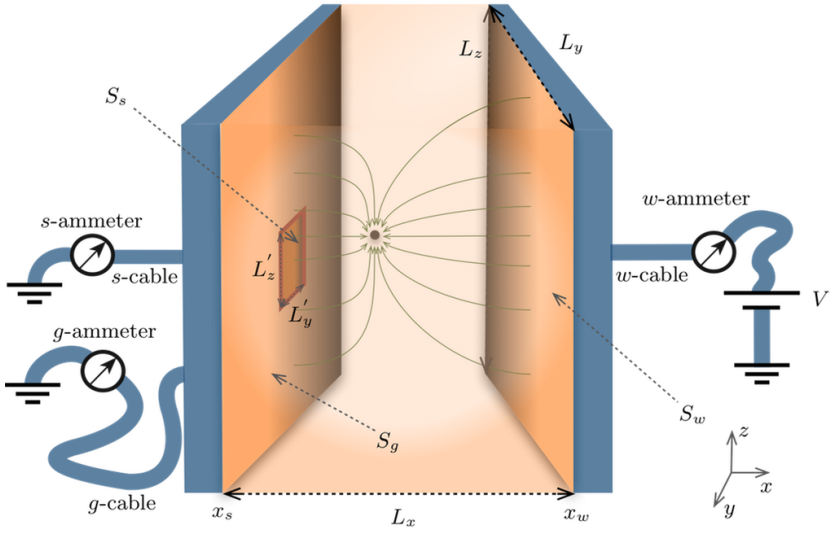

FIGURE 4.4: Schematic representation of a three terminal device to measure the Bohmian velocity in a mesoscopic system.

In Figure 4.4 it is reported a schematic representation of the three terminal device proposed here. There are two metallic surfaces working as *sensing electrodes*. The surface on the right S_w satisfies the relation $S_w \gg L_x^2$, thus the total current measured by the w-ammeter follows the relation given by Equation (4.12) found in Section 4.1.2.1. Therefore, the w-ammeter would measure a quantity proportional to the momentum of the particle in the active region of the device (see Equation (4.13)). At the left side of Figure 4.4, it can be seen that a similar metallic surface, S_g, is depicted connected to the g-ammeter. From this surface a small part of it, S_s, is *electrically isolated* and connected to a different ammeter than g, called s-ammeter. This third s-ammeter, because $S_s \ll L_x^2$, would provide a measurement of the total current that is proportional to the position of the particle in the active region of the device (see Equation (4.16) in Section 4.1.2.3). In order to ensure that the two different conditions used in Section 4.1.2.1 and Section 4.1.2.3 are satisfied it has been considered the square of the length L_x as the maximum distance the particle can reach from the surface. Now it is possible to work out the exact procedure for measuring the Bohmian velocity, the w-ammeter measures weakly the momentum of the particle, these values will be post-selected by positions measurement performed by the s-ammeter.

4.2.1 Derivation of Bohmian Velocity Weak Value

With the operators defined in Section 4.1.1 it is possible to derive mathematically how the Bohmian velocity can be obtained from a weak measurement procedure with post selection for the device geometry just exposed. The reader can found analogous mathematical developments in Refs. [34, 80, 83]. One is interest in the quantity $E[p_w|x_s]$, i.e. the ensemble average values of the (weak measured) momentum p_w conditioned to the fact that (strong) position x_s is effectively measured. Using standard probabilities formulas, this quantity can be simply computed as:

$$E[p_w|x_s] = \frac{\int dp_w p_w \mathcal{P}(p_w \cap x_s)}{\mathcal{P}(x_s)}, \tag{4.18}$$

where $\mathcal{P}(p_w \cap x_s)$ is the joint probability of two sequential measurement p_w and x_s, and $\mathcal{P}(x_s)$ is the probability of x_s. The quantity $\mathcal{P}(x_s)$ is computed as follows:

$$\mathcal{P}(x_s) = \int dp_w \mathcal{P}(p_w \cap x_s) = \int dp_w \langle\psi|\hat{I}_w^\dagger \hat{U}_\tau^\dagger \hat{I}_s^\dagger \hat{I}_s \hat{U}_\tau \hat{I}_w|\psi\rangle, \tag{4.19}$$

where $|\psi\rangle \equiv |\psi_0\rangle$ is the initial wave function, $\hat{U}_\tau$ the unitary evolution operator and the probability $\mathcal{P}$ is computed as $\langle\psi|...|\psi\rangle$ using Born's rule. The operators $\hat{I}_{w/s}$ are defined in Equation (4.13) and Equation (4.17) respectively. Therefore Equation (4.19) becomes:

$$\mathcal{P}(x_s) = \int\int dp' dp'' e^{-\frac{(p'-p'')^2}{4\sigma_w^2}} \langle\psi|p'\rangle\langle p'|\hat{U}_\tau^\dagger \hat{I}_s^\dagger \hat{I}_s \hat{U}_\tau|p''\rangle\langle p''|\psi\rangle, \tag{4.20}$$

with the assumption $e^{-\frac{(p'-p'')^2}{4\sigma_w^2}} \approx 1$, that is equivalent to $\sigma_w \to \infty$, the last expression becomes:

$$\mathcal{P}(x_s) = \langle\psi|\hat{U}_\tau^\dagger \hat{I}_s^\dagger \hat{I}_s \hat{U}_\tau|\psi\rangle = |\psi(x_s,\tau)|^2. \tag{4.21}$$

The last step needed to obtain the Bohmian velocity from Equation (4.18) is to calculate its numerator:

$$\int dp_w p_w \mathcal{P}(p_w \cap x_s) = \iint dp' dp'' \left(\frac{p'+p''}{2}\right) e^{-\frac{(p'-p'')^2}{4\sigma_w^2}} \langle\psi|p'\rangle\langle p'|\hat{U}_\tau^\dagger \hat{I}_s^\dagger \hat{I}_s \hat{U}_\tau|p''\rangle\langle p''|\psi\rangle. \quad (4.22)$$

Using again the condition $\sigma_w \to \infty$ and the definition $\int p|p\rangle\langle p| = \hat{p}$ one gets

$$\begin{aligned} \int dp_w p_w \mathcal{P}(p_w \cap x_s) &= \mathrm{Re}\left(\langle\psi|\hat{U}_\tau^\dagger \hat{I}_s^\dagger \hat{I}_s \hat{U}_\tau \hat{p}|\psi\rangle\right) \\ &= mJ(x_s,\tau) \end{aligned} \quad (4.23)$$

where Re(...) denotes the real part and $J(x_s,\tau)$ is the usual probability current. Hence, one gets the conclusion:

$$\frac{E[p_w|x_s]}{m} = \frac{J(x_s,\tau)}{|\psi(x_s,\tau)|^2} \equiv v(x_s,\tau), \quad (4.24)$$

where $v(x_s,\tau)$ is exactly Bohmian velocity. A detailed derivation of the result found in Equation (4.24) is reported in Appendix C, in which is also specified the condition $\sigma_w \to \infty$ in relation to σ_s.
Next Section is devoted to show a numerical experiment with the set-up reported in Figure 4.4 in which is possible to obtain the Bohmian velocity through a weak measurement of the momentum post-selected with strong measurement of position.

4.3 Numerical Experiments

The simulations reported in this Section are done following of what shown in Section 3.2. In particular the measurement of post selection of position is obtained without explicitly simulating the s-ammeter, but it is obtained directly from the Bohmian position of the electron in the active region of the device. In fact, a strong measurement of the position reveals nothing else that the position of the Bohmian particle [35]. The surface where the weak measurement is performed is $S_w \approx 10^{-11}\ m^2$ while the length of the device is $L_x = 2,8 \cdot 10^{-7}\ m$. The electron in the metal surface are simulated as described in Section 3.2.2.1.

In Figure 4.5 it is reported the velocity $v(x_s,t)$ obtained from an ensemble of 55000 identically prepared experiments. In particular as initial wave function $\psi(x_1,0)$ has

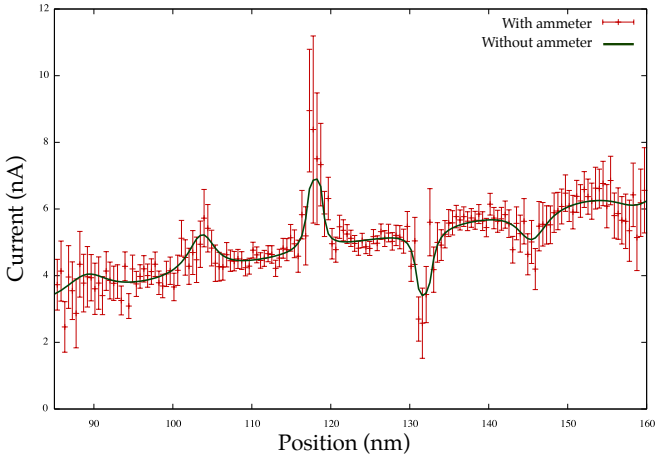

FIGURE 4.5: Red points (with error) Bohmian velocity in position x_s at time $t = 300\ fs$, obtained from an ensemble of 55000 experiments with the inclusion of the electrons in the metal surface (with ammeter) as reported in Section 3.2. The error is calculated from the standard deviation of the ensemble at time t and position x_s divided by the square root of trajectories passing through position x_s at time t. Green solid line Bohmian velocity in position x_s obtained from the same set of simulations without considering the electrons in the metal surface (without ammeter). In the numerical experiment reported in this Section the total current is measured at a frequency $f = 5 \cdot 10^{13}\ Hz$.

been chosen a superposition of two gaussian wave packets which have the central position spatially separated of 50 nm (as it can be seen at the initial time in Figure 4.6). Each gaussian wave packet has the same dispersion of 3 nm and the same energy of 0.0905 eV. The velocity field exhibits the typical maximum and minima of the interference pattern. In Figure 4.6 the modulus square of the wave function in function of time is reported.

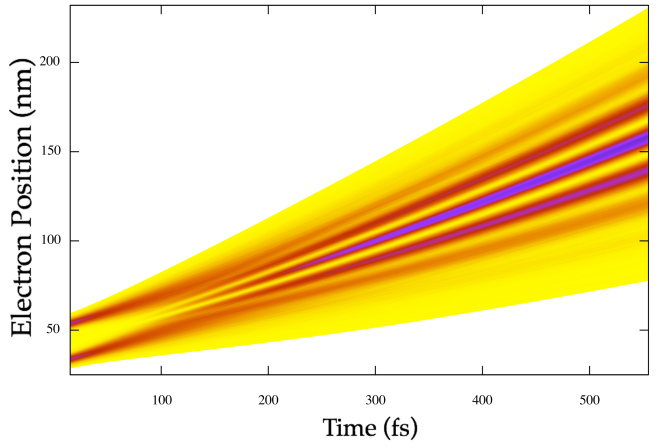

FIGURE 4.6: Density plot of the modulus squared of the wave function in function of time. It can be easily seen how the two initial wave packets spread forming the usual interference pattern. This figure has been obtained only from the trajectories without ammeter used for simulating the experiments.

In Figure 4.7 b) are reported the trajectories reconstructed with the procedure detailed in Section 4.2.1 from the 55000 simulations. In Figure 4.7 a) are reported the trajectories

obtained without considering the electrons in the metal surface.

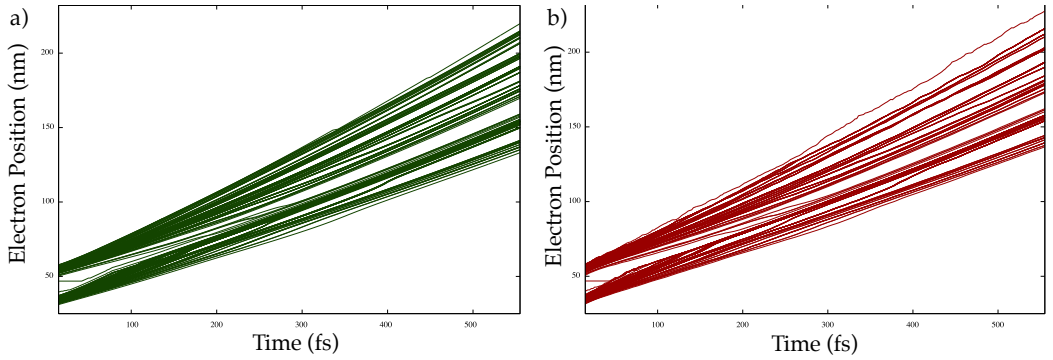

FIGURE 4.7: Bohmian trajectories obtained from simulation without ammeter a) and with ammeter b).

It is important to mention that the trajectories reconstructed in Figure 4.7 are obtained calculating the proportionality constant in Equation (4.12) not using the constant α found in Equation (4.10) but directly from the numerical simulations without ammeter. One can see in Figure 4.7 that there is an excellent agreement between the trajectories obtained from the weak measurement procedure and the exact ones.

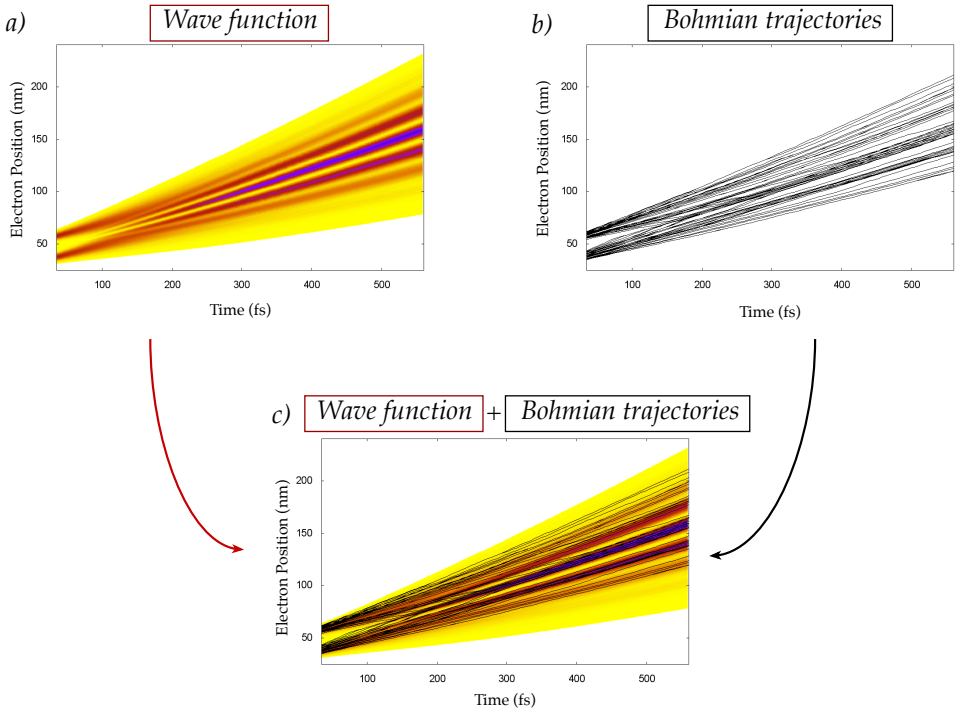

FIGURE 4.8: a) Same wave function reported in Figure 4.6. b) Trajectories obtain form the weak measurement procedure described in the text. c) Wave function and Bohmian trajectories in the same plot. As explained in the text, Bohmian trajectories are more dense near the maximum of the interference pattern while are less dense near the minimums.

As a final result, in Figure 4.8 is reported the comparison of the trajectories obtained from the procedure described in Section 4.2.1 with the same wave function depicted in Figure 4.6. It can be seen that, as expected from Bohmian Mechanics, the trajectories are more dense near the maximum and are less dense near the minimum of the interference pattern of the wave function.

Chapter 5

Time-Dependent Problems in Quantum Transport

The present Chapter is devoted to two problems in quantum transport. The two problems are neither strictly related to each other nor to the foregoing Chapter, but both rely on the techniques developed so far. In Section 5.1, inspired by a recent experiment [14], two particles scattering probabilities for a HOM-type (Hong-Ou-Mandel) experiment are analyzed. The time-dependent nature of this problem is addressed here, by considering as initial states localized wave packets instead of plane waves: this leads to surprising and interesting results. In Section 5.2, the time-dependent nature of the evolution of the conditional wave function is used in understanding the origin of quantum noise in mesoscopic system. As it will be seen, this analysis leads to a two-time measure of a quantum system. It will be argued that quantum noise is easily understood and computed within Bohmian Mechanics. All the discussion about the collapse done in Chapter 2.1, and the numerical example studied in Section 3.1, will be used extensively, as well as the numerical simulation techniques.

5.1 Detection at the Same Place of Two Simultaneously Emitted Electrons

The present Section is inspired by a recent experiment [14] in which two initial electrons wave packets (with opposite central momentums) are spatially localized at each side of a barrier. Then, after impinging upon a tunneling barrier, each wave packet splits into transmitted and reflected components. Contrarily to what is claimed in the literature, it is shown that the probability of detecting two (identically injected) electrons at the

same side of the barrier is different from zero in very common (single or double barrier) scenarios and for any type of (normalizable) state. For some particular resonant energies and wave packets, the transmitted and reflected components become orthogonal and the mentioned probabilities reproduce those values associated to distinguishable particles. These unexpected non-zero probabilities are still present when Coulomb interaction or non-symmetrical potential are considered. On the other hand, for initial wave packets close to Hamiltonian eigenstates, the usual zero probability for electrons at the same side of the barrier found in the literature is recovered. The far-reaching consequences of these non-zero probabilities in the evaluation of quantum noise in some scenarios is briefly addressed.

The present Section is divided as follows: Hereafter a brief introduction of the problem and the main motivations are given. In Section 5.1.1 the general expressions for the probabilities of detecting two electrons are defined. In Section 5.1.2, numerical test for typical tunneling scenarios with symmetric (Section 5.1.2.1) or non-symmetric (Section 5.1.2.2) potentials are presented. Among others, to go beyond the Fermi liquid picture of (non-interacting) electrons, a subsection (Section 5.1.2.3) is dedicated to investigate the effect of including Coulomb interaction among the electrons in a two-particle system. Additionally, a single barrier potential, which is a physical system closer to the experiment mentioned above, is also analyzed numerically (Section 5.1.2.4). In all the four scenarios discussed in Section 5.1.2 clear non-zero probabilities of detecting two electrons at the same side of the barrier are obtained. Section 5.1.3 is dedicated to summarize the main results achieved in the present Section and to indicate further consequences of the results obtained.

The ultimate reason why the quantum theory gives rise to a host of puzzling and fascinating phenomena is because many-particle quantum systems are defined in a high-dimensional and abstract configuration space. For example, in a system of identical particles, only those wave functions whose probability density in the configuration space remains unchanged under permutations of particles are acceptable. When this happens, it is said that the system has exchange interaction. One consequence of the exchange interaction is the Pauli repulsion, that forces electrons to avoid common positions.

In systems with stationary probability distributions, the effect of the exchange interaction in the scattering probability needs to be discussed only once. On the other hand, one can envision a richer phenomenology in scenarios with time-dependent probability distributions when, for example, electrons share common positions at the final time, but

not at the initial one. A typical scenario for discussing exchange and tunneling phenomena with time-dependent probability distributions is shown in the scheme of Figure 5.1. Two electrons with the same energy and opposite momentum are injected simultaneously from two different sources. During the interaction with a tunneling barrier, each wave packet splits into a transmitted and a reflected part. At the final time, transmitted and reflected components of different electrons share common positions and the effect of the exchange interaction becomes relevant. This typical scenario in the study of quantum transport in mesoscopic systems shown in Figure 5.1 can also be interpreted as a type of two-particle interference Hong-Ou-Mandel (HOM) experiment developed some time ago for photons [43].

Within the (Landau) Fermi liquid theory [47–49], these type of experiments are traditionally analyzed by describing the (quasi-particle) electrons as mono-energetic scattering states [16, 17]. The creation and annihilation operators in the second quantization formalism provide a very elegant and powerful formalism to include exchange interaction into tunneling problems. The (anti-symmetrical) initial state with one electron at each side of the barrier is defined by $|\Psi\rangle = \hat{a}_L^\dagger \hat{a}_R^\dagger |0\rangle$. The scattering theory for mono-energetic states predicts that the probability of finding one electron on the left and one electron on the right of the barrier is:

$$\mathcal{P}^S_{\mathcal{LR}} = |\langle 0|\hat{b}_L \hat{b}_R \hat{a}_L^\dagger \hat{a}_R^\dagger |0\rangle|^2 = 1, \tag{5.1}$$

where the upperindex S indicates scattering formalism. Equivalently, the probability of finding both electrons on the left is:

$$\mathcal{P}^S_{\mathcal{LL}} = |\langle 0|\hat{b}_L \hat{b}_L \hat{a}_L^\dagger \hat{a}_R^\dagger |0\rangle|^2 = 0 \tag{5.2}$$

and both electrons on the right is:

$$\mathcal{P}^S_{\mathcal{RR}} = |\langle 0|\hat{b}_R \hat{b}_R \hat{a}_L^\dagger \hat{a}_R^\dagger |0\rangle|^2 = 0. \tag{5.3}$$

Explicit computations of these probabilities are written in Appendix D. The same scattering formalism (with the proper commutations properties for the creation and annihilation operators) has been also used to successfully analyze this type of HOM experiments for photons [16–18, 78].

In principle, one can imaging two clear limits for the defined physical quasi-particle states. The first limit is assuming that the (quasi-)electrons are described by point-like states in real space (very narrow wave packets). This limit is obviously unphysical. The other limit is describing (quasi-)electrons by point-like states in the momentum space (infinitely space extended wave packets). In fact, this second limit has been demonstrated to be very successful in the literature. The celebrated scattering probabilities presented in Equation (5.1), Equation (5.2) and Equation (5.3) fit within this second limit. However, it seems reasonable to expect that the quasi-particle state that better captures the physics of the system described in Figure 5.1, is an initial state with some type of localization: an intermediate state between a point-like state in real space and point-like state in momentum space (probably, quite close to the typical point-like states in momentum state, but not exactly identical to them). In fact, the concept of quasi-particle wave packets was used by Kohn et al. [40] some years ago when analyzing the effect of the physical borders on localized (not infinite) systems. Equivalently, the concept of one-particle wave function that still captures many-body correlations has been deduced by Oriols et al. [68] through the use of the *conditional wave function*.

With this motivation, the mentioned two-particle scattering probabilities are analyzed using localized time-dependent wave packets as initial states. It is computed the probability of detecting two electrons at the same side of the barrier from the anti-symmetric solution of the time-dependent Schrödinger equation in the configuration space.[1] The main result is that in many scenarios (double and single barrier) the probability of finding two identically injected electrons at the same side of the barrier differs from zero (contrarily to what is claimed in the literature for time-independent scattering eigenstates, i.e. Equation (5.2) and Equation (5.3)). The main conclusions about these non-zero probabilities are developed for arbitrary shapes of the wave packets. On the other hand, typical Gaussian wave packets (including point-localized or fully-extended mono-energetic states as two limiting cases) are used to test and illustrate these non-zero probabilities with numerical results. These results are in agreement with the recent experiment of Bocquillon *et al.* [14], where unexpected non-zero probabilities of detecting

[1] The only assumption is that this type of two-electron interference experiments can be perfectly understood from non-relativistic quantum mechanics, as most of the electron problems in chemistry and solid-state physics.

both electrons at the same side of the barriers were obtained. They used single-electron sources in order to ensure that two spatially localized wave packets with disjoint support were prepared at the initial time. In addition, non-zero probabilities were also found when beams of electrons were used by Liu *et al.* in a similar experiment [56]. This suggests that these non-zero probabilities are not due to experimental spurious effects,[2] but due to the fundamental wave packet nature of the electrons present in such experiments. The study of the quantum transport by describing (quasi) electrons by wave packets was initiated by Loudon [55] when he considered the effect of the initial overlapping between two wave packets on the scattering probabilities (not after the interaction with the barrier as considered in this work, as depicted in Figure 5.1). However, this type of studied was mainly ignored in the literature.

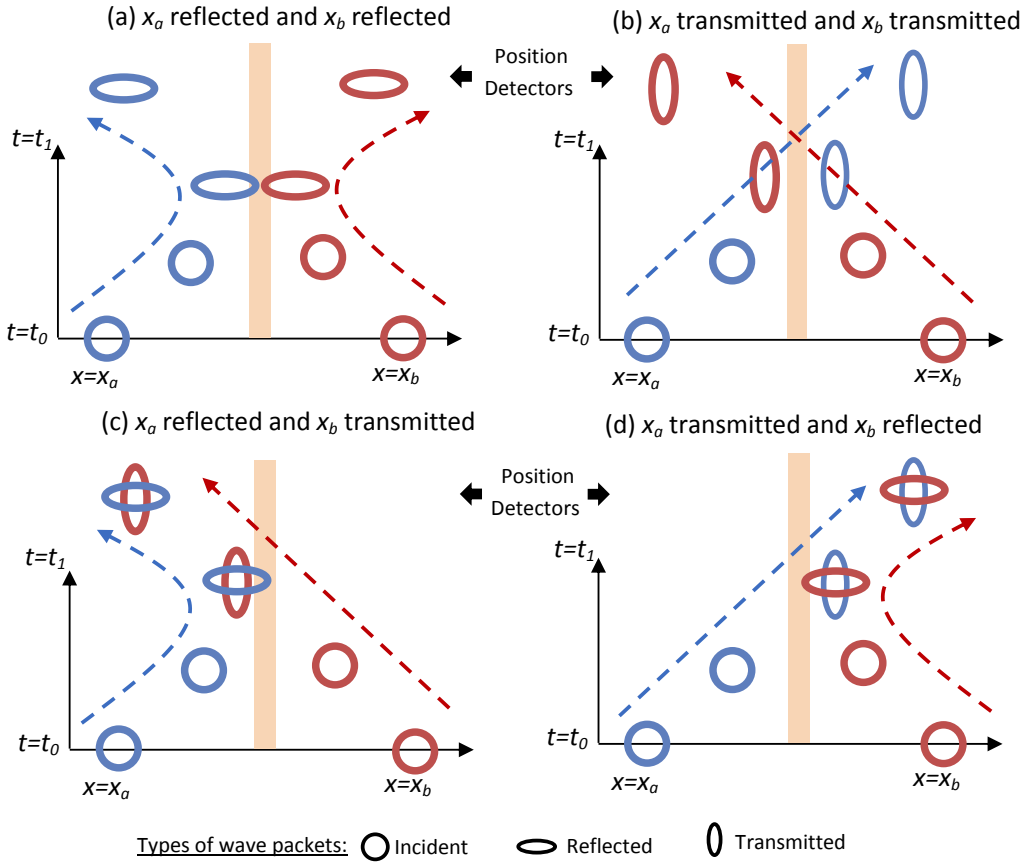

FIGURE 5.1: Two identically injected wave packets from the left x_a and from the right x_b of a scattering barrier. Solid regions represent the barrier region and shaded regions represent the particle detectors. (a) and (b) each particle is detected on a different side of the barrier at final time t_1 when the interaction with the barrier has almost finished. (c) and (d) both particles are detected on the same side of the barrier.

[2] *"The noise is not completely suppressed, in part because of non-idealities in the beam splitter's scattering matrix."*[56]. *"The states are not perfectly identical as shown by the fact that the dip does not go to zero."* [14].

5.1.1 Two-Particle Probabilities

Consider two particles injected from two different sources and impinging upon a tunneling barrier as indicated in Figure 5.1. In order to simplify the discussion, it is assumed that electrons have identical spin orientations. Each one is individually defined in a 1D physical space. The two-particle quantum system can be defined by the (orbital) wave function $\Phi \equiv \Phi(x_1, x_2, t)$ in the 2D configuration space. Such wave function is the solution of the many-particle (non-relativistic) Schrödinger equation:

$$i\hbar\frac{\partial\Phi}{\partial t} = \left[-\frac{\hbar^2}{2m}\frac{\partial^2}{\partial x_1^2} - \frac{\hbar^2}{2m}\frac{\partial^2}{\partial x_2^2} + V(x_1, x_2)\right]\Phi, \tag{5.4}$$

where m is the electron (boson) masses and $V(x_1, x_2)$ takes into account the two-particle Coulomb interaction between the electrons and also the one-particle interaction between one electron and a tunneling barrier. The exchange interaction is introduced in the shape of the initial wave function $\Phi(x_1, x_2, t_0)$. The anti-symmetrical/symmetrical (orbital) many-particle wave function for Fermions/Bosons is:

$$\Phi(x_1, x_2, t_0) = \frac{\phi_a(x_1, t_0)\phi_b(x_2, t_0) \mp \phi_a(x_2, t_0)\phi_b(x_1, t_0)}{\sqrt{2}}. \tag{5.5}$$

The above expression can be interpreted as the determinant/permanent of a 2×2 matrix constructed from the one-particle wave function $\phi_a(x, t_0)$ and $\phi_b(x, t_0)$ [22]. Hereafter, upper/lower signs correspond to (non-relativistic) massive Fermions/Bosons. Although electrons (Fermions) are mainly analyzed, probabilities will be also computed for (massive) Bosons. The initial one-particle wave functions $\phi_a(x, t_0)$ and $\phi_b(x, t_0)$ in Equation (5.5) are completely general. The only relevant condition for $\phi_a(x, t_0)$ is that its modulus square is normalizable to unity and it is totally located at the left of the barrier at time $t = t_0$. Identical conditions for $\phi_b(x, t_0)$ which is localized at the right. Additionally, according to the type of HOM experiment discussed here, both wave packets have opposite (central) momentum so that they impinge upon the barrier after a while, as depicted in Figure 5.1. By construction, the time evolution of $\Phi(x_1, x_2, t)$ using Equation (5.4) preserves the initial norm and the initial (anti)symmetry of the wave function.

It is possible to give an intuitive and simple argument of why it is reasonable to expect non-zero probability for finding both electrons at the same side of the barrier. Pauli principle forbids two fermions being at the same position with the same state [69–71]. However, a pertinent question appears: *When is reasonable the assumption that the reflected and transmitted states are exactly identical?* Certainly, both transmitted and

reflected states are identical when only one state is available in the spatial region where they coincide. This restriction on the available states is evident when the initial state has a unique (well-defined) energy E_k, i.e. a mono-energetic state. Then, because of the elastic nature of the interaction with the barrier (i.e. energy conservation), only one state at the right of the barrier and one at the left with the same energy E_k (and the pertinent momentum going outside from the barrier) are available at the final time. Nevertheless, as stated previously, here it is required a superposition of mono-energetic eigenstates (i.e. a wave packet) to describe an initial state with a spatially localized support outside of the barrier region. Then, in principle, there is the possibility of different time-evolutions for the transmitted and reflected components. In such time-dependent scenarios, one can expect probabilities different from zero (as mentioned before) as indicated in Figure 5.1 c) and Figure 5.1 d). Notice the different shapes of the reflected and transmitted wave packet in Figure 5.1.

Consider a particular time t_1 large enough so that the interaction with the barrier is almost finished, i.e. the probability presence inside the barrier region is negligible. Then, using Born's rule [22] in the 2D configuration space, $\{x_1, x_2\}$, the probability of detecting one electron at each side of the barrier (on regions $\mathcal{S}_{\mathcal{LR}}$ or $\mathcal{S}_{\mathcal{RL}}$ of the configuration space depicted in Figure 5.2 a)) at this time $t = t_1$ is:

$$\mathcal{P}_{\mathcal{LR}} = \int_{\mathcal{S}_{\mathcal{LR}}} |\Phi|^2 dx_1 dx_2 + \int_{\mathcal{S}_{\mathcal{RL}}} |\Phi|^2 dx_1 dx_2 = 2 \int_{\mathcal{S}_{\mathcal{LR}}} |\Phi|^2 dx_1 dx_2. \tag{5.6}$$

Due to the exchange symmetry, the wave function on $\mathcal{S}_{\mathcal{LR}}$ is identical to that on $\mathcal{S}_{\mathcal{RL}}$, as seen in Figure 5.2 a). The two integral in the left hand side of Equation (5.6) are exactly equal, so the total contribution of finding one electron at each side of the barrier is twice one of the integrals. Equivalently, the probability of detecting the two electrons at the left of the barrier (on the region $\mathcal{S}_{\mathcal{LL}}$ of the configuration space) is:

$$\mathcal{P}_{\mathcal{LL}} = \int_{\mathcal{S}_{\mathcal{LL}}} |\Phi|^2 dx_1 dx_2. \tag{5.7}$$

Finally, the probability of two electrons at the right of the barrier (on the region S_{RR}) is:

$$\mathcal{P}_{\mathcal{RR}} = \int_{\mathcal{S}_{\mathcal{RR}}} |\Phi|^2 dx_1 dx_2. \tag{5.8}$$

$\mathcal{P}_{\mathcal{LR}}$, $\mathcal{P}_{\mathcal{LL}}$ and $\mathcal{P}_{\mathcal{RR}}$ are defined as two-particle probabilities. In Figure 5.2 a) the probability presence of the initial two-particle state is plotted in the 2D configuration space. According to Equation (5.5), the wave packet $\phi_a(x_1,t_0)\phi_b(x_2,t_0)$ has its support on $\mathcal{S}_{\mathcal{LR}}$, while the wave packet $\phi_a(x_2,t_0)\phi_b(x_1,t_0)$ on $\mathcal{S}_{\mathcal{RL}}$. There is no initial probability presence in the other regions. The first relevant issue seen on the regions $\mathcal{S}_{\mathcal{LL}}$ and $\mathcal{S}_{\mathcal{RR}}$ of Figure 5.2 b) is that $\mathcal{P}_{\mathcal{LL}} \neq 0$ and $\mathcal{P}_{\mathcal{RR}} \neq 0$. The reason of these non-zero probabilities is explained in details in next Section. In general, it is important to notice that there is no reason to expect that the probability of detecting two electrons at the left of the barrier is equal to the probability of detecting them at the right, $\mathcal{P}_{\mathcal{RR}} \neq \mathcal{P}_{\mathcal{LL}}$ as seen in Figure 5.2 b).

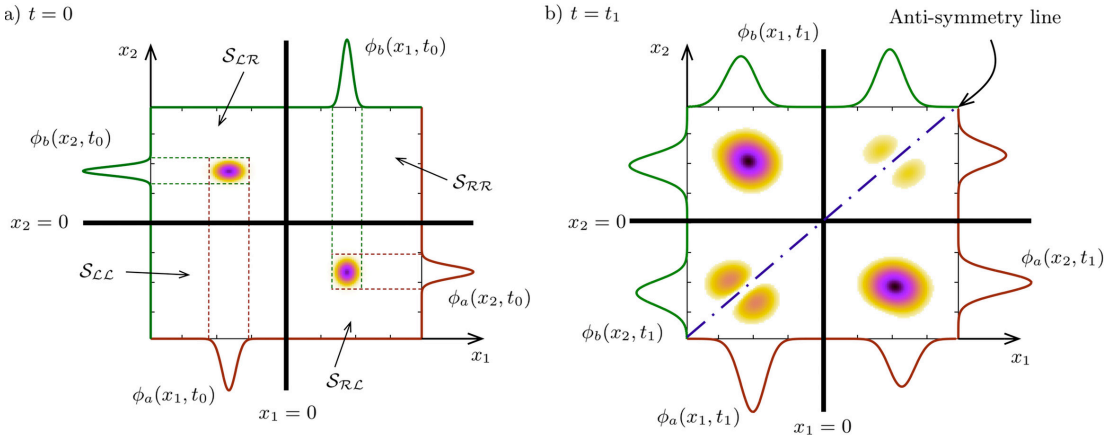

FIGURE 5.2: a) Modulus square of the wave function $\Phi(x_1,x_2,t_0)$ at the initial time t_0 in the configuration space $\{x_1,x_2\}$. With black solid line is represented the scattering barrier. Along the axes the single particle wave packet $\phi_a(x,t_0)$ are reported (red solid line), $\phi_b(x,t_0)$ (green solid line) for both variables (x_1 and x_2). The dotted line visualize how the anti-symmetrical wave function is constructed. The different regions of configuration space $\mathcal{S}_{\mathcal{LL}},\mathcal{S}_{\mathcal{LR}},\mathcal{S}_{\mathcal{RL}}$ and $\mathcal{S}_{\mathcal{RR}}$ are explicitly indicated. b) Modulus square of the wave function $\Phi(x_1,x_2,t_1)$ at the final time t_1 (such that the interaction with the barrier is already accomplished). Along the axes $\phi_a(x,t_1)$ (red solid line) and $\phi_b(x,t_1)$ (green solid line) for both variables $\{x_1,x_2\}$ are reported . With dashed dotted blue line the anti-symmetry line for Fermions is indicated. As asserted in the text the probabilities $\mathcal{P}_{\mathcal{RR}} \neq \mathcal{P}_{\mathcal{LL}} \neq 0$.

To certify the unavoidable fundamental (not spurious) origin of the non-zero probabilities for $\mathcal{P}_{\mathcal{LL}}$ and $\mathcal{P}_{\mathcal{RR}}$, hereafter, the same idealized conditions used in Refs. [12, 16, 17, 78] when they discuss the two-particle probabilities are considered. The two wave packets $\phi_a(x,t_0)$ and $\phi_b(x,t_0)$ are taken as identical as possible. In particular, the following three conditions are imposed:

- Condition (i): A separable potential $V(x_1,x_2)$ in Equation (5.4) without Coulomb interaction:

$$V(x_1,x_2) = V_B(x_1) + V_B(x_2), \tag{5.9}$$

where $V_B(x)$ is the symmetrical potential energy of a tunneling barrier, i.e. $V_B(x) = V_B(-x)$, with $x = 0$ at the center of the barrier region. See Figure 5.3 a).

- Condition (ii): All parameters of the initial wave packet a and b are identical, except for the initial central momentums which accomplishes $k_b = -k_a$ and central positions $x_b = -x_a$. See Figure 5.3 a).
- Condition (iii): Electrons are injected exactly at the same time.

Because of these conditions, as discussed in Appendix E, the two initial wave packets are defined with (almost) identical parameters. In particular, one has $g_a(k) = g_b(-k)$ where $g_a(k) = \langle \phi_a(x, t_0) | \psi_k(x) \rangle$ is the complex value that weights the superposition of the scattering states to build the wave packet $\phi_a(x, t_0)$. See Equation (E.4) in Appendix E. An identical definition is given for $g_b(k)$.

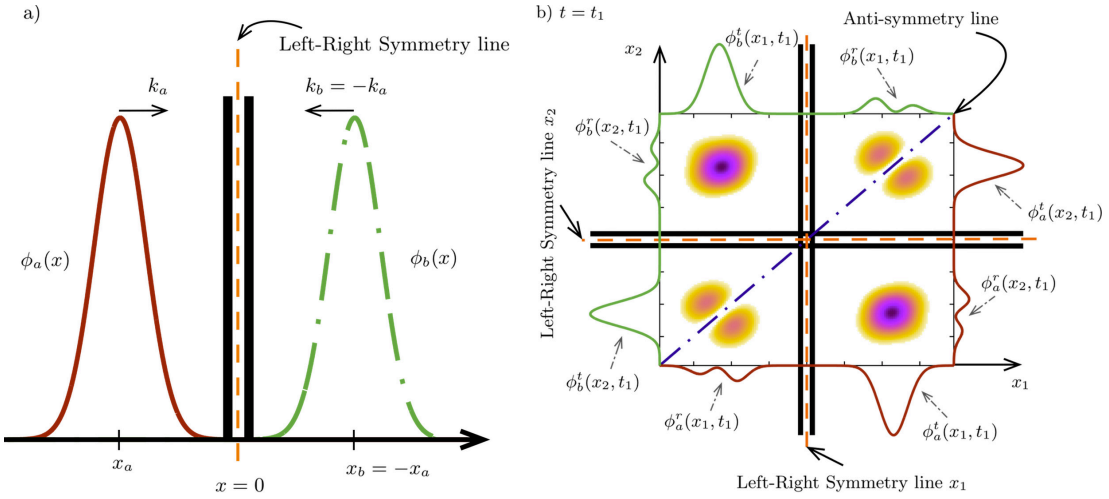

FIGURE 5.3: a) Schematic representation of the initial wave packets in the physical space under the conditions (i), (ii) and (iii). With black solid line the double barrier structure is depicted. With orange dashed line the Left-Right symmetry of the problem is depicted. With red solid line wave packet $\phi_a(x)$ centered in x_a and with momentum k_a is depicted. With green dashed dotted line the wave packet $\phi_b(x)$ centered in $x_b = -x_a$ and momentum $k_b = -k_a$ is reported . b) Modulus square of the wave function $\Phi(x_1, x_2, t_1)$ at the final time t_1 at the configuration points $\{x_1, x_2\}$. With dashed dotted blue line the anti-symmetry line for Fermions is indicated and with orange dashed lines the Left-Right symmetry for each degree of freedom (x_1 and x_2) is reported. Along the axes, the modulus square of the ϕ_a (red line) and ϕ_b (green line) wave functions are plotted for each degree of freedom (x_1 and x_2). The upper indices r or t indicate reflected or transmitted components, respectively.

Under these conditions, it is possible to anticipate the evolution of $\Phi(x_1, x_2, t)$ and also the origin of the non-zero probabilities for arbitrary wave packets. The initial (anti-symmetrical) wave function of two electrons $\Phi(x_1, x_2, 0)$ considered is defined by Equation (5.5). Since the time-evolution of Schrödinger equation satisfies the superposition principle, it is possible to discuss the time-evolution of $\phi_a(x_1, t_0)\phi_b(x_2, t_0)$ and

$\phi_a(x_2,t_0)\phi_b(x_1,t_0)$ independently. Then, since the Hamiltonian is separable, the evolution of $\phi_a(x,t)$ and $\phi_b(x,t)$ can be computed from two simpler single particle Schrödinger equations. At a time $t=t_1$, after the interaction with the barrier, each wave packet splits into two (non-overlapping) components:

$$\phi_a(x,t_1) = \phi_a^r(x,t_1) + \phi_a^t(x,t_1), \tag{5.10}$$

$$\phi_b(x,t_1) = \phi_b^r(x,t_1) + \phi_b^t(x,t_1), \tag{5.11}$$

where the upper indices r and t refer to the reflected and transmitted component of each wave packet (ϕ_a and ϕ_b), respectively. Then, the two particle wave function in the region of the configuration space $\mathcal{S}_{\mathcal{LL}}$ at $t=t_1$ is:

$$\Phi(x_1,x_2,t_1)\big|_{\mathcal{S}_{\mathcal{LL}}} = \frac{\phi_a^r(x_1,t_1)\phi_b^t(x_2,t_1) - \phi_a^r(x_2,t_1)\phi_b^t(x_1,t_1)}{\sqrt{2}}. \tag{5.12}$$

Notice that the region $\mathcal{S}_{\mathcal{LL}}$ was initially empty of probability, as seen in Figure 5.2 a). The initial wave packet $\phi_a(x_1,t_0)$ on $\mathcal{S}_{\mathcal{LR}}$ (which is identical to the one plotted in Figure 5.2 a)) evolves into the part $\phi_a^r(x_1,t_1)$ on $\mathcal{S}_{\mathcal{LL}}$ in Figure 5.3 b). Equivalently, the initial wave packet $\phi_b(x_2,t_0)$ in Figure 5.2 a) evolves into the part $\phi_b^t(x_2,t_1)$ on $\mathcal{S}_{\mathcal{LL}}$ in Figure 5.3 b). Identical explanations for the presence of $\phi_b^t(x_1,t_1)$ and $\phi_a^r(x_2,t_1)$ on $\mathcal{S}_{\mathcal{LL}}$. Clearly, since $\mathcal{P}_{\mathcal{LL}}$ in Equation (5.7) is computed from an integral of non-negative real numbers, the requirement for obtaining the result $\mathcal{P}_{\mathcal{LL}}=0$ in Equation (5.12) is that $\phi_a^r(x_1,t_1)\phi_b^t(x_2,t_1) = \phi_a^r(x_2,t_1)\phi_b^t(x_1,t_1)$ at all positions $\{x_1,x_2\}\in\mathcal{S}_{\mathcal{LL}}$.[3] This last condition can only be obtained when $\phi_b^t(x,t_1)=\phi_a^r(x,t_1)$ and $\phi_a^t(x,t_1)=\phi_b^r(x,t_1)$. On the contrary, if the transmitted and reflected wave packet components differ, i.e. if the time-evolution giving the transmitted component $\phi_a^t(x,t_1)$ is different from $\phi_b^r(x,t_1)$, then one gets $\Phi(x_1,x_2,t_1)\neq 0$, which implies $\mathcal{P}_{\mathcal{LL}}\neq 0$. Analogous consideration can be done for the configuration space region $\mathcal{S}_{\mathcal{RR}}$.

After discussing the origin of the non-zero probabilities, here a technical question is addressed that it will be tested later numerically. The conditions (i), (ii) and (iii) impose an additional symmetry on the problem. Apart from the intrinsic anti-symmetry of the wave function implicit in Equation (5.5), there is an additional Left-Right symmetry. This means that, being $x=0$ the center of the barrier region as depicted in Figure 5.3 a), the wave function under the separable Hamiltonians of Equation (5.9) has to satisfy $\Phi(x_1,x_2,t) = -\Phi(-x_1,-x_2,t)$ at all times. This additional symmetry implies that the

[3] By construction, only in the configuration space points $\{x_1,x_2\}\in\mathcal{S}_{\mathcal{LL}}$ such that $x_1=x_2$ the wave function is always strictly zero (see anti-symmetry line in the Figure 5.3 b)).

probability of detecting two electrons on the left is exactly equal to detect them on the right, i.e. $\mathcal{P}_{\mathcal{LL}} = \mathcal{P}_{\mathcal{RR}}$ as depicted in Figure 5.3 b). However, in general, when conditions (i), (ii) and (iii) are not satisfied, one has $\mathcal{P}_{\mathcal{LL}} \neq \mathcal{P}_{\mathcal{RR}}$ as depicted in the preceding Figure 5.2 b).

The exact values of $\mathcal{P}_{\mathcal{LR}}$, $\mathcal{P}_{\mathcal{LL}}$ and $\mathcal{P}_{\mathcal{RR}}$ depend on the effective overlapping between $\phi_a^t(x,t_1)$ and $\phi_b^r(x,t_1)$. In Appendix E analytical calculations are developed for the range of values that the probabilities Equation (5.6)-Equation (5.8) can take when conditions (i), (ii) and (iii) are assumed. When reflected and transmitted wave packets are identical as indicated in Equation (E.13), expressions (5.6)-(5.8) can be rewritten as:

$$\mathcal{P}_{\mathcal{LL}}^{M} = \mathcal{P}_{\mathcal{RR}}^{M} = RT \mp RT, \tag{5.13}$$

$$\mathcal{P}_{\mathcal{LR}}^{M} = (R \pm T)^2, \tag{5.14}$$

which corresponds to the well-known result $\mathcal{P}_{\mathcal{LL}}^{M} = \mathcal{P}_{\mathcal{LL}}^{S} = 0$, $\mathcal{P}_{\mathcal{RR}}^{M} = \mathcal{P}_{\mathcal{RR}}^{S} = 0$ and $\mathcal{P}_{\mathcal{LR}}^{M} = \mathcal{P}_{\mathcal{LR}}^{S} = 1$ mentioned in Equations (5.1), (5.2) and (5.3) for Fermions. Additionally, one has $\mathcal{P}_{\mathcal{LL}}^{M} = \mathcal{P}_{\mathcal{RR}}^{M} = 2RT$ and $\mathcal{P}_{\mathcal{LR}}^{M} = (R-T)^2$ for Bosons. Notice that the sum of the three probabilities is equal to one (for Fermions or Bosons) because a unitary evolution is considered. The upper index M denotes that the overlapping between the transmitted and reflected components is maximum. In summary, it has been tested that the general definitions of the two-particle probabilities in Equations (5.6)-(5.8) exactly reproduce, as a particular example, the results found in the literature for scattering states in Refs. [16, 17, 51, 52, 78].

For other scenarios, for example a double barriers with wave packets with resonant energies, it is shown in Appendix E that the transmitted and reflected components become orthogonal. Then, the probabilities (5.6)-(5.8) in this type of experiments at resonances can be written as:

$$\mathcal{P}_{\mathcal{LL}}^{m} = \mathcal{P}_{\mathcal{RR}}^{m} = RT, \tag{5.15}$$

$$\mathcal{P}_{\mathcal{LR}}^{m} = R^2 + T^2. \tag{5.16}$$

where the upper index m here indicates that the overlapping between transmitted and reflected components is zero (minimum). Again, the sum of the probabilities is one because of the unitary evolution. These last probabilities $\mathcal{P}_{\mathcal{LL}}^{m}, \mathcal{P}_{\mathcal{RR}}^{m}$ and $\mathcal{P}_{\mathcal{LR}}^{m}$ show no

difference between Fermions or Bosons. In fact, these results are identical to the probability of distinguishable particles. In conclusion, even with both electrons at the same position at the same time, the Pauli principle has no effect in these HOM scenarios because the wave nature of electrons is described by different (orthogonal) wave functions. It is important to emphasize that, in general, the two-particle probabilities in Equations (5.6)-(5.8) can take any value between the limits imposed by Equations (5.13)-(5.14) and Equations (5.15)-(5.16). It is important to stress that all the previous results are valid for any shape of quasi-particle wave packets.

5.1.2 Numerical Results

This section is dedicated to confirm numerically the predicted non-zero probabilities in different and general scenarios. The procedure for the numerical computation of the probabilities $\mathcal{P}_{\mathcal{LR}}$, $\mathcal{P}_{\mathcal{LL}}$ and $\mathcal{P}_{\mathcal{RR}}$ is the following. First, time-evolve an (anti-symmetrical) initial state, defined by Equation (5.5), with the Schrödinger equation in the configuration space. Second, at the final time t_1, compute the different probabilities Equations (5.6)-(5.8) from the modulus square of the wave function through Born's rule, without any approximation.

5.1.2.1 Two-Particle Scenario with a Separable and Symmetrical Double Barrier Potential

Consider the double barrier drawn in Figure 5.3 a) and also in the inset of Figure 5.4. The potential profile is built by two barriers of 0.4 eV of height and 0.8 nm of width between a quantum well of 5.6 nm. This potential profile has Left-Right symmetry. The $x = 0$ is situated at the center of the quantum well. The (effective) mass of the electrons (m) is 0.067 times the free electron mass. The first resonant energy of such structure is $E_R = 0.069\ eV$. At the initial time t_0, the initial state is defined for numerical convenience by two Gaussian wave packets, $\phi_a(x, t_0)$ and $\phi_b(x, t_0)$ [22] whose spatial support is located at the left and right of the barrier, respectively. Notice that such Gaussian wave packets have point-localized or fully-extended mono-energetic states as two limiting cases. Both wave packets have the same central energy $E_a = E_b$, but opposite central wave vectors $k_b = -k_a$ and central positions $x_a = -x_b$. In Figure 5.4 the time evolutions of expressions (5.6)-(5.8) are depicted. First, it can be observed that for a wave packet whose energy is far from the resonant energy E_R, one obtains $\mathcal{P}^S_{\mathcal{LR}} \equiv \mathcal{P}^M_{\mathcal{LR}} = 1$, $\mathcal{P}^S_{\mathcal{LL}} = \mathcal{P}^M_{\mathcal{LL}} = 0$ and $\mathcal{P}^S_{\mathcal{RR}} = \mathcal{P}^M_{\mathcal{RR}} = 0$, at $t_1 = 0.7\ ps$, as predicted by and expressions (5.1)-(5.3) and also by expressions (5.13)-(5.14). However, for the resonant energy $E_a = E_b = E_R$ one gets the results $\mathcal{P}_{\mathcal{LR}} \equiv \mathcal{P}^m_{\mathcal{LR}} = 1-2RT$, $\mathcal{P}_{\mathcal{LL}} \equiv \mathcal{P}^m_{\mathcal{LL}} = RT$ and

$\mathcal{P}_{\mathcal{RR}} \equiv \mathcal{P}^m_{\mathcal{RR}} = RT$ that correspond to the values of indistinguishable particles predicted by expressions (5.15)-(5.16). Notice that, to test these last expressions numerically, this potential profile and wave packets give $T = 0.806$ and $R = 0.194$, where R and T are the single particle reflection and transmission coefficients. As explained (see Appendix E), the latter set of probabilities correspond to a scenario in which the transmitted and reflected components are orthogonal. In other words, the transmitted wave packet is basically built by a superposition of resonant scattering states, while the reflected one by mainly non-resonant scattering states.

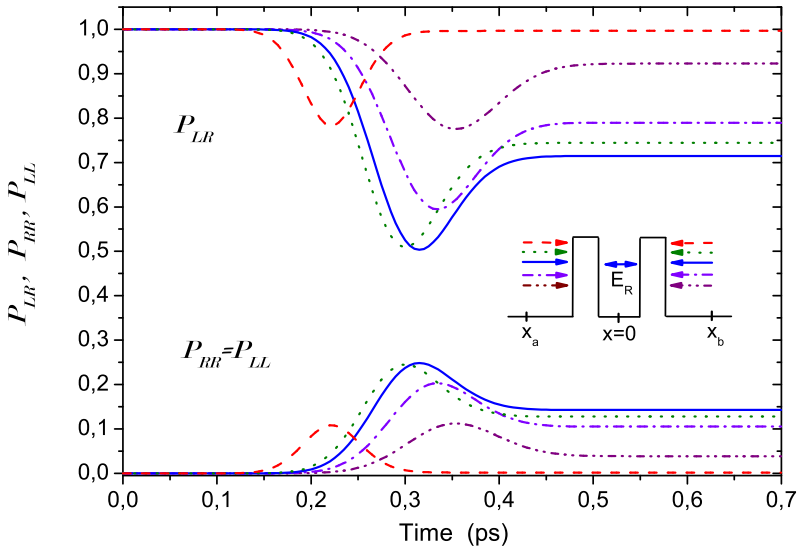

FIGURE 5.4: Time evolution of $\mathcal{P}_{\mathcal{LR}}$ (upper lines) and $\mathcal{P}_{\mathcal{LL}} = \mathcal{P}_{\mathcal{RR}}$ (lower lines) from $\Phi(x_1, x_2, t)$ built by two initial wave packets located at $x_a = -175$ nm and $x_b = 175$ nm with opposite momentums and equal spatial dispersions $\sigma_a = \sigma_b = 35$ nm. The energies are $E_a = E_b = 0.12$ eV (red dashed line), $E_a = E_b = 0.085$ eV (green dot line), $E_a = E_b = E_R = 0.069$ eV (blue solid line), $E_a = E_b = 0.06$ eV (dash dot violet line) and $E_a = E_b = 0.05$ eV (dash dot dot purple). The inset shows the potential profile.

As mentioned in Section 5.1, dealing with the time-dependent Schrödinger equation implies that the results depends also on the initial wave packet shape. In Figure 5.5, the dependence of the two-particle probabilities of Figure 5.4 on the *size* of the initial wave packet is studied. The size of the initial wave packet is defined as the double of the full width at half maximum (FWHM) of the probability presence of the Gaussian wave packet at $t = t_0$. Such size can be related with the spatial dispersion σ_x of the initial wave packet from the relation $2 \times FWHF = 4\sqrt{\ln(2)}\sigma_x$. In the limit of $\sigma_x \to \infty$, a wave packet approaches to a scattering state.

The maximum wave packet dimensions considered in Figure 5.5 are much larger than typical reservoir sizes in quantum transport with semiconductors [81] and one can clearly see $\mathcal{P}_{\mathcal{LL}} = \mathcal{P}_{\mathcal{RR}} \neq 0$. In addition, if one considers barriers much higher than 0.4 eV,

the resonance becomes much sharper and wave packets with $\sigma_x \approx 1\ \mu m$ still show $\mathcal{P}_{\mathcal{LL}} = \mathcal{P}_{\mathcal{RR}} \neq 0$.

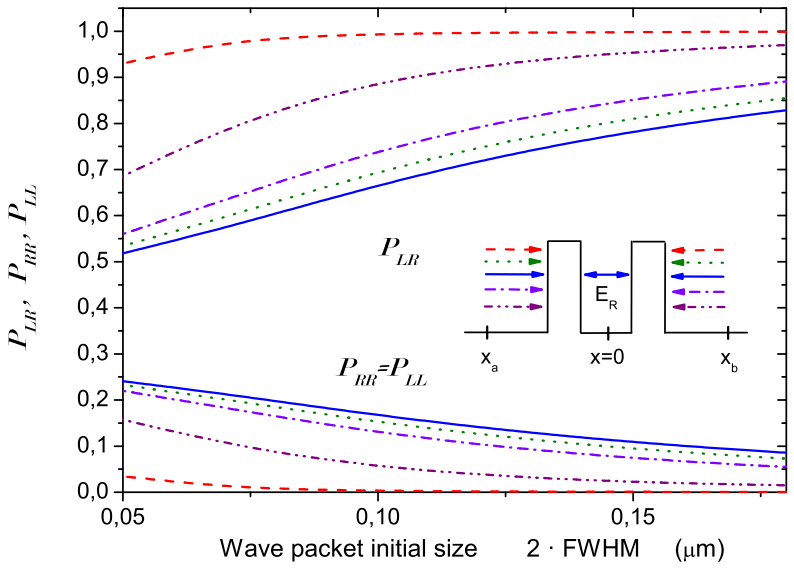

FIGURE 5.5: The probabilities of $\mathcal{P}_{\mathcal{LR}}$ (upper lines) and $\mathcal{P}_{\mathcal{LL}} = \mathcal{P}_{\mathcal{RR}}$ (lower lines) from $\Phi(x_1, x_2, t_1)$ at time $t_1 = 0.7$ ps with the same initial wave packets and energies of Figure 5.4 but with variable spatial dispersion $\sigma_x = \sigma_a = \sigma_b$. The inset shows the potential profile.

5.1.2.2 Two-Particle Scenario with a Separable and Non-Symmetrical Double Barrier Potential

Here it is analyzed which is the role of symmetry of the potential in the computation of non-zero probabilities. In typical mesoscopic systems, the potential profile is not Left-Right symmetrical. For example, when an external battery is included. It implies an asymmetric potential profile, as indicated in the inset of Figure 5.6. Then, the conditions (i), (ii) and (iii) are not applicable and the two-particle probabilities (5.6)-(5.8) present an even more rich phenomenology.

Consider the same scenario studied in Figure 5.4 with an applied bias of $0.05\ V$ (see the inset of Figure 5.6). The kinetic energy of the a-wave packet is $E_a = E_R = 0.043\ eV$ equal to the new resonant energy. The kinetic energy of the b-wave packet is, $E_b = E_R = (0.043 + 0.05)\ eV$. Different initial positions are selected to ensure that the wave packets coincide in the barrier region, at the time $x_a/v_a^c = x_b/v_b^c$, with the initial central velocity $v_a^c = \hbar k_a^c/m = 4.75\ 10^5\ m/s$ and $v_b^c = -4.88\ 10^5\ m/s$. In any case, at time $t_1 = 0.8\ ps$, it is found a rich phenomenology for the two-particle probabilities with $\mathcal{P}_{\mathcal{LL}} \neq \mathcal{P}_{\mathcal{RR}} \neq 0$. As mentioned, the additional Left-right symmetry is not present.

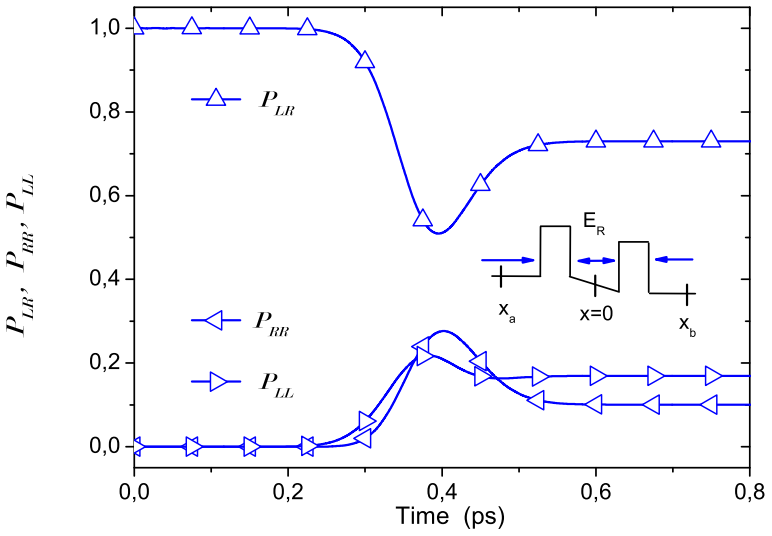

FIGURE 5.6: Time evolution of $\mathcal{P}_{\mathcal{LR}}$, $\mathcal{P}_{\mathcal{LL}}$ and $\mathcal{P}_{\mathcal{RR}}$ (solid blue lines) for $\Phi(x_1, x_2, t)$ built from two initial wave packets located at $x_a = -175$ nm and $x_b = 257$ nm with equal spatial dispersions $\sigma_a = \sigma_b = 35\ nm$. The inset shows the potential profile.

5.1.2.3 Two-Particle Scenario with Non-Separable Double Barrier Potential

At this point, it is analyzed if the assumption of quasi-particle is a fundamental issue in the non-zero probabilities. In order to go beyond the Fermi liquid theory it is computed the Coulomb interaction among two electrons in the type of HOM configuration considered here. It is considered the wave functions $\Phi(x_1, x_2, t)$ solutions of Equation (5.4) with the same initial expression (5.5) but with a non-separable potential:

$$V(x_1, x_2) = V_B(x_1) + V_B(x_2) + C \cdot V_C(x_1, x_2), \tag{5.17}$$

being $V_C(x_1, x_2)$ the Coulomb interaction between electrons. The constant C takes into account the strength of the interacting Hamiltonian (i.e. $C = 0$ means separable Hamiltonian). The following expression is used:

$$V_C(x_1, x_2) = \frac{q^2}{4\pi\epsilon_r\epsilon_0} \frac{1}{\sqrt{(x_1 - x_2)^2 + a_C^2}} f(x_1, x_2), \tag{5.18}$$

with $\epsilon_r = 11.6$ and ϵ_0 is the free space dielectric constant. To avoid numerical irrelevant complications, the parameter $a_C = 1.2\ nm$ avoids the divergence character of the Coulomb potential when $x_1 = x_2$. The function $f(x_1, x_2) = exp(-(x_1^2 + x_2^2)/\sigma_C)$, with $\sigma_C = 5\ nm$, allows us to define the Coulomb interaction only in the active region of the device. These conditions mimic the solution of the 3D Poisson equation in a resonant

tunneling diode with screening [67].[4] In Figure 5.7, it is plotted the potential $V(x_1, x_2)$ defined in Equation (5.17) with $C = 5$, and with the same potential barriers $V_B(x)$ discussed in Section 5.1.2.1. The diagonal line $x_1 = x_2$ shows the region of maximum Coulomb potential. The Coulomb potential in Figure 5.7 is still symmetrical and so the Left-Right symmetry is preserved.

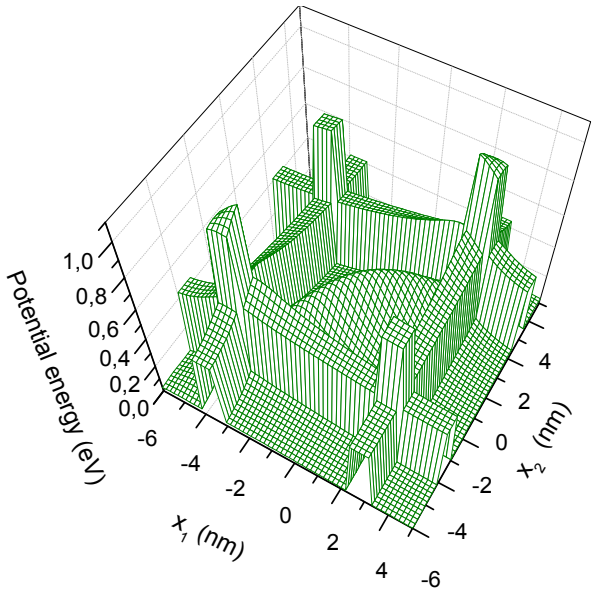

FIGURE 5.7: Potential $V(x_1, x_2)$ in the configuration space $\{x_1, x_2\}$ with Coulomb interaction in a double barrier when C=5.

In Figure 5.8 and Figure 5.9 the two-particle probabilities for an energy $E_a = E_b = E_R = 0.069\ eV$ and $E_a = E_b = 0.06\ eV$ respectively, are plotted for different values of the constant C defined in Equation (5.17). Exactly the same double barrier defined in Section 5.1.2.1 is considered with the same wave packets with $\sigma_x = 35\ nm$ and $x_a = -175\ nm$ and $x_b = 175\ nm$. So, the consideration of more realistic scenarios with Coulomb interaction (not directly included in the analytical computations of Appendix D and Appendix E) does not tend to recover the results $\mathcal{P}^M_{\mathcal{LL}} = \mathcal{P}^S_{\mathcal{LL}} = 0$, $\mathcal{P}^M_{\mathcal{RR}} = \mathcal{P}^S_{\mathcal{RR}} = 0$ and $\mathcal{P}^M_{\mathcal{LR}} = \mathcal{P}^S_{\mathcal{LR}} = 1$ mentioned in Equations (5.1)-(5.3), but just the contrary. Again, $\mathcal{P}_{\mathcal{LR}} \neq 1$ and $\mathcal{P}_{\mathcal{LL}} = \mathcal{P}_{\mathcal{RR}} \neq 0$.

5.1.2.4 Two-Particle Scenario with Single Barrier Potential

One could argue that the anomalous probabilities $\mathcal{P}_{\mathcal{LL}}$ and $\mathcal{P}_{\mathcal{RR}}$ will not be accessible in a single barrier scenario because of the poorer energy dependence of the transmission and reflection coefficients. Here a single barrier is used instead of the double barrier potential considered above. This single barrier scenario is much closer to the experiments mentioned in Section 5.1 [14, 56]. In Figure 5.10 the two-particle probabilities in the

[4] Equation (5.18) is exactly the same expression used in Section 2.3.1.1.

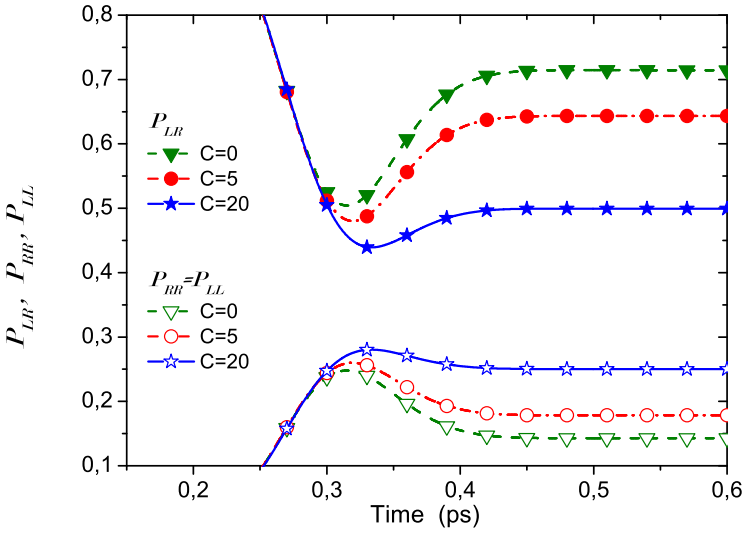

FIGURE 5.8: Time evolution of $\mathcal{P}_{\mathcal{LR}}$ (upper lines) and $\mathcal{P}_{\mathcal{LL}} = \mathcal{P}_{\mathcal{RR}}$ (lower lines) from $\Phi(x_1, x_2, t)$ built by two initial wave packets located at $x_a = -175$ nm and $x_b = 175$ nm with opposite momentums, equal spatial dispersions $\sigma_a = \sigma_b = 35$ nm and equal energy $E_a = E_b = 0.069$ eV. The values of the constant C in Equation (5.17) are $C = 0$ (green dashed line with triangles), $C = 5$ (red dashed dot line with circles), and $C = 20$ (blue solid line with stars).

case of a single barrier of width 12.4 nm and height 0.04 eV are plotted for three different energies as a function of the initial wave packet size. Again, only for initial wave packets with a very large spatial support (close to a Hamiltonian eigenstate) the results $\mathcal{P}^M_{\mathcal{LL}} = \mathcal{P}^S_{\mathcal{LL}} = 0$, $\mathcal{P}^M_{\mathcal{RR}} = \mathcal{P}^S_{\mathcal{RR}} = 0$ and $\mathcal{P}^M_{\mathcal{LR}} = \mathcal{P}^S_{\mathcal{LR}} = 1$ are recovered. In particular, in Figure 5.10 is plotted the energy $E_a = E_b = E_{T=1/2} = 0.045$ eV for the incident wave packets, where $E_{T=1/2}$ means that half of the wave packet is transmitted and half is reflected, in other words that the barrier works effectively as an electron beam splitter.

As shown for the double-barrier structure, also in the case of a single barrier, the probabilities $\mathcal{P}_{\mathcal{LL}} = \mathcal{P}_{\mathcal{RR}}$ are different from zero depending on the wave packet size. The divergence from the results mentioned in Equations (5.1)-(5.3) is even more dramatic when considering Coulomb interaction among electrons. In Figure 5.11 the probabilities $\mathcal{P}_{\mathcal{LR}}$, $\mathcal{P}_{\mathcal{LL}}$ and $\mathcal{P}_{\mathcal{RR}}$ are plotted as a function of time for different values of the interaction constant C in Equation (5.18). The same values reported in Section 5.1.2.3 are used. The larger value of C provides the larger discrepancies with the values $\mathcal{P}^M_{\mathcal{LL}} = \mathcal{P}^S_{\mathcal{LL}} = 0$, $\mathcal{P}^M_{\mathcal{RR}} = \mathcal{P}^S_{\mathcal{RR}} = 0$ and $\mathcal{P}^M_{\mathcal{LR}} = \mathcal{P}^S_{\mathcal{LR}} = 1$.

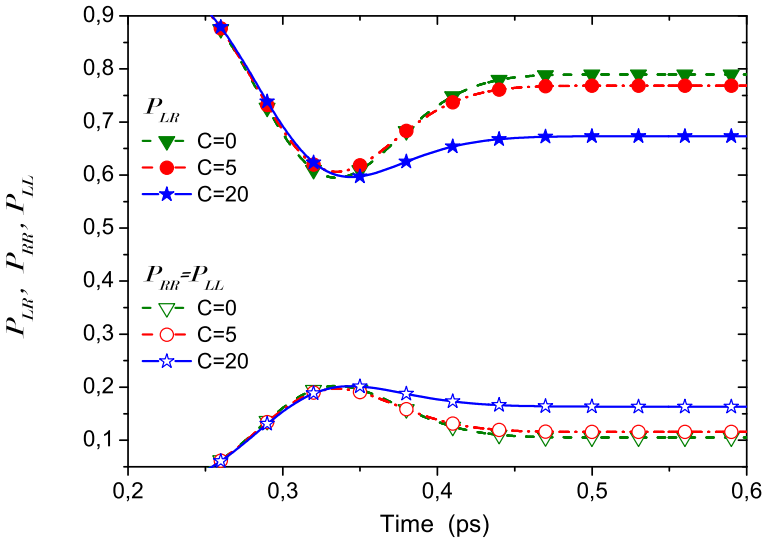

FIGURE 5.9: Time evolution of $\mathcal{P}_{\mathcal{LR}}$ (upper lines) and $\mathcal{P}_{\mathcal{LL}} = \mathcal{P}_{\mathcal{RR}}$ (lower lines) from $\Phi(x_1, x_2, t)$ built by two initial wave packets located at $x_a = -175$ nm and $x_b = 175$ nm with opposite momentums, equal spatial dispersions $\sigma_a = \sigma_b = 35\ nm$ and equal energy $E_a = E_b = 0.06\ eV$. The values of the constant C in Equation (5.17) are $C = 0$ (green dashed line with triangles), $C = 5$ (red dashed dot line with circles), and $C = 20$ (blue solid line with stars).

5.1.3 Final Considerations

In the previous theoretical and numerical examples it has been considered two electrons injected simultaneously from both sides of a tunneling barrier including exchange interaction. This is a typical scenario for quantum transport in electron devices and it can be also considered as a type of interference HOM experiment. Ia has been taken into account explicitly quasi-particle wave packets to describe electrons. Electrons are initially associated to wave packets whose supports are located either at the left or at right of the barrier. In the literature it is argued that the probability of detecting the two electrons at the same side of the barrier is zero [12, 16, 17, 78]. On the contrary, the discussion above demonstrate analytically and numerically that for any type of wave packet non-zero values for such probabilities are achieved.

The physical origin of this non-zero probability is due to the different time-evolution suffered by the reflected and transmitted components of the wave packet. This difference between components appears in quite common scenarios (with single or double barrier potentials, with or without Coulomb interaction). For some particular resonant energies, the transmitted and reflected components are so different that they indeed become orthogonal. Then, the two-particle probabilities of these electrons with exchange interaction reproduce the probabilities predicted for distinguishable electrons. On the

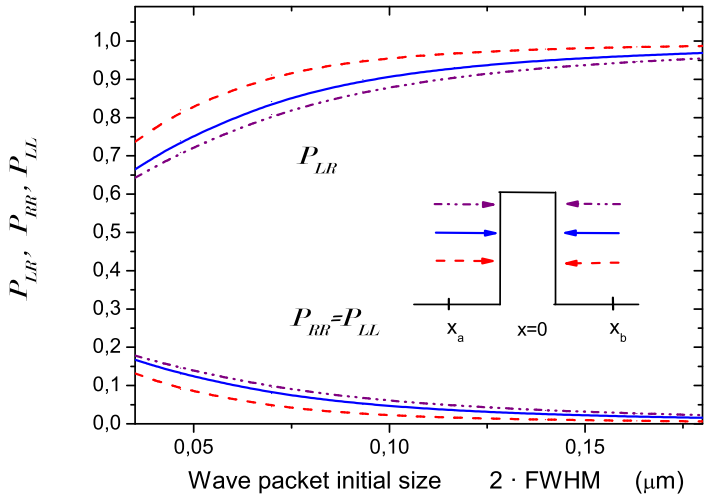

FIGURE 5.10: The probabilities of $\mathcal{P}_{\mathcal{LR}}$ (upper lines) and $\mathcal{P}_{\mathcal{LL}} = \mathcal{P}_{\mathcal{RR}}$ (lower lines) from $\Phi(x_1, x_2, t_1)$ at time $t_1 = 0.8$ ps with initial wave packets located at $x_a = -175$ nm and $x_b = 175$ nm with opposite momentums and with variable spatial dispersion $\sigma_x = \sigma_a = \sigma_b$. The energies are $E_a = E_b = 0.035\ eV$ (red dashed line), $E_a = E_b = E_{T=1/2} = 0.045\ eV$ (blue solid line) and $E_a = E_b = 0.055\ eV$ (dash dot dot purple line). The inset shows the potential profile of a single barrier.

contrary, for initial wave packets with a large spatial support (approaching to a Hamiltonian eigenstate), the usual two-particle probabilities for indistinguishable particles reported in the literature [12, 16, 17, 78] are exactly reproduced.

The non-zero probabilities presented above suggest a fundamental (not spurious) origin of the unexpected probabilities found in the experiments of Refs. [14, 56]. It is important to emphasize that the non-zero probabilities discussed analytically (and tested numerically) have far-reaching consequences. In fact, in some scenarios, the celebrated Landauer-Büttiker model [16, 17, 51, 52] for quantum noise needs to be revisited. This model was developed within the (Landau) Fermi liquid theory [47–49] under the assumptions of quasi-particle mono-energetic initial states. This last assumption leads to expressions (5.1)-(5.3) with zero-probabilities of detecting electrons at the same side. It has been explicitly shown that the consideration of quasi-particle wave packets shows non-zero probabilities in quite common scenarios. It is important to underline that the consequence on noise has been preliminary addressed in [59], where it is explicitly shown that the unexpected non-zero probability of several particles are still (experimentally) accessible for a many-particle system in the limit of low phase-space density (high temperature). For high phase-space density (low temperature) the mentioned probabilities tend to zero and the fluctuation-dissipation theorem [44, 64] is satisfied. In addition, it has been shown that the inclusion of the Coulomb interaction between electrons (going beyond the Fermi liquid theory) does also exhibit this unexpected non-zero probabilities.

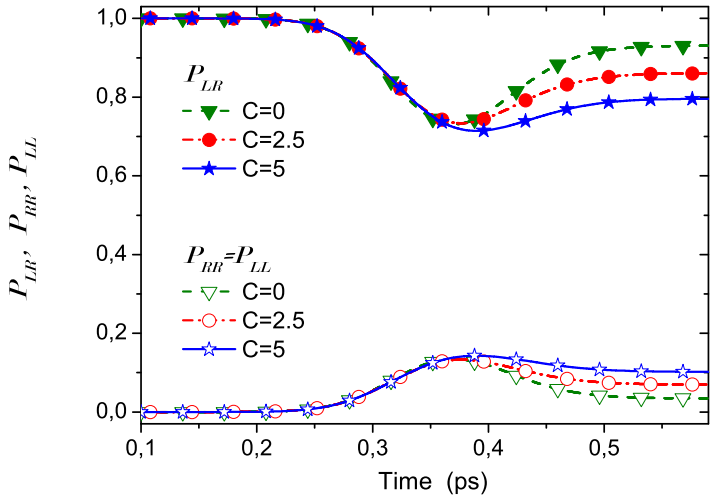

FIGURE 5.11: The probabilities of $\mathcal{P}_{\mathcal{LR}}$ (upper lines) and $\mathcal{P}_{\mathcal{LL}} = \mathcal{P}_{\mathcal{RR}}$ (lower lines) from $\Phi(x_1, x_2, t)$ built by two initial wave packets located at $x_a = -175$ nm and $x_b = 175$ nm with opposite momentums, equal spatial dispersions $\sigma_a = \sigma_b = 35\ nm$ and equal energy $E_a = E_b = E_{T=1/2} = 0.045\ eV$. The values of the constant C in Equation (5.17) are $C = 0$ (green dashed line with triangles), $C = 2.5$ (red dashed dot line with circles), and $C = 5$ (blue solid line with stars).

5.2 Quantum Noise with Bohmian Mechanics Simulations

As mentioned at the beginning of this Chapter, in this Section, a different topic is treated. In particular it is analyzed quantum noise properties of electron devices from Bohmian point of view. It will be argued that quantum noise is easily understood and computed within Bohmian Mechanics.

Historically, the definition of noise was related to the sound: A noise is an unwanted, unpleasant and confusing type of sound.[5] However, such definition is ambiguous. What does it mean unwanted, unpleasant or confusing? An attempt to provide a more academic definition comes from music: Noise is a non-harmonious or discordant group of sounds. Again, however, the definition is not free from ambiguities because one man's noise is another man's music [52].

A more scientific definition closer to electrical devices comes from communications: A noise is an electric disturbance that interferes with or prevents reception of a signal or of information. For example, the buzz in a telephone call. Thus, one realizes that once a precise definition of what is a signal is given, the meaning of what is noise becomes perfectly clear: It is the difference between the measured value and the signal.

[5] In fact, the word noise is etymologically derived from the Latin word *nausea*, meaning seasickness.

5.2.1 Quantum Noise in Electrical Devices from an Experimental Point of View

As discussed above, the answer to what is noise in electrical devices depends on the definition of the electrical signal. For most DC applications, the signal is just the time-averaged value of the current. For frequency applications, the signal is equivalently defined as a time-averaged value, but using a shorter time interval (related to the inverse of the operating frequency). In other applications, mainly digital applications, the signal is related to the time-averaged value of the voltage in a capacitor. Hereafter, it will be assumed that the electrical signal is the DC value of the current, referenced by the symbol $\langle I \rangle$. All fundamental and practical issues discussed here for the DC signal (and its noise) can be easily and straightforwardly extended to those other types of electrical signals.

What is measured in a laboratory for the DC signal is the time-average value of the instantaneous current $I(t)$ in a unique device during a large period of time T:

$$\langle I \rangle = \lim_{T \to \infty} \frac{1}{T} \int_0^T I(t) dt. \tag{5.19}$$

Once the signal $\langle I \rangle$ is defined as the DC value, in principle, the noise can be quantified by time-averaging the difference between the measured value of the current $I(t)$ and the signal in a unique device:

$$\triangle I^2 = \lim_{T \to \infty} \frac{1}{T} \int_0^T (I(t) - \langle I \rangle)^2 dt, \tag{5.20}$$

where the square of the difference avoids positive and negative cancellations.

At this point, it is very important to realize that $I(t)$ presents very rapid fluctuations that cannot be captured by the standard laboratory apparatus. Any experimental setup, that measures the current fluctuations, behaves as a low-pass filter (i.e. the current fluctuations at frequencies higher than the apparatus cut-off frequency are not measured). Therefore, the experimentally accessible information about the current fluctuations is not given by Equation (5.20), but by the power spectral density of the fluctuations $S(\omega)$ (and its related magnitudes). From the Wiener-Khinchine relation, the power spectral density can be defined as the Fourier transform of the time-average definition of this autocorrelation function $\triangle R(\tau)$:

$$\triangle R(\tau) = \lim_{T\to\infty} \frac{1}{T} \int_0^T \triangle I(t_1)\triangle I(t_1+\tau)dt_1, \tag{5.21}$$

where $\triangle I(t) = I(t) - \langle I \rangle$. A straightforward development shows that Equation (5.21) can be rewritten as $\triangle R(\tau) = R(\tau) - \langle I \rangle^2$ with:

$$R(\tau) = \lim_{T\to\infty} \frac{1}{T} \int_0^T I(t_1)I(t_1+\tau)dt_1. \tag{5.22}$$

Then, the Fourier transform of Equation (5.21) gives the noise power spectral density $S(\omega)$:

$$S(\omega) = \int_{-\infty}^{\infty} \triangle R(\tau) e^{-i\omega\tau} d\tau. \tag{5.23}$$

It is quite trivial to realize that the definition of the spectral density $S(\omega)$ in Equation (5.23) and Equation (5.21) is consistent with the definition of the total noise[6] in Equation (5.20):

$$\triangle I^2 = \int_{-\infty}^{\infty} S(\omega) d\omega, \tag{5.24}$$

where the definition of the delta function $\delta(\tau) = \int_{-\infty}^{\infty} e^{-i\omega\tau} d\omega$ has been used.

It is very relevant for the rest of the Section to realize that the measurement of $S(\omega)$ through the function $R(\tau)$ defined in Equation (5.22) requires the knowledge of the measured value of the current during all t. Thus, one has to make predictions about the evolution of the electronic device while being (continuously) measured. In a classical scenario, such discussion about measurement is generally ignored. On the contrary, for quantum systems, it has very relevant implications because the evolution of a system with or without measurement can be dramatically different (as seen in Section 2.1).

If the electronic device satisfies the ergodic theorem [39, 72]. A continuous measurement of the system can be avoided. In what sense ergodicity can simplify noise computations

[6] Technically, $S(\omega)$ defined in Equation (5.23) is non-negative and symmetric with respect to ω. Then, since only positive frequencies ω are measured in a laboratory, the measured density includes $S(\omega)$ and $S(-\omega)$ and the integral of the noise spectrum measured in a laboratory runs from 0 till ∞.

is shown hereafter. In general, the *mathematical* concept of a random process is used to deal with noise. A random process requires a sample space. In the case considered here, one can define an ensemble of *identical* electrical devices[7], each one labeled by the sample space variable γ. Then, the (instantaneous) current is labeled by the random process $I^{\gamma}(t)$. For a fixed time, t_1, the quantity $I^{\gamma}(t_1)$ is a random variable. For a fixed device γ_1, the function $I^{\gamma_1}(t)$ is a well-defined non-random function of time. Finally, $I^{\gamma_1}(t_1)$ is just a real number. Often the sample space variable γ is omitted in the notation. The DC value of the current in Equation (5.19) can be alternatively defined for an ergodic system as:

$$\langle I \rangle = \sum_i I_i(t_1) P(I_i(t_1)), \tag{5.25}$$

where $P(I_i(t_1))$ is the probability of getting I_i at time t_1. These probabilities are defined as the ratio of the number of devices providing I_i divided by the total number of devices. It is important to realize that the experimental evaluation of Equation (5.25) requires only one measurement of the current at t_1 in a large number of *identical* γ-devices. Then, the theoretical predictions of Equation (5.25) does only need to determine the free (without measuring apparatus) evolution of the electronic device from the initial time t_0 till t_1. See a detailed discussion in Appendix F on how ergodicity avoids the complications of the measurement in a quantum system. Obviously, one can compute the total noise represented in Equation (5.20) from a unique measurement in ergodic system:

$$\triangle I^2 = \sum_i (I_i(t_1) - \langle I \rangle)^2 P(I_i(t_1)). \tag{5.26}$$

However, the noise measured in a laboratory is not given by $\triangle I^2$, but $S(\omega)$ in Equation (5.23). It is important to repeat the reason explained in Equation (5.20): The amount of noise generated by an instantaneous current evolving from $I(t_1) = 5$ mA to $I(t_2) = 10$ mA during a time interval of $t_2 - t_1 = \tau = 1$ fs, is not captured from state-of-the-art laboratory apparatuses (which already has difficulties to capture noise at frequencies higher than few Terahertzs). From an experimental point of view, in fact, it is easy to get $S(\omega \to 0)$, but impossible to get $S(\omega \to \infty)$. The noise power spectral density $S(\omega)$ can be computed from the ensemble average version of the autocorrelation defined in Equation (5.22) as:

[7] At this point, one could say that, in typical laboratory experiments, only one electronic device is available (not an ensemble of them). Then, as a practical definition of ensemble, it can be defined the instantaneous current measured in different time-intervals: $I^{\gamma_1}(t)$ for the instantaneous current measured during the first time interval, $I^{\gamma_2}(t)$ for the second interval, and so on.

$$R(t_1, t_2) = \sum_i \sum_j I_j(t_2) I_i(t_1) P\big(I_j(t_2), I_i(t_1)\big). \tag{5.27}$$

In general, it can be assumed that the instantaneous current in an electronic device behaves as a wide-sense stationary random process. Then, $\langle I \rangle$ in Equation (5.25) is constant and time-independent. Identically, the autocorrelation function in Equation (5.27) depends only on the time difference $\triangle R(t_1, t_1 + \tau) = \triangle R(\tau)$ with $t_2 = t_1 + \tau$. Finally, one uses Equation (5.23), with $\triangle R(\tau)$ computed from Equation (5.27), to get the noise power spectral density $S(\omega)$.

It is important to emphasize (for a posterior discussion) that the probability $P\big(I_j(t_2), I_i(t_1)\big)$ implies the knowledge of how the following two-measurement process for each electronic device: It evolves freely from t_0 till t_1 when the current is measured giving the value I_i. Then, it evolves without measurement until time t_2, when the system is measured again giving I_j. In summary, even if the ergodicity argument is invoked, the noise computation through the autocorrelation function requires, at least, a two times measurement in a single device (and the average over all γ-devices).

It is important to underline that the previous discussion is valid for either classical or quantum devices. The adjective *quantum* emphasizes that the signal and the noise are computed or measured in an electronic device governed by quantum laws [10, 18, 24, 51]. If the electronic device is not ergodic, expression (5.22) requires a continuous measurement of the current $I(t)$. On the contrary, for an ergodic electron device, expression (5.25) requires one unique measurement, while expression (5.27) requires a two-times measurement when dealing with the power spectral density $S(\omega)$.

Up to here, one realizes that the definition of quantum noise seems very trivial. Then, why does the concept of quantum noise have a halo of mystery around it?

5.2.2 Quantum Noise in Electrical Devices from a Computational Point of View

The previous definition on what is quantum noise does not answer the question on how it is possible to compute it. If one wishes to predict the values $I(t)$ used in Equation (5.20) and Equation (5.22) or the probabilities $P(I)$ and $P\big(I_j(t_2), I_i(t_1)\big)$ for Equation (5.25) and Equation (5.27), one requires a quantum theory.

There are several quantum theories available in the literature that, by construction, are empirically equivalent when explaining all quantum phenomena. As said in Chapter 2, the so-called Copenhagen or orthodox interpretation [19, 42], Bohmian mechanics [15, 35, 68] or the many-worlds theory [36]. Any theory has usually two different planes. First the formalism, which is a set of mathematical rules (using elements such as wave functions, operators, trajectories) that allows to make practical computations that reproduce experimental results. The formalism of a theory provides an answer to the question: How quantum noise is computed? The second plane of a theory is its interpretation. It tries to provide a deep connection on how the mathematical rules and its elements explain how nature works. The interpretation of the theory provides answers to the question: Which is the physical origin of quantum noise? Each quantum theory will provide its own answers to both questions.

Many people argue that the only important part of a quantum theory (once it is known that is empirically valid) is its formalism because it is the only part one needs to make computations. Certainly, one can make noise computations using any of the available formalisms without worrying about its interpretation. At the end of the day, by construction, each theory should give the same predictions. Other people argue that even when one is only interested in computations, a correct understanding of the interpretational issues of each theory is fruitful because it provides an enlarged vision on how correctly apply the theory in unsolved problems (abandoning the *shut up and calculate* philosophy [63]). This point will be addressed later, in Section 5.2.4.

At this point, it is important to clarify why quantum noise is specially sensible to fundamental quantum mechanical issues. Any electrical device (or any experiment) is connected to a measuring apparatus. In the case considered here, an ammeter to get the electrical current. Quantum noise is sensible to the (ammeter) measuring process. As stated in Equation (5.27), in order to obtain the noise, the quantum system has to be measured, at least, twice. As already said in the present Thesis, this two-time measurement faces directly with the perturbation of the quantum wave function when a measurement is performed: this is the *the collapse of the wave function* exposed in Section 2.1. Can be ignored? Definitively not if temporal correlations need to be correctly predicted. See for example, Ref. [17]: *"The fluctuations ... are a consequence of a probabilistic reflection and transmission probability (a wave phenomena) and are a consequence of the fact that detectors register either a transmitted or a reflected particle (a particle phenomena)"*. The measurement process is hidden in the word *detectors*.

It is worthwhile also to mention that the fundamental understanding/computing of the measurement process can be largely relaxed when dealing with DC predictions. They can be computed from an ensemble of devices with only one measurement in each device,

so one can ignore the evolution of the quantum system after the measurement. See Appendix F to enlarge this point.

At this point all the discussion provided in Section 2.1 that a first glance would seem somehow abstract and useless turns out to be very fruitful when analyzing quantum noise in electrical devices (a very specific and practical problem). There, it was considered a typical scenario when discussing quantum noise: a flux of electrons impinging upon a partially transparent barrier (located in the middle of the active region). Electron transport through the barrier takes place by tunneling. Electron is either transmitted or reflected, but not both! [16, 24, 61] One gets a transmitted electron with a probability T, while a reflected one with probability $R = 1 - T$. To simplify the discussion, it is considered a constant injection of electrons (at zero temperature), one by one. Each electron, after measurement at time t_1, will appear randomly at the left or the right of the barrier. The time averaged number of transmitted electrons will be proportional to T, but the number of transmitted electrons fluctuates instantaneously because of the randomness of the transmission. These fluctuations on the number of transmitted electrons (when compared with the DC signal) are named partition noise [10, 17, 61]. There are many other sources of noise in electrical devices, for example, the $1/f$ noise which becomes very relevant at low frequencies [10, 18] and the so-called thermal noise.

5.2.3 Computational Ability of Bohmian Mechanics in Solving Quantum Noise

The present section is mainly devoted to summarizing the main results obtained Section 2.1 when discussing the collapse of the wave function and to apply them to quantum noise. There it was analyzed the simple, but paradigmatic problem, of an electron impinging on a tunneling barrier that was partially transmitted and partially reflected. It was seen that the Orthodox Interpretation, which only has the wave function evolving unitarily according to the Schrödinger equation, needs to postulate the collapse of the wave function in order to reproduce a non-unitary evolution when the system is measured. Instead, Bohmian Mechanics, with the use of the conditional wave function, achieves a non unitary evolution simply slicing a unitary evolution, in a larger configuration space where the detector is explicitly taken into account.

Thus the partition noise within Bohmian Mechanics is simply derived without postulating any further axiom to the theory, while in the Orthodox Interpretation of Quantum Mechanics is awkwardly postulated. The proper evolution of the conditional wave function already gives what is needed. This fact, in author's opinion, implies also a more

easy computational use of the conditional wave function when addressing quantum noise problems. Hereafter a motivation for this last assertion is given.

It has been previously seen the main features of Bohmian mechanics in explaining in a quite trivial way the partition noise in a tunneling barrier. However, as it occurs for all theories, there is a huge step between its general formulation and its practical application. In fact, it happens many times that the practical problem one want to solve is unsolvable both analytically and numerically and some kind of approximations are always required.

In principle it has been seen in Section 2.1.2 (theoretically) and in Section 3.1.4.1 (numerically) that to reproduce the collapse of the wave function in Bohmian mechanics one has to include a suitable interaction with an external apparatus. Then one can write down the Schrödinger equation for the complete system including all the electrons in the active region of the device plus all the particles composing the detector. But solving numerically this problem is obviously impossible. Again, the *many-body problem* appears. Then one should look for suitable approximations able to reduce the complexity of the problem. It is important to emphasize that the (technical) approximations that will be shown, do not alter the general framework previously presented in Chapter 2.

First kind of approximation:

- The first kind of approximation one has to address regards the inclusion of the apparatus in the simulations. It seems that its inclusion is unavoidable in order to provide the collapse of the wave function. And this is true, but in the particular case of quantum noise in electrical devices the fact of *playing* with (Bohmian) trajectories will greatly simplify the problem. In Section 3.2.1, it has been reported how any experimental value is calculated in Bohmian mechanics. The important thing achieved there is that any expectation value of a given operator is simply calculated as a function of the actual particles positions over an ensemble of repeated experiments (see Equation (3.43) in Section 3.2.1). Thus what really matters in the computation of a property of the quantum system are only the trajectories of the Bohmian particles (not the wave functions). Therefore, if the trajectories without measuring apparatus are enough accurate (this means if the error on these trajectories due to neglecting the apparatus is reasonably small compared to the exact solution) one can get accurate results with a minimal computational effort. In the case of the *transmitted charge detector* of Section 3.1, it has been demonstrated [7] that the error due to the exclusion of the apparatus from the simulations is almost negligible for the computation of the trajectories (see Figure 3.4 of Section 3.1.5). In this way it is possible to decrease enormously the computational

burden, removing all the degrees of freedom related to the apparatus from the computations.

It can be provided a more didactic discussion on why the previous technical approximation for the measuring apparatus works quite well when using Bohmian trajectories. In Section 2.1.1, it has been concluded that the reason why the wave function evolution in Figure 2.1 was wrong is because the wrong possibility that an electron that is transmitted at time t_1 is later reflected at time t_2. This unphysical result simply disappears when using Bohmian trajectories: the dynamic of a transmitted electron at time t_1 will be determined *locally* by the guidance law Equation (1.2) that only takes into account the transmitted part of the wave function. Then, it is possible, for all practical purposes, to completely ignore the reflected part of the wave function. Therefore, at time t_2, this electron will remain as a transmitted electron with full certainty. Thus if the trajectory without detector is enough accurate it does not matter if the collapse of the wave function is taken into account or not.[8]

Second kind of approximation:

- Once the apparatus has been *practically* eliminated from the computations, a second kind of approximation regards the interactions among the electrons of the device. The active region of the electronic device can contain hundreds of electrons. Also in this case, as it has been mentioned, the many-particle Schrödinger equation can be solved only for very few degrees of freedom. While in the first approximation it has been excluded some degrees of freedom (the ones of the apparatus) because its interaction with the system was small enough to certify that the perturbation of the (system) trajectories was negligible, this is not the case for this second approximation. A way to include short-range and long-range Coulomb interaction beyond the mean field approximation is the algorithm presented in Section 2.3.2. As already said, the advantage of the algorithm in Section 2.3.2 using the *conditional wave function* instead of the many-particle Schrödinger equation is that, in order to find approximate trajectories one does not need to evaluate the wave function and potential energies in the whole configuration space, but only over a smaller number of configuration points, associated with those trajectories defining the highest probabilities according to the modulus squared of the wave function.

[8] It is important to emphasize that, in principle, the measuring apparatus has also a role in the classical simulation of electronic devices. Such interaction with the apparatus is included at a classical level, at best, by a proper boundary conditions for the scalar potential of the Hamiltonian (i.e. the Poisson equation) ensuring overall charge neutrality. Obviously, this kind of approximations can also be included.

In order to have a full simulator one has to include also the fact that an electron device is an open system, where many parameters can only be estimated from the knowledge of their statistical (typical) distribution. Apart from the uncertainty in the initial position in the quantum trajectories (the α distribution explained in Section 3.2.1), one has also take into account the uncertainty on the properties of the injected electrons (initial energies, momentums, etc) which it is referred to the parameter $h = \{1, ..., M_h\}$. From now on γ refers to α and h. At finite temperature, the thermal noise introduces fluctuations on the energies of the electrons entering inside the device. As discussed in the introduction of Section 5.2.1, the study of the noise in electrical devices due to the partition noise of the barrier plus the thermal noise of the injection are traditionally known as quantum shot noise [10, 16, 17, 24, 52, 61]. In many systems, one obtains the well known Schottky's result [76] or Poissonian shot noise, $S_{II\ shot}(0) = 2q\langle I\rangle$, for the noise power spectral density defined in Equation (5.23) at zero frequency $w = 0$.

If one selects a particular (large) set of wave packets with values α and h for selecting their initial conditions. It is referred to such selection as α_1 and h_1. The wave packets and trajectories are evolved as explained in the second kind of approximation above (i.e. the *small entanglement approximation* of Section 2.3.2). Within the two approximation mentioned above, the total current value can be calculated as the sum of the particle or conduction current plus the displacement current:

$$\begin{aligned} I^{\alpha,h}(t) &= I_c^{\alpha,h}(t) + I_d^{\alpha,h}(t) = \\ &= \int_S \sum_{i=1}^{N} q_i v_i(X_i^{\alpha,h}(t))\delta(x_D - X_i^{\alpha,h}(t)) \cdot ds + \\ &+ \int_S \sum_{i=1}^{N} \epsilon(x_D) \frac{dE(x_D; X_i^{\alpha,h}(t), t)}{dt} \cdot ds, \end{aligned} \tag{5.28}$$

where S is the surface where one want to calculate the current, x_D are the points of the chosen surface, $\epsilon(x_D)$ is the dielectric constant in the same surface and $E(x_D; X_i^{\alpha,h}(t), t)$ is the electric field in the surface S which depends on the actual position of all the electrons.

Once $I^{\alpha_1,h_1}(t)$ is known for a large interval of time, the algorithm to compute the current fluctuations is quite simple following Equation (5.21) and Equation (5.23). This discussion can be familiar for those people who works in semi-classical approaches. In fact, the Bohmian procedure is very similar to that of, for instance, the Monte-Carlo simulations of the Boltzmann equation. But instead of being the electric-field the one

who *guides* the electrons, it is the wave function, through the guiding velocity field in Equation (1.2).

5.2.4 Discussion

Computations of quantum noise are quite complex because noise is generally quantified in terms of temporal correlations. Such correlations must include the time-evolution of a quantum system during and after one measurements. Usually, many quantum computations do only require a final measurement, so that their time-evolution from the initial until the final times is uniquely determined by the unitary (Schrödinger like) evolution. As discussed in Chapter 2, this unitary evolution is not enough to compute time correlations which require mixing unitary and non-unitary (the so-called collapse of the wave function) time evolutions.

There are several (empirically equivalent) quantum theories. Each quantum theory has its own formalism that is able to connect the experimental values with some abstracts elements such as wave functions, operators, trajectories, etc. that are able to satisfactorily reproduce (or predict) experimental results. Obviously, each theory also gives a different interpretation on its origin. In any case, at the end of the day, the same empirical predictions are achieved by using the Orthodox Interpretation of Quantum Mechanics or Bohmian Mechanics.

Because the Bohmian formulation uses trajectories to compute experimental results, it has been seen that a very reasonable approximation to include collapse can be achieved with a very small computational effort. A simulator named BITLLES has been developed by X. Oriols and his researching group based on the above exposed ideas [11]. It has been emphasized that the presented formalism and the procedure for computing the properties of a system (in the case above current, noise, etc.) have many similarities with the one used in semi-classical simulations (for example Monte-Carlo of the Boltzmann equation [62]). In any case, the Bohmian formalism is not at all a semi-classical approach but a complete quantum theory that can be applied to study any non-relativistic quantum phenomena.

Now, it is possible to provide an answer to the question: *What is the ultimate origin of quantum noise according to the Orthodox Interpretation?* A crucial role in the understanding of the quantum noise within the orthodox theory is played by the random collapse of the wave function due to measurements. Without the rule of the collapse, the wave function follows a deterministic law dictated by the Schrödinger equation. The partition noise in the tunneling barrier discussed in Figure 2.2 is due to the action of the

operator which implements the collapse of the wave function (selecting the final wave function stochastically among the set of available eigenstates).

Alternatively, one can also answer to the question: *What is the origin of quantum noise according to Bohmian Mechanics?* Bohmian Mechanics is a fully deterministic theory. Once the initial positions of all particles (of the universe) are fixed, the evolution of the trajectories (*a motion choreographed by the wave function*) is perfectly determined. It can be shown that the Bohmian universe, though deterministic, evolves in such a manner that an *appearance* of randomness emerges in an ensemble of identically prepared subsystem. Each element of the ensemble, for example an electronic device, is defined by the same conditional wave function of the electronic device and the initial positions are randomly distributed according to the modulus squared of the wave function [29]. This is the α distribution of the conditional wave function explained in Section 3.2.1 that accounts for the (non-explicitly simulated) environment. Being the evolution of the conditional wave function highly non-linear, the quantum randomness emerges in the same manner as for a classical chaotic system: the randomness in each experiment is a consequence of the dynamical evolution of the conditional wave function and of the uncertainty of the initial position of the particle, which is ultimately due to the global quantum equilibrium of the *entire system*, namely if the wave function is Ψ the configuration of the particles are distributed according to the probabilistic distribution $|\Psi|^2$ (for a more detailed discussion on this issue see [29, 30]). It is important to notice that the measurement has no special role.

In summary, according to the orthodox interpretation, the partition noise has its origin in the stochasticity of the orthodox measurement process. On the contrary, Bohmian mechanics says that the origin of noise is the uncertainty of the initial position of the trajectory in each realization of the experiment. Although both theories give the same predictions, in the author's opinion, the latter has a more natural and understandable explanation of the origin of quantum noise. The collapse in Bohmian theory is so naturally derived that the quantum measurement problem is somehow demystified. Then, the halo of mystery around the concept of quantum noise disappears.

Preferences between the explanation of the origin of quantum noise in terms of the orthodox or Bohmian interpretations are subjective in author's opinion. Therefore, above objective arguments have been also developed about the computational advantages of the Bohmian formalism. The facts that the measuring apparatus, what it is called the ammeter, is directly treated into the Hamiltonian of the Schrödinger equation and that the currents values are computed from trajectories (not from the wave functions) allows to study system *plus* apparatus scenarios (or look for reasonable approximations).

Quantum noise is a quite paradigmatic example where the differences between Bohmian approach and Orthodox Interpretation of Quantum Mechanics arise. Its discussion it has been put at the end of the present thesis in order to close somehow a circle: At the beginning, it has been argued that Bohmian Mechanics can provide an alternative way of understanding and computing quantum phenomena, quantum noise is undoubtedly a powerful example supporting this argument. When explaining quantum noise from Bohmian point of view, it has been used the collapse of the conditional wave function (trivially achieved from a slicing of a unitary evolution in a larger configuration space) in explaining the two times measurement needed for quantum noise computation and it has been used an algorithm to solve the many particle problem able to compute any values of quantum properties through the only use of (approximate) quantum trajectories.

Appendix A

Going Beyond the Small Entanglement Approximation

In Section 2.3.1 the limits of the *small entanglement approximation* have been analyzed for a non-separable potential. In this Appendix it is analyzed if the scheme presented there could be extended to improve the accuracy of the approximation. The main lesson learnt in Section 2.3.1 was that if one is able to reduce the many-particle wave function (in the configuration space) into a problem of single particle wave functions, the numerical complexity of the many-particle wave function in configuration space is enormously decreased. It has been observed that the main difficulty is due to the unknown terms A_i and B_i of Equation (2.19). One can observe that by construction, ψ_1 obeying Equation (2.15) exactly reproduces the usual Bohmian trajectory $X_1(t)$, and similarly for other particles. Hence, a proper ensemble will exactly reproduce all statistical predictions of ordinary quantum theory – provided the one-particle effective potentials $V_i^{\rm eff}(x,t)$ are defined appropriately. There is no difficulty with the conditional potential terms, e.g., $V[x, X_2(t), t]$. But the above definitions of A_1 and B_1 involve ψ_1' and ψ_1'' which are, in turn, defined in terms of the configuration space wave function in Equations (2.20) and (2.21). Here are discussed two different possibilities, both are a derivation of an original proposal of T. Norsen in Ref. [65].

One possibility for defining the terms A_1 and B_1 has been developed in [66]. For simplicity, one can define the particle-1-associated potential fields $a_1(x_1,t)$, $b_1(x_1,t)$, etc., as follows:

$$a(x_1,t) = \frac{\psi_1'(x_1,t)}{\psi_1(x_1,t)}, \tag{A.1}$$

$$b(x_1,t) = \frac{\psi_1''(x_1,t)}{\psi_1(x_1,t)}, \tag{A.2}$$

$$c(x_1,t) = \frac{\psi_1'''(x_1,t)}{\psi_1(x_1,t)}, \tag{A.3}$$

and so on. Then Equation (2.19) for the full effective potential which drives the evolution of particle 1's single-particle wave function ψ_1 can be re-written as

$$V_1^{\text{eff}}(x_1,t) = V(x_1,X_2(t),t) + i\hbar\frac{dX_2}{dt}a(x_1,t) - \frac{\hbar^2}{2m_2}b(x_1,t). \tag{A.4}$$

Then the full configuration-space Schrödinger equation may be used to find out how $a(x,t)$ and $b(x,t)$ must evolve in order to exactly reproduce the standard Bohmian trajectories. The important thing here is that the results can be written exclusively in terms of this infinite network of potential fields. For example, the field a should satisfy its own partial differential equation of the form

$$\begin{aligned}\frac{\partial a}{\partial t} &= \frac{i\hbar}{2m_1}\left[\frac{\partial^2 a}{\partial x_1^2} + 2\frac{\partial a}{\partial x_1}\frac{(\partial\psi_1/\partial x_1)}{\psi_1}\right] + \\ &\quad + \frac{i\hbar}{2m_2}\left[c - ab\right] + \frac{dX_2}{dt}\left[b - a^2\right] - \frac{i}{\hbar}\frac{\partial V}{\partial x_2}\Big|_{x_2=X_2(t)}.\end{aligned} \tag{A.5}$$

And similarly, b will satisfy an evolution equation of the form

$$\begin{aligned}\frac{\partial b}{\partial t} &= \frac{i\hbar}{2m_1}\left[\frac{\partial^2 b}{\partial x_1^2} + 2\frac{\partial b}{\partial x_1}\frac{(\partial\psi_1/\partial x_1)}{\psi_1}\right] + \frac{i\hbar}{2m_2}\left[d - b^2\right] + \frac{dX_2}{dt}\left[c - ab\right] \\ &\quad - \frac{2i}{\hbar}a\frac{\partial V}{\partial x_2}\Big|_{x_2=X_2(t)} - \frac{i}{\hbar}\frac{\partial^2 V}{\partial x_2^2}\Big|_{x_2=X_2(t)}.\end{aligned} \tag{A.6}$$

The c and d which appear here need their own time-evolution equations (which will in turn involve further potentials e and f), and so on. The result is a countably infinite network of potential fields obeying coupled time-evolution equations. These potentials then of course appear in the Schrödinger-type equations governing the single-particle pilot-wave fields which guide the particles. The exact statistical predictions of quantum theory are reproduced, but the configuration space wave function Ψ is nowhere to be found. It has been used Ψ, of course, to find out how the potentials a, b, c, etc., must interact and evolve in order to reproduce the usual Bohmian particle trajectories.

But once one has Equations Equation (A.4) as well as Equation (A.5), (A.6), etc., the universal wave function Ψ is not need at all!

Nevertheless, solving an infinite network of interacting potentials seems does not reduce the complexity of the problem. The solution is rather simple, the infinite coupled equation can be cut at some level (for example one can think to stop between b and c). This first proposal has an advantage: the fields a, b, c etc. defined above can be interpreted as additional potential to the conditional potential in the evolution of the single particle conditional wave function. But at the same time are numerically ill defined: As matter of fact, whenever the modulus squared of the conditional wave function $|\psi_1(x_1,t)|^2$ is small the definition of in Equation (A.1) leads to numerical errors. The present author has developed an algorithm cutting the potential whenever the modulus squared of the conditional wave function is small which leads to the same results exposed in the following of the present section, but it seems an ad-hoc solution that must be changed and verified in different physical situation. In order to overcome this problem, a different (but related scheme) can be used. This is exactly the one proposed by T. Norsen in Ref. [65].

One can directly use the terms ψ_1' and ψ_1'' appearing in Equation (2.15) and write down their dynamical evolutions. Again, they will depends of high order terms such as ψ_1''', ψ_1'''' and so on. The result obtained in [65] is the following:

$$\begin{aligned} i\hbar\frac{\partial\psi_1^{(n)}(x_1,t)}{\partial t} &= -\frac{\hbar^2}{2m_1}\frac{\partial^2\psi_1^{(n)}(x_1,t)}{\partial x_1^2} - \frac{\hbar^2}{2m_2}\psi_1^{(n+2)}(x_1,t) \\ &+ i\hbar\frac{dX_2(t)}{dt}\psi_1^{(n+1)}(x_1,t) + P_n, \end{aligned} \tag{A.7}$$

where the potential term P_n is:

$$P_n \equiv \sum_{i=0}^{n}\binom{n}{i}\frac{\partial^i V}{\partial x_2^i}(x_1,X_2(t),t)\psi_1^{(n-i)}(x_1,t). \tag{A.8}$$

In order to check if including more terms in the evolution of the conditional wave function leads to an improvement of the *small entanglement approximation* it has been tested in the same physical situation described in Section 2.3.1.1 including only ψ' and ψ'' for each particle. For each particle is solved the following system of coupled equation:

$$
\begin{aligned}
i\hbar\frac{\partial\psi_1(x_1,t)}{\partial t} &= -\frac{\hbar^2}{2m_1}\frac{\partial^2\psi_1(x_1,t)}{\partial x_1^2} - \frac{\hbar^2}{2m_2}\psi_1''(x_1,t) \\
&+ i\hbar\frac{dX_2(t)}{dt}\psi_1'(x_1,t) + V(x_1,X_2(t))\psi_1(x_1,t), \qquad \text{(A.9)} \\
i\hbar\frac{\partial\psi_1'(x_1,t)}{\partial t} &= -\frac{\hbar^2}{2m_1}\frac{\partial^2\psi_1'(x_1,t)}{\partial x_1^2} + V(x_1,X_2(t))\psi_1'(x_1,t) \\
&+ \frac{\partial V}{\partial x_2}\Big|_{x_2=X_2(t)}\psi_1(x_1,t), \qquad \text{(A.10)} \\
i\hbar\frac{\partial\psi_1''(x_1,t)}{\partial t} &= -\frac{\hbar^2}{2m_1}\frac{\partial^2\psi_1''(x_1,t)}{\partial x_1^2} + V(x_1,X_2(t))\psi_1''(x_1,t) \\
&+ \frac{\partial V}{\partial x_2}\Big|_{x_2=X_2(t)}\psi_1'(x_1,t) + \frac{\partial^2 V}{\partial x_2^2}\Big|_{x_2=X_2(t)}\psi_1(x_1,t). \qquad \text{(A.11)}
\end{aligned}
$$

Equations (A.9), (A.10) and (A.11) are solved simultaneously. Some numerical and technical approximation are implemented to solve the above system of equation. Firstly, ψ_1 at every discrete time step Δt is normalized because Equation (A.9) is non-linear and non-unitary. Secondly, one can note that in the evolution of ψ' and ψ'' have been disregarded the terms ψ_1'' and ψ_1''' for the former and ψ_1''' and ψ_1'''' for the latter (defining the present approximation). Even though ψ_1'' is known from Equation (A.11) it is not involved in the evolution of ψ_1' in Equation (A.10) because it would imply a different numerical treatment similar to Equation (A.9) but generating an instability of the all scheme.

With the approximations just exposed, in Figure A.1 is reported the deviation (calculated as before form Equation (2.27)) form the exact 2D solution of the approximate trajectories with the present scheme. It can be noted that the deviation is enormously decreased if the terms ψ_1' and ψ_1'' are included. It is worthwhile to notice that the y axis is logarithmic scale.

The algorithm just presented has still numerical instability for values of the parameter $C \geq 1$: it is an ongoing project of the present author to improve the above numerical scheme in order to achieve numerical stability. Nevertheless, the main point addressed here is that the inclusion of additional terms (in the case studied here only two) leads to enormous increase in the accuracy of the numerical scheme to reproduce the Bohmian trajectories without using the many particle wave function but only single particle mathematical objects.

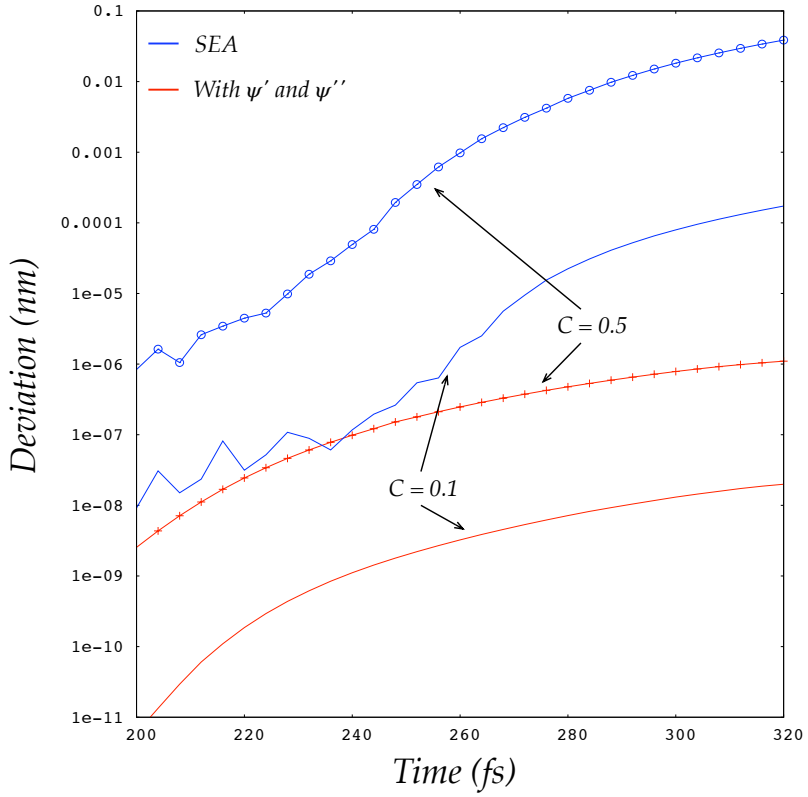

FIGURE A.1: Blue lines, deviation calculated from Equation (2.32) as a function of time from the exact 2D trajectories of the 1D SEA solution of Equations (2.30) and (2.31). Red lines, deviation calculated from Equation (2.32) as a function of time from the exact 2D trajectories of the 1D solution of Equations (A.9), (A.10) and (A.11) for each particle. Solid lines are for $C = 0.1$ while lines with points are for $C = 0.5$ in Equation (2.27).

Appendix B

Analytical Formula for the Electric Flux Through a Surface

In this Appendix an analytical formula for the electric field generated by a particle in a surface is computed. In Section 3.1.3 it has been obtained that the flux is:

$$\Phi(E_x(x,y,z;x_D)) = \int_0^{L_z}\int_0^{L_y} \frac{q}{4\pi\epsilon}\frac{(x_D-x)}{[(x_D-x)^2+(y'-y)^2+(z'-z)^2]^{3/2}}dy'dz'. \quad \text{(B.1)}$$

It is convenient to integrate first in dy'. Before doing that, the following substitution is considered

$$\alpha^2 = (x_D-x)^2+(z'-z)^2,$$

thus Equation (B.1) becomes

$$\Phi(E_x(x,y,z;x_D)) = \int_0^{L_z}\int_0^{L_y} \frac{q}{4\pi\epsilon}\frac{(x_D-x)}{[(y'-y)^2+\alpha^2]^{3/2}}dy'dz'. \quad \text{(B.2)}$$

Performing the change of variables

$$\begin{aligned} y' - y &= \alpha \tan(t), \\ dy' &= \alpha(1+\tan^2(t))dt = \frac{\alpha}{\cos^2(t)}dt, \end{aligned} \tag{B.3}$$

one gets:

$$\begin{aligned} \Phi(E_x(x,y,z;x_D)) &= \frac{q}{4\pi\epsilon}\int_0^{L_z}\int_{\tan^{-1}(-\frac{y}{\alpha})}^{\tan^{-1}(\frac{L_y-y}{\alpha})} \frac{(x_D-x)}{[\alpha^2\tan^2(t)+\alpha^2]^{3/2}}\frac{\alpha}{\cos^2(t)}dtdz' = \\ &= \frac{q}{4\pi\epsilon}\int_0^{L_z}\int_{\tan^{-1}(-\frac{y}{\alpha})}^{\tan^{-1}(\frac{L_y-y}{\alpha})} \frac{x_D-x}{\frac{\alpha^3}{\cos^3(t)}}\frac{\alpha}{\cos^2(t)}dtdz' = \\ &= \frac{q}{4\pi\epsilon}\int_0^{L_z}\int_{\tan^{-1}(-\frac{y}{\alpha})}^{\tan^{-1}(\frac{L_y-y}{\alpha})} \frac{(x_D-x)\cos(t)}{\alpha^2}dtdz' = \\ &= \frac{q}{4\pi\epsilon}\int_0^{L_z} dz' \left[\frac{\sin(t)}{\alpha^2}\right]_{\tan^{-1}(-\frac{y}{\alpha})}^{\tan^{-1}(\frac{L_y-y}{\alpha})}. \end{aligned} \tag{B.4}$$

Recalling that

$$\sin(t) = \frac{\tan(t)}{\sqrt{\tan^2(t)+1}} = \frac{(y'-y)}{\sqrt{(y'-y)^2+\alpha^2}}, \tag{B.5}$$

where in the last equality of Equation (B.5) it has been used the relation (B.3). Then the first integral becomes:

$$\begin{aligned} &\Phi(E_x(x,y,z;x_D)) = \\ = &\frac{q}{4\pi\epsilon}\int_0^{L_z} dz' \left[\frac{(x_D-x)(y'-y)}{[(x_D-x)^2+(z'-z)^2]\sqrt{(x_D-x)^2+(y'-y)^2+(z'-z)^2}}\right]_0^{L_y} = \\ = &\frac{q}{4\pi\epsilon}\int_0^{L_z} dz' \left(\frac{(x_D-x)(L_y-y)}{[(x_D-x)^2+(z'-z)^2]\sqrt{(x_D-x)^2+(L_y-y)^2+(z'-z)^2}} + \right. \\ + &\left. \frac{y'(x_D-x)}{[(x_D-x)^2+(z'-z)^2]\sqrt{(x_D-x)^2+(y)^2+(z'-z)^2}}\right) = \\ = &\frac{q}{4\pi\epsilon}\int_0^{L_z} dz'(F_1+F_2). \end{aligned} \tag{B.6}$$

At this point the second integral in dz' has to be performed. It can be observed that one has to integrate the sum of two functions which have the same structure, so one can compute explicitly only the first one, i.e. F_1.

$$\begin{aligned} I_1 &= \frac{q}{4\pi\epsilon}\int_0^{L_z} dz' F_1 \\ &= \frac{q}{4\pi\epsilon}\int_0^{L_z} dz' \frac{(x_D-x)(L_y-y)}{[(x_D-x)^2+(z'-z)^2]\sqrt{(x_D-x)^2+(L_y-y)^2+(z'-z)^2}}. \end{aligned} \tag{B.7}$$

Now calling $a=(x_D-x)$, $b=(L_y-y)$, $a^2+b^2=c^2$ and making the change of variable

$$\begin{aligned} z'-z &= c\tan(t), \\ dz' &= \frac{c}{\cos^2(t)}dt, \end{aligned}$$

the integral I_1 becomes:

$$\begin{aligned} I_1 &= \frac{q}{4\pi\epsilon}\int_{\tan^{-1}(-\frac{z}{c})}^{\tan^{-1}(\frac{L_z-z}{c})} \frac{ab}{[c^2-b^2+c^2\tan^2(t)]\sqrt{c^2+c^2\tan^2(t)}}\frac{c}{\cos^2(t)}dt = \\ &= \frac{q}{4\pi\epsilon}\int_{\tan^{-1}(-\frac{z}{c})}^{\tan^{-1}(\frac{L_z-z}{c})} \frac{ab}{\left[\frac{c^2}{\cos^2(t)}-b^2\right]\sqrt{\frac{c^2}{\cos^2(t)}}}\frac{c^2}{\cos^2(t)}dt = \\ &= \frac{q}{4\pi\epsilon}\int_{\tan^{-1}(-\frac{z}{c})}^{\tan^{-1}(\frac{L_z-z}{c})} \frac{ab}{\left[\frac{c^2}{\cos^2(t)}-b^2\right]}\frac{1}{\cos(t)}dt = \\ &= \frac{q}{4\pi\epsilon}\int_{\tan^{-1}(-\frac{z}{c})}^{\tan^{-1}(\frac{L_z-z}{c})} \frac{ab\cos(t)}{c^2-b^2\cos^2(t)}dt = \\ &= \frac{q}{4\pi\epsilon}\int_{\tan^{-1}(-\frac{z}{c})}^{\tan^{-1}(\frac{L_z-z}{c})} \frac{ab\cos(t)}{c^2-b^2+b^2\sin^2(t)}dt = \\ &= \frac{q}{4\pi\epsilon}\int_{\tan^{-1}(-\frac{z}{c})}^{\tan^{-1}(\frac{L_z-z}{c})} \frac{ab\cos(t)}{a^2+b^2\sin^2(t)}dt = \\ &= \frac{q}{4\pi\epsilon}\int_{\tan^{-1}(-\frac{z'}{c})}^{\tan^{-1}(\frac{L_z-z}{c})} \frac{\frac{b}{a}\cos(t)}{1+\frac{b^2}{a^2}\sin^2(t)}dt. \end{aligned} \tag{B.8}$$

At this point, with another change of variable

$$\beta = \frac{b}{a}\sin(t),$$
$$d\beta = \frac{b}{a}\cos(t)dt,$$

the integral I_1 is simply:

$$\begin{aligned}
I_1 &= \frac{q}{4\pi\epsilon}\int_{\frac{b}{a}\sin(\tan^{-1}(-\frac{z}{c}))}^{\frac{b}{a}\sin(\tan^{-1}(\frac{L_z-z}{c}))}\frac{d\beta}{1+\beta^2} = \frac{q}{4\pi\epsilon}\left[\tan^{-1}(\beta)\right]_{\frac{b}{a}\sin(\tan^{-1}(-\frac{z}{c}))}^{\frac{b}{a}\sin(\tan^{-1}(\frac{L_z-z}{c}))} = \\
&= \frac{q}{4\pi\epsilon}\left[\tan^{-1}\left(\frac{b}{a}\sin(t)\right)\right]_{\tan^{-1}(-\frac{z}{c})}^{\tan^{-1}(\frac{L_z-z}{c})} = \\
&= \text{Equation (B.5)}\frac{q}{4\pi\epsilon}\left[\tan^{-1}\left(\frac{b}{a}\frac{\tan(t)}{\sqrt{\tan^2(t)+1}}\right)\right]_{\tan^{-1}(-\frac{z}{c})}^{\tan^{-1}(\frac{L_z-z}{c})} = \\
&= \frac{q}{4\pi\epsilon}\left[\tan^{-1}\left(\frac{b}{a}\frac{(z'-z)}{\sqrt{(z'-z)^2+c^2}}\right)\right]_0^{L_z} = \\
&= \frac{q}{4\pi\epsilon}\left[\tan^{-1}\left(\frac{L_y-y'}{x_D-x}\frac{(z'-z)}{\sqrt{(x_D-x)^2+(L_y-y')^2+(z'-z)^2}}\right)\right]_0^{L_z} = \\
&= \frac{q}{4\pi\epsilon}\tan^{-1}\left(\frac{(L_y-y)(L_z-z)}{(x_D-x)\sqrt{(x_D-x)^2+(L_y-y)^2+(L_z-z)^2}}\right) + \\
&- \frac{q}{4\pi\epsilon}\tan^{-1}\left(\frac{-z(L_y-y)}{(x_D-x)\sqrt{(x_D-x)^2+(L_y-y)^2+(z)^2}}\right) \\
&= \frac{q}{4\pi\epsilon}\tan^{-1}\left(\frac{(L_y-y)(L_z-z)}{(x_D-x)\sqrt{(x_D-x)^2+(L_y-y)^2+(L_z-z)^2}}\right) + \\
&+ \frac{q}{4\pi\epsilon}\tan^{-1}\left(\frac{z(L_y-y)}{(x_D-x)\sqrt{(x_D-x)^2+(L_y-y)^2+(z)^2}}\right).
\end{aligned} \tag{B.9}$$

Where in the last equality it has been used the fact that $\tan^{-1}(-x) = -\tan^{-1}(x)$. In the same manner one can calculate the integral of F_2,

$$\begin{aligned}
I_2 &= \frac{q}{4\pi\epsilon}\int_0^{L_z} dz' F_2 = \frac{q}{4\pi\epsilon}\tan^{-1}\left(\frac{y(L_z-z)}{(x_D-x)\sqrt{(x_D-x)^2+(y)^2+(L_z-z)^2}}\right) + \\
&+ \frac{q}{4\pi\epsilon}\tan^{-1}\left(\frac{zy}{(x_D-x)\sqrt{(x_D-x)^2+(y)^2+(z)^2}}\right),
\end{aligned} \tag{B.10}$$

obtaining the final result:

$$\begin{aligned}\Phi(E_x(x,y,z;x_D)) &= \frac{q}{4\pi\epsilon}\tan^{-1}\left(\frac{(L_y-y)(L_z-z)}{(x_D-x)\sqrt{(x_D-x)^2+(L_y-y)^2+(L_z-z)^2}}\right)+\\ &+ \frac{q}{4\pi\epsilon}\tan^{-1}\left(\frac{z(L_y-y)}{(x_D-x)\sqrt{(x_D-x)^2+(L_y-y')^2+(z)^2}}\right)+\\ &+ \frac{q}{4\pi\epsilon}\tan^{-1}\left(\frac{y(L_z-z)}{(x_D-x)\sqrt{(x_D-x)^2+(y)^2+(L_z-z)^2}}\right)+\\ &+ \frac{q}{4\pi\epsilon}\tan^{-1}\left(\frac{zy}{(x_D-x)\sqrt{(x_D-x)^2+(y)^2+(z)^2}}\right). \qquad \text{(B.11)}\end{aligned}$$

In the simple case in which the particle is located in $x = (x, L_y/2, L_z/2)$ and is able to move only in the x direction the last expression becomes:

$$\Phi(E_x(x;x_D)) = \frac{q}{\pi\epsilon}\tan^{-1}\left(\frac{L_yL_z}{4(x_D-x)\sqrt{(x_D-x)^2+(\frac{L_y}{2})^2+(\frac{L_z}{2})^2}}\right), \qquad \text{(B.12)}$$

where one can observe that the relevant parameter is $S = L_yL_z$ the area in which the electric field is evaluated. When $L_y = L_z \equiv L$ and $S = L^2$ the expression (B.12) become

$$\Phi(E_x(x;x_D)) = \frac{q}{\pi\epsilon}\tan^{-1}\left(\frac{S}{4(x_D-x)\sqrt{(x_D-x)^2+\frac{S}{2}}}\right), \qquad \text{(B.13)}$$

which is the main result used in the text of the thesis.

Appendix C

Derivation of the Bohmian Velocity Through Weak Measurement Procedure

In this Appendix it is presented a detailed derivation of Equation (4.24) in Section 4.2.1. Starting from:

$$v(x_s,\tau) = \frac{E[p_w|x_s]}{m} = \frac{1}{m}\frac{\int dp_w p_w \mathcal{P}(p_w \cap x_s)}{\mathcal{P}(x_s)}, \tag{C.1}$$

one can calculate the denominator of the last expression as:

$$\begin{aligned}
\mathcal{P}(x_s) = & \int dp_w \mathcal{P}(p_w \cap x_s) \\
= & \int dp_w dp_w \langle\psi|\hat{I}_w^\dagger \hat{U}_\tau^\dagger \hat{I}_s^\dagger \hat{I}_s \hat{U}_\tau \hat{I}_w|\psi\rangle \\
= & \iint dp' dp'' \left[C_w^2 \int dp_w e^{-\frac{(p'-p_w)^2}{2\sigma_w^2}} e^{-\frac{(p''-p_w)^2}{2\sigma_w^2}} \right] \langle\psi|p'\rangle\langle p'|\hat{U}_\tau^\dagger \hat{I}_s^\dagger \hat{I}_s \hat{U}_\tau|p''\rangle\langle p''|\psi\rangle,
\end{aligned} \tag{C.2}$$

where in the last line it has been used the definition Equation (4.13). One can focus only in the integral between squared parenthesis in the last line of Equation (C.2)

$$
\begin{aligned}
& C_w^2 \int dp_w e^{-\frac{(p'-p_w)^2}{2\sigma_w^2}} e^{-\frac{(p''-p_w)^2}{2\sigma_w^2}} = \\
= \; & C_w^2 \int dp_w e^{-\frac{p_w^2}{\sigma_w^2}+p_w\left(\frac{p'}{\sigma_w^2}+\frac{p''}{\sigma_w^2}\right)-\frac{p'^2}{2\sigma_w^2}-\frac{p''^2}{2\sigma_w^2}} = \\
= \; & e^{-\frac{(p'-p'')^2}{4\sigma_w^2}}
\end{aligned} \tag{C.3}
$$

where it has been used $C_w = (\sqrt{\pi}\sigma_w)^{-1/2}$. Thus Equation (C.2) becomes:

$$
\begin{aligned}
\mathcal{P}(x_s) = & \iint dp'dp'' e^{-\frac{(p'-p'')^2}{4\sigma_w^2}} \langle\psi|p'\rangle\langle p'|\hat{U}_\tau^\dagger \hat{I}_s^\dagger \hat{I}_s \hat{U}_\tau|p''\rangle\langle p''|\psi\rangle \\
= & \iint dp'dp''\langle\psi|p'\rangle e^{-\frac{(p'-p'')^2}{4\sigma_w^2}} \langle p''|\psi\rangle \left[C_s^2 \int dx e^{-\frac{(x-x_s)^2}{\sigma_s^2}} \langle p'|\hat{U}_\tau^\dagger|x\rangle\langle x|\hat{U}_\tau|p''\rangle\right]
\end{aligned} \tag{C.4}
$$

Recalling that:

- (i) $\hat{U}_\tau = \int dp|p\rangle\langle p|e^{-i\frac{p^2\tau}{2m\hbar}}$,
- (ii) $\langle x|p\rangle = \frac{1}{\sqrt{2\pi\hbar}} e^{i\frac{px}{\hbar}}$,
- (iii) $\langle x|\hat{U}_\tau|p''\rangle = \langle x|\int dp|p\rangle\langle p|e^{-i\frac{p^2\tau}{2m\hbar}}|p''\rangle = \frac{1}{\sqrt{2\pi\hbar}} e^{-i\frac{p''^2\tau}{2m\hbar}+i\frac{p''x}{\hbar}}$,

it is possible to work out the integral between squared parenthesis in Equation (C.4),

$$
\begin{aligned}
& C_s^2 \int dx e^{-\frac{x^2}{\sigma_s^2}+x\left(\frac{2x_s}{\sigma_s^2}+i\frac{p''}{\hbar}-i\frac{p'}{\hbar}\right)-\frac{x_s^2}{\sigma_s^2}-i\frac{p''^2\tau}{2m\hbar}+i\frac{p'^2\tau}{2m\hbar}} = \\
= \; & e^{-\frac{\sigma_s^2}{4\hbar^2}(p'-p'')^2} e^{-\frac{i}{\hbar}x_s p'+i\frac{p'^2\tau}{2m\hbar}} e^{\frac{i}{\hbar}x_s p''-i\frac{p''^2\tau}{2m\hbar}} = \\
= \; & e^{-\frac{\sigma_s^2}{4\hbar^2}(p'-p'')^2} \langle p'|\hat{U}_\tau^\dagger|x_s\rangle\langle x_s|\hat{U}_\tau|p''\rangle.
\end{aligned} \tag{C.5}
$$

Therefore Equation (C.4) becomes:

$$
\mathcal{P}(x_s) = \iint dp'dp'' e^{-\frac{(p'-p'')^2}{4\sigma_w^2}} e^{-\frac{\sigma_s^2}{4\hbar^2}(p'-p'')^2} \langle\psi|p'\rangle\langle p'|\hat{U}_\tau^\dagger|x_s\rangle\langle x_s|\hat{U}_\tau|p''\rangle\langle p''|\psi\rangle, \tag{C.6}
$$

if the condition

$$\sigma_w \gg \frac{\hbar}{\sigma_s} \tag{C.7}$$

is satisfied then Equation (C.6) simply becomes:

$$\mathcal{P}(x_s) = \langle\psi|\hat{U}_\tau^\dagger \hat{I}_s^\dagger \hat{I}_s \hat{U}_\tau|\psi\rangle = |\psi(x_s,\tau)|^2, \tag{C.8}$$

which is the result, Equation (4.21), obtained in Section 4.2.1.
Now, it is possible to calculate the numerator of Equation (C.1):

$$\begin{aligned}&\int dp_w p_w \mathcal{P}(p_w \cap x_s) = \\ &= \iint dp' dp'' \left[C_w^2 \int dp_w p_w e^{-\frac{(p'-p_w)^2}{2\sigma_w^2}} e^{-\frac{(p''-p_w)^2}{2\sigma_w^2}} \right] \langle\psi|p'\rangle\langle p'|\hat{U}_\tau^\dagger \hat{I}_s^\dagger \hat{I}_s \hat{U}_\tau|p''\rangle\langle p''|\psi\rangle,\end{aligned} \tag{C.9}$$

again it is possible to calculate the integral between squared parenthesis in the last expression,

$$\begin{aligned} & C_w^2 \int dp_w p_w e^{-\frac{(p'-p_w)^2}{2\sigma_w^2}} e^{-\frac{(p''-p_w)^2}{2\sigma_w^2}} = \\ = \; & e^{-\frac{(p'-p'')^2}{4\sigma_w^2}} C_w^2 \int dp_w p_w e^{-\frac{\left[p_w - \frac{(p'+p'')}{2}\right]}{\sigma_w^2}} = \\ = \; & \left(\frac{p'+p''}{2}\right) e^{-\frac{(p'-p'')^2}{4\sigma_w^2}}. \end{aligned} \tag{C.10}$$

Then Equation (C.9) becomes:

$$\begin{aligned}&\int dp_w p_w \mathcal{P}(p_w \cap x_s) = \\ &= \iint dp' dp'' \left(\frac{p'+p''}{2}\right) e^{-\frac{(p'-p'')^2}{4\sigma_w^2}} \langle\psi|p'\rangle\langle p'|\hat{U}_\tau^\dagger \hat{I}_s^\dagger \hat{I}_s \hat{U}_\tau|p''\rangle\langle p''|\psi\rangle,\end{aligned} \tag{C.11}$$

making the same steps done from Equation (C.4) till Equation (C.6), Equation (C.11) becomes:

$$\int dp_w p_w \mathcal{P}(p_w \cap x_s) =$$
$$= \iint dp' dp'' \left(\frac{p' + p''}{2} \right) e^{-\frac{(p'-p'')^2}{4\sigma_w^2}} e^{-\frac{\sigma_s^2}{4\hbar^2}(p'-p'')^2} \langle \psi | p' \rangle \langle p' | \hat{U}_\tau^\dagger | x_s \rangle \langle x_s | \hat{U}_\tau | p'' \rangle \langle p'' | \psi \rangle \quad \text{(C.12)}$$

If Equation (C.7) is satisfied then Equation (C.12) becomes:

$$\begin{aligned} \int dp_w p_w \mathcal{P}(p_w \cap x_s) &= \frac{1}{2} \left[\langle \psi | \hat{p} \hat{U}_\tau^\dagger \hat{I}_s^\dagger \hat{I}_s \hat{U}_\tau | \psi \rangle + \langle \psi | \hat{U}_\tau^\dagger \hat{I}_s^\dagger \hat{I}_s \hat{U}_\tau \hat{p} | \psi \rangle \right] = \\ &= \mathrm{Re} \left(\langle \psi | \hat{U}_\tau^\dagger \hat{I}_s^\dagger \hat{I}_s \hat{U}_\tau \hat{p} | \psi \rangle \right) \end{aligned} \quad \text{(C.13)}$$

where in the last expression it has been used the property $\hat{p} = \int p|p\rangle\langle p| dp$. If one writes the momentum operator in position representation easily realizes that the expression between parenthesis in the last line of Equation (C.13) is

$$\langle \psi | \hat{U}_\tau^\dagger \hat{I}_s^\dagger \hat{I}_s \hat{U}_\tau \hat{p} | \psi \rangle = -i\hbar \psi^*(x_s, \tau) \frac{\partial}{\partial x_s} \psi(x_s, \tau) \quad \text{(C.14)}$$

and thus its real part is

$$\begin{aligned} \mathrm{Re} \left(\langle \psi | \hat{U}_\tau^\dagger \hat{I}_s^\dagger \hat{I}_s \hat{U}_\tau \hat{p} | \psi \rangle \right) &= \frac{\hbar}{2i} \left(\frac{\partial \psi(x_s, \tau)}{\partial x_s} \psi^*(x_s, \tau) - \frac{\partial \psi^*(x_s, \tau)}{\partial x_s} \psi(x_s, \tau) \right) \\ &= m J(x_s, \tau). \end{aligned} \quad \text{(C.15)}$$

Therefore, the right hand side of Equation (C.1) becomes:

$$\frac{1}{m} \frac{\int dp_w p_w \mathcal{P}(p_w \cap x_s)}{\mathcal{P}(x_s)} = \frac{J(x_s, \tau)}{|\psi(x_s, \tau)|^2} = v(x_s, \tau), \quad \text{(C.16)}$$

which is the result obtain in Section 4.2.1.

Appendix D

Analytical Two-Particle Probabilities from the Scattering Formalism with Mono-Energetic Initial States

In this Appendix it is reproduced the results of the two-particle scattering probabilities for indistinguishable particles developed in Refs. [12, 16, 17, 78] and summarized in Equations (5.1)-(5.3). In the scattering formalism, input states are described by annihilation operators $\hat{a}_L$ and $\hat{a}_R$ or creation operators $\hat{a}_L^\dagger$ and $\hat{a}_R^\dagger$, being L and R the left and right lead. Analogously, the output states are described by $\hat{b}_i$ and $\hat{b}_i^\dagger$ with $i = L, R$. The connection between the $\hat{a}_i$ and the $\hat{b}_i$ is provided by the scattering matrix [16, 18] through the relation

$$\begin{pmatrix} b_L \\ b_R \end{pmatrix} = \begin{pmatrix} r & t' \\ t & r' \end{pmatrix} \begin{pmatrix} a_L \\ a_R \end{pmatrix}, \tag{D.1}$$

where the probability amplitude coefficients are such that $|r|^2 = |r'|^2 = R$ and $|t|^2 = |t'|^2 = T$ where R and T are respectively the reflection and transmission probabilities that satisfy the condition $T + R = 1$. Analogously the creation operators $\hat{a}_i^\dagger$ and the $\hat{b}_i^\dagger$ are related by the adjoint scattering matrix $s^\dagger$. The scattering matrix satisfies the relation $s^\dagger s = I$. For fermions the $\hat{a}_i$ operators obey to the anti-commutation relations

$$\{\hat{a}_i, \hat{a}_j^\dagger\} = \delta_{ij}, \tag{D.2}$$

and the $\hat{b}_i$ operators follows

$$\{\hat{b}_i, \hat{b}_j^\dagger\} = \delta_{ij}, \tag{D.3}$$

with $i, j = L, R$. Equation (D.2) and Equation (D.3) reflect the underling anti-symmetry of the wave function.

Hereafter it is interesting to focus on the physical situation depicted in figure 5.1. An input state is constructed by one electron incident from the left and the other from the right. Both with a unique and equal (in modulus) momentum. With the help of the creation and annihilation operators it is possible to write the input state as $|\Psi\rangle = \hat{a}_L^\dagger \hat{a}_R^\dagger |0\rangle$, where $|0\rangle$ is the vacuum state of the system.

Using the scattering matrix (Equation (D.1)) and the anti-commutation relation (Equation (D.2) and Equation (D.3)) it is possible to obtain the probability of finding one particle on the left and the other on the right, $\mathcal{P}^S_{\mathcal{LR}}$, as:

$$\begin{aligned}
\mathcal{P}^S_{\mathcal{LR}} &= |\langle 0|\hat{b}_L \hat{b}_R \hat{a}_L^\dagger \hat{a}_R^\dagger |0\rangle|^2 = \\
&= |\langle 0| \left(r\hat{a}_L + t'\hat{a}_R\right) \left(t\hat{a}_L + r'\hat{a}_R\right) \hat{a}_L^\dagger \hat{a}_R^\dagger |0\rangle|^2 = \\
&= |\langle 0| r t \hat{a}_L \hat{a}_L \hat{a}_L^\dagger \hat{a}_R^\dagger + r r' \hat{a}_L \hat{a}_R \hat{a}_L^\dagger \hat{a}_R^\dagger + t' t \hat{a}_R \hat{a}_L \hat{a}_L^\dagger \hat{a}_R^\dagger + t' r' \hat{a}_R \hat{a}_R \hat{a}_L^\dagger \hat{a}_R^\dagger |0\rangle|^2 = \\
&= |\langle 0| \left(r r' - t' t\right) \hat{a}_L \hat{a}_R \hat{a}_L^\dagger \hat{a}_R^\dagger |0\rangle|^2 = \\
&= |\left(t' t - r r'\right)|^2 = \left(t' t - r r'\right) \left(t'^* t^* - r^* r'^*\right) = \\
&= T^2 + R^2 - t' t r^* r'^* - r r' t'^* t^* = (T + R)^2,
\end{aligned} \tag{D.4}$$

where in the last equality of Equation (D.4) it has been used the property of the scattering matrix $s^\dagger s = s s^\dagger = I$. Analogously, it is calculated the probability for two particles on the left, $\mathcal{P}^S_{\mathcal{LL}}$, as:

$$\begin{aligned}
\mathcal{P}^S_{\mathcal{LL}} &= |\langle 0|\hat{b}_L \hat{b}_L \hat{a}_L^\dagger \hat{a}_R^\dagger |0\rangle|^2 \\
&= |\langle 0| \left(r\hat{a}_L + t'\hat{a}_R\right) \left(r\hat{a}_L + t'\hat{a}_R\right) \hat{a}_L^\dagger \hat{a}_R^\dagger |0\rangle|^2 = \\
&= |\langle 0| r r \hat{a}_L \hat{a}_L \hat{a}_L^\dagger \hat{a}_R^\dagger + r t' \hat{a}_L \hat{a}_R \hat{a}_L^\dagger \hat{a}_R^\dagger + t' r \hat{a}_R \hat{a}_L \hat{a}_L^\dagger \hat{a}_R^\dagger + t' t' \hat{a}_R \hat{a}_R \hat{a}_L^\dagger \hat{a}_R^\dagger |0\rangle|^2 = \\
&= |\langle 0| \left(r t' - t' r\right) \hat{a}_L \hat{a}_R \hat{a}_L^\dagger \hat{a}_R^\dagger |0\rangle|^2 = 0.
\end{aligned} \tag{D.5}$$

Finally, the probability of detecting two particles on the right, $\mathcal{P}^S_{\mathcal{RR}}$, is calculated as:

$$\begin{aligned}
\mathcal{P}^{S}_{\mathcal{RR}} &= |\langle 0|\hat{b}_R\hat{b}_R\hat{a}^{\dagger}_L\hat{a}^{\dagger}_R|0\rangle|^2 \\
&= |\langle 0|\left(t\hat{a}_L + r'\hat{a}_R\right)\left(t\hat{a}_L + r'\hat{a}_R\right)\hat{a}^{\dagger}_L\hat{a}^{\dagger}_R|0\rangle|^2 = \\
&= |\langle 0|tt\hat{a}_L\hat{a}_L\hat{a}^{\dagger}_L\hat{a}^{\dagger}_R + tr'\hat{a}_L\hat{a}_R\hat{a}^{\dagger}_L\hat{a}^{\dagger}_R + r't\hat{a}_R\hat{a}_L\hat{a}^{\dagger}_L\hat{a}^{\dagger}_R + r'r'\hat{a}_R\hat{a}_R\hat{a}^{\dagger}_L\hat{a}^{\dagger}_R|0\rangle|^2 = \\
&= |\langle 0|\left(tr' - r't\right)\hat{a}_L\hat{a}_R\hat{a}^{\dagger}_L\hat{a}^{\dagger}_R|0\rangle|^2 = 0. \qquad \text{(D.6)}
\end{aligned}$$

It is interesting to notice that these probabilities are developed under the assumption (implicit in the scattering formalism) that each initial state $\hat{a}^{\dagger}_L|0\rangle$ or $\hat{a}^{\dagger}_R|0\rangle$ is a mono-energetic state. Different initial states are considered in Section 5.1. Within the scattering formalism, a superposition of $\hat{a}^{\dagger}_L\hat{a}^{\dagger}_R|0\rangle$ with different momentums will be required to reproduce the variability of the two-particle probabilities studied in the main tex of the thesis.

Appendix E

Analytical Two-Particle Probabilities for Arbitrary Wave Packets

A general expression for the probabilities $\mathcal{P}_{\mathcal{LR}}$, $\mathcal{P}_{\mathcal{LL}}$ and $\mathcal{P}_{\mathcal{RR}}$ in Equations (5.6)-(5.8) for an arbitrary normalizable wave packet is developed in this Appendix. Conditions (i), (ii) and (iii) mentioned in Section 5.1.1 are explicitly assumed. The solution of time dependent Schrödinger equation with the separable potentials can be found from two decoupled single-particle Schrödinger equations. After impinging with the barrier, at the time t_1 mentioned in the text, each initial one-particle wave function splits into (non-overlapping) transmitted (t) and reflected (r) components defined in Equation (5.10) and Equation (5.11).

From the set of four available reflected and transmitted components, the set of sixteen complex integrals is defined as follows:

$$I_{e,f}^{c,d} = \int_g^h dx\ \phi_e^c(x,t_1)\ \phi^{*d}_f(x,t_1), \tag{E.1}$$

where the upper indices c and d are related to transmitted (t) and reflected (r) components, while the sub indices e and f to the initial position of the one-particle wave packets (a left and b right). The limits of the spatial integration, not explicitly indicated in $I_{e,f}^{c,d}$, are $g = -\infty, h = 0$ when both components are present at the left of the barrier, while $g = 0, h = \infty$ at the right. With the definitions of Equation (E.1), the transmission and reflection coefficients of the a-wave packet are rewritten as $T_a = I_{a,a}^{t,t}$ and $R_a = I_{a,a}^{r,r}$, respectively. Identically, it is defined $T_b = I_{b,b}^{t,t}$ and $R_b = I_{b,b}^{r,r}$. By construction, $I_{e,f}^{c,d} = (I_{f,e}^{d,c})^*$.

Using the definitions in Equations (5.10)-(5.11) and (E.1), one gets the property:

$$I_{a,b}^{r,t} + I_{a,b}^{t,r} = \int_{-\infty}^{\infty} dx\ \phi_a\ \phi_b^* = \int_{-\infty}^{\infty} dk\ g_a(k)\ g_b^*(k), \tag{E.2}$$

where it has been defined

$$g_a(k) = \langle \phi_a(x,t_0) | \psi_k(x) \rangle = \int_{-\infty}^{\infty} \phi_a(x,t_0) \psi_k^*(x) dx, \tag{E.3}$$

being $\psi_k(x)$ the scattering state (with k its wave vector). Accordingly, the wave packet $\phi_a(x,t)$ can be written by superposition as:

$$\phi_a(x,t) = \frac{1}{\sqrt{2\pi}} \int_{-\infty}^{\infty} g_a(k) \Delta e^{-\frac{iE_k \Delta t}{\hbar}} \psi_k(x) dk. \tag{E.4}$$

Identical definition for $g_b(k)$. Notice that the scenario depicted in figure 5.1 implies that there is no overlapping between $g_a(k)$ and $g_b(k)$ because they have opposite momentums at the initial time. This no overlapping condition is true initially and it also remains valid at any later time because $\psi_k(x)$ are Hamiltonian eigenstates. Then, one gets $I_{a,b}^{r,t} + I_{a,b}^{t,r} = 0$.

Using $I_{e,f}^{c,d} = (I_{f,e}^{d,c})^*$, the probability of detecting two particles at the left of the barrier in Equation (5.7), at $t = t_1$, can be straightforwardly developed as:

$$\mathcal{P}_{\mathcal{LL}} = \int_{-\infty}^{0} dx_1 \int_{-\infty}^{0} dx_2\ \ |\Phi|^2 = R_a T_b \mp |I_{a,b}^{r,t}|^2. \tag{E.5}$$

Identically, the probability of detecting two particles at the right of the barrier is:

$$\mathcal{P}_{\mathcal{RR}} = T_a R_b \mp |I_{a,b}^{r,t}|^2. \tag{E.6}$$

Finally, using also the previous identity $I_{a,b}^{r,t} = -I_{a,b}^{t,r}$, the probability of one particle at each side is:

$$\begin{aligned} \mathcal{P}_{\mathcal{LR}} &= \frac{R_a R_b + T_a T_b}{2} \pm |I_{a,b}^{r,t}|^2 + \frac{R_a R_b + T_a T_b}{2} \pm |I_{a,b}^{r,t}|^2 = \\ &= R_a R_b + T_a T_b \pm 2|I_{a,b}^{r,t}|^2. \end{aligned} \tag{E.7}$$

Notice that the term $\pm|I_{a,b}^{r,t}|$ accounts for the difference between Fermions and Bosons. For these general conditions, one can check that $\mathcal{P}_{\mathcal{LL}}+\mathcal{P}_{\mathcal{RR}}+\mathcal{P}_{\mathcal{LR}} = R_a R_b + T_a T_b + 2T_a R_b$. Since $1 = R_a + T_a$ and $1 = R_b + T_b$, one finally gets $\mathcal{P}_{\mathcal{LL}} + \mathcal{P}_{\mathcal{RR}} + \mathcal{P}_{\mathcal{LR}} = 1$, for either Fermions or Bosons.

Under the conditions (i), (ii) and (iii) mentioned in Section 5.1.1, the expression of $I_{a,b}^{r,t}$ can be further developed. Define a new wave packet $\Upsilon_a(x,t_1)$ as follows: $\Upsilon_a(x,t_1) =$

$\phi_a^r(x,t_1)$ for all $x \in (-\infty, 0]$ and $\Upsilon_a(x,t_1) = 0$ elsewhere. This new wave packet can be written at t_1 as:

$$\Upsilon_a(x,t_1) = \frac{1}{\sqrt{2\pi}} \int_{-\infty}^{\infty} g_a(k) \Delta e^{-\frac{iE_k \Delta t_1}{\hbar}} r(k) e^{-ikx} dk, \tag{E.8}$$

where $r(k)$ is the reflection (complex) amplitude of the scattering state $\psi_k(x)$. Notice that $\Upsilon_a(x,t_1)$ does not contain the incident plane wave $exp(ikx)$ included in $\psi_k(x)$. The reason is because, at time t_1, the superposition of these incident terms $exp(ikx)$ do not contribute to the wave function at the left of the barrier. Identically, it is defined $\Upsilon_b(x,t_1) = \phi_b^t(x,t_1)$ for all $x \in (-\infty, 0]$ and $\Upsilon_b(x,t_1) = 0$ elsewhere. At t_1:

$$\Upsilon_b(x,t_1) = \frac{1}{\sqrt{2\pi}} \int_{-\infty}^{\infty} g_b(k) \Delta e^{-\frac{iE_k \Delta t_1}{\hbar}} t(k) e^{-ikx} dk, \tag{E.9}$$

where $t(k)$ is the transmission (complex) amplitude of the scattering state $\psi_k(x)$. Because of conditions (i), (ii) and (iii), one can consider $g(k) \equiv g_a(k) = g_b(-k)$. Then, using expressions (E.8) and (E.9) one gets:

$$I_{a,b}^{r,t} = \int_{-\infty}^{\infty} dx \Upsilon_a \Upsilon^*_b = \int_{-\infty}^{\infty} dk |g(k)|^2 r(k) t^*(k), \tag{E.10}$$

where the spatial integral in Equation (E.10) extends from $-\infty$ to ∞ because, by construction, $\Upsilon_a(x,t_1)$ and $\Upsilon_b^*(x,t_1)$ are zero at $x \in (0, \infty)$. It has also been used the property of the scattering states $t(k) = t(-k)$. It is interesting to compare Equation (E.10) with the well-known expression for the computation of the (one-particle) transmission coefficient:

$$T = T_b = T_a = I_{a,a}^{t,t} = \int_{-\infty}^{\infty} dk |g(k)|^2 |t(k)|^2, \tag{E.11}$$

and (one-particle) reflection coefficient:

$$R = R_b = R_a = I_{a,b}^{r,r} = \int_{-\infty}^{\infty} dk |g(k)|^2 |r(k)|^2. \tag{E.12}$$

Notice that, under the conditions (i), (ii) and (iii), the transmission $T = T_b = T_a$ and reflection $R = R_b = R_a$ coefficients are equal for the a and b wave packets. One can observe that T and R take real values, while $I_{a,b}^{r,t}$ take complex ones.

From Equation (E.10), it is a straightforward procedure to deduce the maximum allowed value for $|I_{a,b}^{r,t}|^2$. The maximum value is $|I_{a,b}^{r,t}|^2 = RT$. It corresponds to an scenario where $r(k)$ and $t(k)$ are (almost) constant in the support of $g(k)$. Then, from Equation (E.10), one obtains $I_{a,b}^{r,t} \approx r(k^c) t^*(k^c)$ with k^c defined as the central wave vector of the wave packet. It can be straightforwardly demonstrated that this value implies that the shapes

of the a-reflected $\phi_r^a(x,t)$ and b-transmitted $\phi_t^b(x,t)$ wave packets are identical up to an arbitrary (complex) constant:

$$\phi_a^r(x,t_1) = \phi_b^t(x,t_1)e^{\alpha+i\beta}, \tag{E.13}$$

being α and β two real position-independent constants. For such scenarios, Equations (E.5)-(E.7) can be rewritten as $\mathcal{P}_{\mathcal{LL}}^M$, $\mathcal{P}_{\mathcal{RR}}^M$ and $\mathcal{P}_{\mathcal{RR}}^M$ in Equation (5.13) and Equation (5.14). The upper index M is used in Equation (5.13) and Equation (5.14) to indicate that the probabilities correspond to the maximum value of $|I_{a,b}^{r,t}|^2$. Equation (5.13) and Equation (5.14) exactly reproduce the results found in the literature for scattering states in Refs. [16, 17, 51, 52, 78].

However, the possibility of a minimum value $|I_{a,b}^{r,t}|^2 = 0$ in Equation (E.10) is in general ignored in the literature. This corresponds to an scenario where $r(k)$ and $t(k)$ vary very rapidly between 1 and 0 on the support of $g(k)$. For example, in a sharp resonance. Then, from Equation (E.10), one gets $I_{a,b}^{r,t} \approx 0$. This value means that $\phi_r^a(x,t)$ and $\phi_t^b(x,t)$ in Equation (E.1) are orthogonal. In fact, the different schematic symbols of the wave packets in Figure 5.1 want to emphasize this point. When $|I_{a,b}^{r,t}|^2 = 0$, Equations (E.5)-(E.7) can be rewritten as $\mathcal{P}_{\mathcal{LL}}^m$,$\mathcal{P}_{\mathcal{RR}}^m$ and $\mathcal{P}_{\mathcal{LR}}^m$ in Equation (5.15) and Equation (5.16). The upper index m in Equation (5.15) and Equation (5.16) indicates that these probabilities correspond to the minimum value of $|I_{a,b}^{r,t}|^2$. The probabilities in Equations (5.15)-(5.16) show no difference between indistinguishable (Fermions or Bosons) or distinguishable particles.

Appendix F

The Quantum DC Current in Ergodic Systems

The DC current in a laboratory $\langle I \rangle$ can be computed by time-averaging the measured value of the total current $I(t)$ from a *unique device* during a large (ideally infinite) period of time τ as mentioned in Equation (5.19). If one can justify the ergodicity of the electronic device, one can alternatively compute $\langle I \rangle$ from an ensemble-average of all possible values of the current I_i measured, at one particular time t, over an *ensemble of (identical) devices* as seen in Equation (5.25). For DC quantum transport computations, Equation (5.25) is greatly preferred because it deals directly with the probabilistic interpretation of the wave function. It is important to realize that while Equation (5.19) implies measuring the quantum current many times, Equation (5.25) involves only one measurement. One does not need to worry about the evolution of the wave function after the measurement when using Equation (5.25). It is possible to define the eigenstates $|\psi_i\rangle$ of a particular operator I, as those vectors that satisfy the equation $I|\psi_i\rangle = I_i|\psi_i\rangle$. The eigenvalue I_i is one of the M possible measured values in Equation (5.24).[1] Since the entire set of eigenstate form a basis for the Hilbert space, the wave function can be decomposed as $|\psi(t)\rangle = \sum_{i=1}^{M} c_i(t)|\psi_i\rangle$, with $c_i(t) = \langle\psi_i|\psi(t)\rangle$. Then, one can rediscover Equation (5.24) as follow:

$$\begin{aligned} \langle I \rangle &= \langle\psi(t)|I|\psi(t)\rangle = \\ &= \sum_{j=1}^{M} c_j^*(t)\langle\psi_j| \sum_{i=1}^{M} I_i c_i(t)|\psi_i\rangle = \sum_{i=1}^{M} I_i P(I_i), \end{aligned} \tag{F.1}$$

[1] For simplicity it is assumed that there is no degeneracy. The qualitative discussion does not change if degeneracy is considered.

where it has been used the orthonormal property of the eigenstates $\langle\psi_j|\psi_i\rangle = \delta_{ij}$ and the definition of the (Born) probability $P(I_i) = |c_i(t)|^2$. It is important to emphasize that $\langle\psi(t)|I|\psi(t)\rangle$ does not require the explicit knowledge of the eigenstates. Only the free evolution of the state $|\psi(t)\rangle$ and the *measuring* operator I are needed.

At this point, it is mandatory to provide some discussion about the use of the ergodic theorem. Strictly speaking, no ergodic theorem exists for an out of equilibrium system [72]. Indeed, the out of equilibrium system is represented by a distribution function, or probability function, that is different from that in equilibrium and arises from a balance between the driving forces and the dissipative forces. The applied bias used to measure the DC current of any device implies that the device is quite likely in a far from equilibrium state. Therefore, the ergodic connection between (5.19) and (5.25) has to be considered as only a very reasonable approximation for DC transport, but not as an exact result [72].

Bibliography

[1] Aharanov, Y., Albert, D. Z. & Vaidman, L.: *How the result of a measurement of a component of the spin of a spin-1/2 particle can turn out to be 100*. Physical Review Letters **60** (14), 1351-1354 (1988).

[2] Alarcón, A. & Oriols, X.: *Computation of quantum electron transport with local current conservation using quantum trajectories*. Journal of Statistical Mechanics: Theory and Experiment **2009**, P01051 (2009).

[3] Alarcón, A., Cartoixa, X. & Oriols, X.: *Towards the explicit computation of bohm velocities associated to n-electron wavefunctions with arbitrary spin-orientations*. Physica Status Solidi C **7**, 2636-2639 (2010).

[4] Alarcón, A., Yaro, S., Cartoixà, X. & Oriols, X.: *Computation of many-particle quantum trajectories with exchange interaction: Application to the simulation of nanoelectronic devices*. Journal of Physics: Condensed Matter **25**, 325601 (2013).

[5] Albareda, G., Suñé, J. & Oriols, X.: *Many-particle hamiltonian for open systems with full coulomb interaction: Application to classical and quantum time-dependent simulations of nanoscale electron devices*. Physical Review B **79**, 075315 (2009).

[6] Albareda, G., Lopez, H., Cartoixà, X., Suñé, J. & Oriols, X.: *Time-dependent boundary conditions with lead-sample Coulomb correlations: Application to classical and quantum nanoscale electron device simulators*. Physical Review B **82**, 085301 (2010).

[7] Albareda, G., Marian, D., Benali, A., Yaro, S., Zanghì, N. & Oriols, X.: *Time-resolved electron transport with quantum trajectories*. Journal of Computational Electronics, Special Issue on Quantum Trasport Beyond DC, **12**(3), 405-419 (2013).

[8] Albareda, G., Marian, D., Benali, A., Alarcòn, A., Yaro, S. & Oriols, X.: Book Chapter *Electron Devices Simulation with Bohmian Trajectories* in *Simulation of*

transport in nanodevices, Volume 1: Principles, models and methods, ISTE Ltd (2014).

[9] Bassi, A. & Ghirardi, G. C.: *The Trieste Lecture of John Stewart Bell.* Journal of Physics A: Mathematical and Theoretical **40** 2919 (2007).

[10] Beenakker, C. & Schönenberger, C.: *Quantum Shot Noise.* Physics Today **56**, 37-43 (2003)

[11] BITLLES is the acronym of *Bohmian Interacting Transport for non-equiLibrium eLEctronic Structures.* See the website *http://europe.uab.es/bitlles*

[12] Blanter, Y. M. & Büttiker, M.: *Shot noise in mesoscopic conductors.* Physical Reports **336**, 1-166 (2000).

[13] Braverman, B. & Simon, C.: *Proposal to Observe the Nonlocality of Bohmian Trajectories with Entangled Photons.* Physical Review Letters **110**, 060406 (2013).

[14] Bocquillon, E., Freulon, V., Berroir, J. M., Degiovanni, P., Plaçais, B., Cavanna, A., Jin, Y. & Feve, G.: *Coherence and Indistinguishability of Single Electrons Emitted by Independent Sources.* Science **339**, 1054 (2013).

[15] Bohm, D.: *A suggested interpretation of the quanta theory in term of "hidden" variables I and II.* Physical Review **85**, 166-193 (1952).

[16] Büttiker, M.: *Scattering theory of thermal and excess noise in open conductors.* Physical Review Letters **65**, 2901-2904 (1990).

[17] Büttiker, M.: *Scattering theory of current and intensity noise correlations in conductors and wave guides.* Physical Review B **46**, 12485-12507 (1992).

[18] Büttiker, M.: *Bunches of Photons–Antibunches of Electrons.* Science **284**, 275 (1999).

[19] Bohr, N.: *Atomic Theory and the Description of Nature.* Cambridge University Press, Cambridge (1934)

[20] Born, M.: *The Classical Mechanics of Atoms.* New York, Ungar (1960).

[21] Cavalcanti, E. G.& Wiseman, H. M.: *Bell Nonlocality, Signal Locality and Unpredictability (or What Bohr Could Have Told Einstein at Solvay Had He Known About Bell Experiments).* Foundation of Physics **42**, 1329-1338 (2012).

[22] Cohen-Tanoudji, C., Diu, B. & Laloë, F.: *Quantum Mechanics.* Wiley, New York (1977).

[23] Colomés, E., Marian, D. & Oriols, X.: *Understandable algorithm for exchange interaction: Quantum noise in nanoelectronic devices.* Computational Electronics (IWCE), 2014 International Workshop on, (2014). doi: 10.1109/IWCE.2014.6865811

[24] de Jong, M.J.M. & Beenakker, C.W.J.: *Shot noise in mesoscopic systems.* In: Sohn, L.L., Kouwenhoven, L.P., Schön, G. (eds.) NATO ASI Series E Vol. 345, pp. 225-262. Kluwer Academic Publishing, Dordrecht (1997)

[25] Dhara, C., de la Torre, G. & Acín, A.: *Can Observed Randomness Be Certified to Be Fully Intrinsic?* Physical Review Letters **112** , 100402 (2014).

[26] Di Ventra, M.: *Electrical Transport in Nanoscale Systems.* Cambridge University Press, Cambridge (2008).

[27] Dirac, P. A. M.: *Quantum mechanics of many-electron systems.* Proceeding of the Royal Society A **213**, 714-733 (1929).

[28] de Broglie, L.: *An introduction to the Study of Wave Mechanics*, New York: Dutton (1930).

[29] Dürr, D., Goldstein, S. & Zanghì, N.: *Quantum Equilibrium and the Origin of Absolute Uncertainty.* Journal of Statistical Physics **67**, 843-907 (1992).

[30] Dürr, D., Goldstein, S. & Zanghì, N.: *Quantum Chaos, Classical Randomness, and Bohmian Mechanics.* Journal of Statistical Physics **68**, 259-270 (1992).

[31] Dürr, D., Goldstein, S. & Zanghì, N.: *Bohmian mechanics and the meaning of the wave function.* In R.S. Cohen, M. Horne, J. Stachel (Eds.), *Experimental Metaphysics – Quantum Mechanical Studies in Honor of Abner Shimony, Volume I* (pp. 25-38). Dordrecht: Kluwer Academic Publishers (1996).

[32] Dürr, D., Goldstein, S. & Zanghì, N.: *Quantum equilibrium and the role of operators as observables in quantum theory.* Journal of Statistical Physics **116**, 959-1055 (2004).

[33] Dürr, D., Goldstein, S., Tumulka, R. & Zanghì, N.: *On the Role of Density Matrices in Bohmian Mechanics.* Foundations of Physics **35**, 449-467 (2005).

[34] Dürr, D., Goldstein, S. & Zanghì, N.: *On the Weak Measurement of Velocity in Bohmian Mechanics.* Journal of Statisitcal Physics **134**, 1023 (2009).

[35] Dürr, D., Goldstein, S. & Zanghì, N.: *Quantum theory without quantum philosophy.* Springer, Berlin (2013).

[36] Everett, H.: *Relative State Formulation of Quantum Mechanics*. Review of Modern Physics **29**, 454-462 (1957)

[37] Feynman, R.: *Feynman Lectures on Gravitation*. Perseus, Cambridge, MA (2002).

[38] Ghirardi, G.C., Rimini, A. & Weber, T.: *Unified dynamics for microscopic and macroscopic systems*. Physical Review D **34**: 470 (1986).

[39] Goldstein, S., Lebowitz, J. L., Mastrodonato, Ch., Tumulka, R. & Zanghì, N.: *Normal typicality and von Neumann's quantum ergodic theorem*. Proc. R. Soc. A **466**, 3203-3224 (2010).

[40] Heinonen, O. & Kohn, W.: *Internal structure of a Landau quasiparticle wave packet*. Physical Review B **36**, 3565 (1987).

[41] Heisenberg, W.: *Physics and Philosophy: the Revolution in Modern Science*. New York: Harper (1958).

[42] Heisenberg, W.: *The Physical Principles of the Quantum Theory*. Dover, New York (1930).

[43] Hong, C. K., Ou, Z. Y., & Mandel, L.: *Measurement of sub picosecond time intervals between two photons by interference*. Physical Review Letters **59 (18)**, 2044 (1987).

[44] Johnson, J.: *Thermal Agitation of Electricity in Conductors*. Physical Review **32**, 97 (1928).

[45] Kocis, S., Braverman, B., Ravets, S., Stevens, M. J., Mirin, R. P., Shalm, L. K. & Steinberg, A. M.: *Observing the Average Trajectories of Single Photons in a Two-Slit Interferometer*. Science **332**, 1170 (2011).

[46] Kraus, K: *States, Effects, and Operations*. Lecture notes in Physics, Volume **190** (1983).

[47] Landau, L. D.: *Theory of Fermi-liquids*. Soviet Physics JETP **3**, 920 (1957).

[48] Landau, L. D.: *Oscillations in a Fermi-liquid*. Soviet Physics JETP **5**, 101 (1957).

[49] Landau, L. D.: *On the theory of the Fermi-liquid*. Soviet Physics JETP **8**, 70 (1959).

[50] Landauer, R. & Martin, Th.: *Equilibrium and Shot Noise in Mesoscopic Systems*. Physica B **175**, 167 (1991).

[51] Landauer, R.: *Solid-State shot noise*. Physical Review B **47**, 16427-16432 (1993).

[52] Landauer, R.: *The noise is the signal.* Nature **392**, 658-659 (1998).

[53] Levitov, L. S., Lee, H. & Lesovik, G. B.: *Electron Counting Statistics and Coherent States of Electric Current.* Journal of Mathematical Physics **37**, 4845-4866 (1996)

[54] Lopreore, C. L. & Wyatt, R. E.: *Quantum Wavepacket Dynamics with Trajectories*, Physical Review Letters **82**, 5190-5193 (1999).

[55] Loudon, R.: *Fermion and boson beam-splitter statistics.* Physical Review A **58**, 4904 (1998).

[56] Liu, R. C., Odom, B., Yamamoto, Y. & Tarucha, S.: *Quantum interference in electron collision.* Nature **391**, 263 (1988).

[57] Lundeen, J. S., Sutherland, B., Patel, A., Stewart, C. & Bamber, C.: *Direct measurement of the quantum wavefunction.* Nature **474**, 188 (2011).

[58] Marian, D., Zanghì & N., Oriols, X.: *On the back-action of THz measurement on the total current of quantum devices.* Computational Electronics (IWCE), 2014 International Workshop on (2014). doi: 10.1109/IWCE.2014.6865844

[59] Marian, D., Colomés, E. & Oriols, X.: *Time-dependent exchange and tunneling: detection at the same place of two electrons emitted simultaneously from different sources.* Submitted, see also arxiv:1408.1990

[60] Marian, D., Colomés, E., Zhan, Z. & Oriols, X.: *Quantum Noise from a Bohmian perspective: fundamental understanding and practical computation in electron devices* Journal of Computational Electronics, Special Issue on Noise Modeling, in press (2015). See also arxiv:1410.0530

[61] Martin, Th. & Landauer, R.: *Wave-packet approach to noise in multichannel mesoscopic systems.* Physical Review B **45**, 1742-1755 (1992).

[62] Mateos, J., González, T., Pardo, D., Hoel, V. & Cappy, A.: *Monte Carlo simulator for the design optimization of low-noise HEMTs.* IEEE Transactions on Electron Devices, **47**, 1950-1956 (2000).

[63] Mermin, N.D.: *What's Wrong with this Pillow?* Physics Today **42**, 9 (1989).

[64] Nyquist, H.: *Thermal Agitation of Electric Charge in Conductors.* Physical Review **32**, 110 (1928).

[65] Norsen, T.: *The Theory of (Exclusively) Local Beables.* Foundation of Physics **40**, 1858-1884 (2010).

[66] Norsen, T., Marian, D. & Oriols, X.: *Can the wave function in configuration space be replaced by single-particle wave functions in physical space?* Synthese, Special Issue: Space-time and the wave function, 1-27 (2014). doi: 10.1007/s11229-014-0577-0, see also arxiv:1410.3676

[67] Oriols, X.: *Quantum trajectory approach to time dependent transport in mesoscopic systems with electron-electron interactions.* Physical Review Letters **98**, 066803 (2007).

[68] Oriols, X. & Mompart, J.: *Applied Bohmian Mechanics: From Nanoscale Systems to Cosmology.* Singapore: Pan Stanford Publishing (2012).

[69] Pauli, W.: *Über den Geschwindigkeitsabhängigkeit der Elektronenmasse auf den Zeemaneffekt.* Z. Physik **31**, 373-385 (1925).

[70] Pauli, W.: *Über den Zusammenhang des Abschlusses der Elektronengruppen im Atom mit der Komplexstruktur der Spektren.* Z. Physik **31**, 765-783 (1925).

[71] Pauli, W.: *Exclusion principle and quantum mechanics.* Nobel Lecture, 13 December, (1946).

[72] Price, P. J.: *Fluctuations of hot electrons.* In: Burgess, R.E. (eds) Fluctuation Phenomena in Solids, pp. 355-380. Academic Press, New York (1965).

[73] Sanz, A. S. & Miret-Artés, S.: *A Trajectory Description of Quantum Processes. I. Fundamentals.* Lecture Notes in Physics **850**, Springer-Verlag (Berlin, 2012).

[74] Sanz, A. S. & Miret-Artés, S.: *A Trajectory Description of Quantum Processes. II. Applications.* Lecture Notes in Physics **831**, Springer-Verlag (Berlin, 2014).

[75] Schilpp, P. A., ed.: *Albert Einstein: Philosopher-Scientist.* The Library of Living Philosophers, vol. 7. (1949).

[76] Schottky, W.: *Über spontane stromschwankungen in verschiedenen elektrizitätsleitern.* Annals of Physics (Leipzig) **57**, 541-567 (1918).

[77] Schrödinger, E.: *The Present Situation in Quantum Mechanics* (translation of 3-part Schrödinger, E. (November 1935). "Die gegenwärtige Situation in der Quantenmechanik"). Naturwissenschaften **23** (49): 823807-828812 (1935).

[78] Schöenenberger, C.: *Two Indistinguishable Electrons Interfere in an Electronic Device.* Science **339**, 1041 (2013).

[79] Traversa, F. L., Buccafurri, E., Alarcón, A., Albareda, G., Clerc, R., Calmon, F., Poncet, A. & Oriols, X.: *Time-Dependent Many-Particle Simulation for Resonant*

Tunneling Diodes: Interpretation of an Analytical Small-Signal Equivalent Circuit. IEEE Transanction on Electronic Devices **58**, 2104-2112 (2011).

[80] Traversa, F. L., Albareda, G., Di Ventra, M. & Oriols, X.: *Robust weak-measurement protocol for Bohmian velocities.* Physical Review A **87**, 052124 (2013).

[81] Venugopal, R., Goasguen, S., Datta, S. & Lundstrom, M. S.: *Quantum mechanical analysis of channel access geometry and series resistance in nanoscale transistors.* Journal of Applied Physics **95**, 292 (2004).

[82] von Neumann, J.: *Mathematical Foundations of Quantum Mechanics* (R. T. Beyer, Trans). Princeton: Princeton University Press (1955). (Original title: *Mathematische Grundlagen der Quantenmechanik*, Berlin 1932).

[83] Wiseman, H. M.: *Grounding Bohmian mechanics in weak values and Bayesianism.* New Journal of Physics **9**, 165 (2007).

[84] Wyatt, R. E.: *Quantum Dynamics with Trajectories*, Springer, (2005).

Acknowledgments

It's difficult to thank all who helped and supported me during my PhD, I hope I am not forgetting anyone.
First of all, I really thank my PhD Supervisor, Prof. Nino Zanghì, for introducing me to Bohmian Mechanics, for his competence, help and support during these three years: without him this Thesis would not exist.
I am very grateful to my External Supervisor, Prof. Xavier Oriols, for passing me his passion for applied Bohmian Mechanics, for his continuous help during the last years and for his kindness in hosting me in his research group in Barcelona: also without him this Thesis would not exist.
Thanks a lot to Matteo for carefully reading the Thesis and for his continuous support.
Thanks to Grande Fra for sharing with me his office in Genova.
Thanks to Sferrazza Papa Francesco for being my friend for too many years.
Thanks to Ferney, Jimena and Sebastian for their hospitality in Sabadell, for their friendship and for having helped me in improving my Spanish.
Thanks to Enrique for correcting my English mistakes, for sharing with me the office in Barcelona, for his friendship and for all the nice time we had in Spain.
Thanks to all my family: Grazia, Massimo, Sauro and Claudia for their encouragement and support.
Thanks to all the rest of the family, Zia Tina, Zia Mari, Zio Nino, Zio Stefano, Matteo, Silvia and Francesco.
Lastly, thanks to Simona for having always believed in me and without whom all this work would not really be started.